2009-01-05
2009-02-28

NBP09-01

Cruise Report

Contents

List of Figures

List of Tables

1 Introduction

Stan Jacobs, Chief Scientist

Three international science projects were accommodated on NB Palmer cruise 09-01. O-274, entitled 'Amundsen Sea Influence on West Antarctic Ice Sheet Stability and Sea Level Rise,' (S Jacobs, A Jenkins & H Hellmer, PIs) seeks to better understand ocean forcing on ice shelf, ice stream and sea ice change, and the sources of ocean freshening. Its several related subcomponents included setting out time series moorings to record temperature, salinity and currents over a period of two years; repeat profiling of water column properties on and near the Amundsen continental shelf; using the UK 'Autosub' to map thermohaline properties, currents and dimensions of the Pine Island Ice Shelf cavity; modeling the ocean circulation; sampling the sea ice, setting out drifters and mass balance buoys and recording sea ice properties underway; swath-mapping the sea floor; and outreach photography and video. B-244, 'Shedding Dynamic Light on Iron Limitation,' (K Arrigo, PI), a US/Netherlands/Canada project, sampled surface and subsurface waters to 300 m with trace metal clean equipment/methods to assess the influence of iron and light on phytoplankton productivity and species distribution. The goal of O-261, 'Sampling the ocean-sea ice interaction in the Pacific center of the Antarctic Dipole,' (X Yuan and J Sprintall, PIs) was to set a deep mooring northwest of the Amundsen Sea continental shelf to monitor the upper ocean role and response in ENSO teleconnections, complemented by German work near the Atlantic Dipole in the Weddell Sea.

Prior to the cruise, responsible Principal Investigators were asked to provide project summaries and plans, which were then circulated to other members of the field parties. Those outlines are attached to this report as appendices, which can now be compared with the work accomplished, detailed in the following sections. Elements of the work were also briefly described in prior weekly science reports to mo-sciweekly@usap.gov et al. For a variety of reasons, none of these projects achieved all of the fieldwork objectives in the time frames or locations anticipated in their underlying proposals. However, some have now come closer than others, some will be continued in forthcoming years, and at least one may have unexpectedly struck paydirt.

Project O-274 would have required >50 days and helicopter support to implement the full program proposed on the Amundsen Sea continental shelf, including a sea ice thickness survey with Alfred Wegener Institute collaborators and the setup of Automatic Weather Stations. In lieu of that, it was allocated 60 days to also accommodate the British Antarctic Survey/Southampton Autosub III project, postponed from prior scheduling on NBP07-02. The cruise length was subsequently shortened, but NBP09-01 experienced an atypically low sea ice cover and generally fair weather, facilitating much of the O-274 work planned in the eastern Amundsen sector. Project B-244 specified work in the Ross Sea, consistent with prior studies and modeling there, but for the first time in several trips to the Amundsen Sea, the NB Palmer started in Punta Arenas rather than McMurdo, and returned to Chile. Project O-261 anticipated an 11-day cruise from McMurdo to set a mooring at 69S, 140W, and after several iterations settled on a site at 66.45S, 129.47W, requiring 4-5 days of 0901 ship time. That mooring was deployed, but had to be quickly recovered as it did not set right in the water column, and could not be re-set without new line. The total ship time needed for all 3 projects was initially projected at 67 days, vs 62 allocated, reduced to 47 days during last summer's fuel crisis/budget crunch, after which 7 days were restored. Average fuel consumption (~5.6K gal/da) has been substantially less than anticipated, mainly due to the light sea ice encountered and substantial time 'on station.' Related costs were also much less than expected, at < $1.90/gal for marine gas at the pump in PUQ.

Acknowledgements

We are grateful for the solid technical and logistic support provided during the cruise by 11-person RPSC crew under the direction of Marine Project Coordinator Eric Hutt, and the 23-person ECO contingent led by Captain Mike Watson. Thanks to those who gave talks during the cruise, showed slides of their travels and made their 0901 pictures available on the local web. The primary financial support for this work has come from the US National Science Foundation, Office of Polar Programs to Columbia and Stanford

Universities and to Raytheon Polar Services Company/Edison Chouest Offshore, and from the UK National Environmental Research Council to the British Antarctic Survey and the National Oceanography Center, Southampton. Other agencies, institutions and individuals have also contributed, including the US Environmental Protection Agency, University of California Santa Cruz, Woods Hole Oceanographic Institute, NASA, the University of New South Wales @ the Australian Defence Force Acadamy, the Royal Netherlands Institute for Ocean Research, INIDEP-Argentina, University of Hawaii, Bruce Huber at the Lamont Earth Observatory, Tim Newberger at Lamont and UC Santa Cruz, and more than a few friends and families who managed the home fronts while we went south for the boreal winter.

2 CTD and LADCP Operations

Robin Robertson, Raul Guerrero, Katie Leonard, Chris Little, Ken Mankoff

2.1 CTD

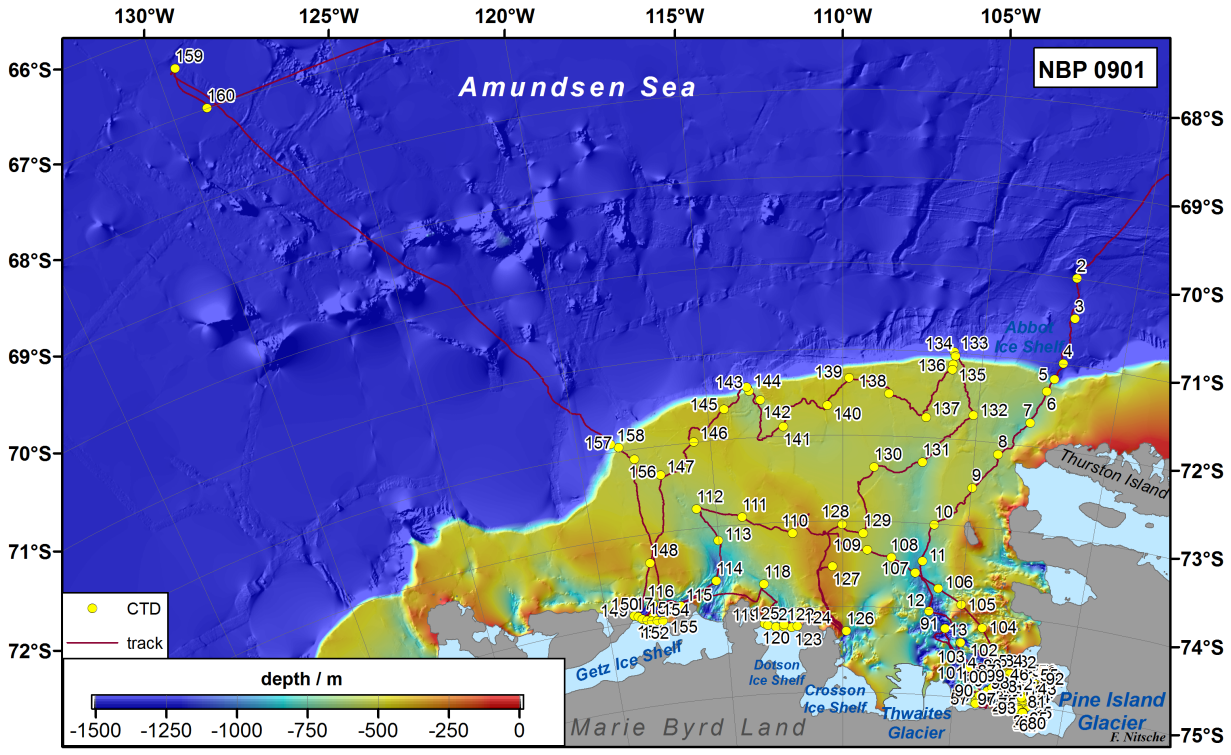

Figure 1: NBP0901 CTD station locations (yellow dots) in the Amundsen Sea with cruise track. Details on station location in PIB are shown in Fig. 2

During NBP0901, 160 CTD casts measuring Conductivity, Temperature and Depth were made with the Sea-Bird SBE 9/11+ system on a 24 bottle SBE32 rosette in support of the O-274, B-244, and O-261 projects. Temperature, conductivity, and dissolved oxygen were measured with dual sensor systems, primary and secondary. The sensors and pumps were mounted vertically on a horizontal frame connected to the rosette frame near the bottom. A single pressure sensor, rated to 6,000 dbar (10,000 psia), provided pressure information for conversion to depth. Additionally, single chlorophyll fluorometer, transmissometer, and PAR sensors were attached to the rosette in support of the DynaLife operations (B-244). The PAR sensor

Instrument	Serial Number	Calibration Date
CTD Fish	097536-0328	8/1/07
Carousel Water Sampler	3211265-0066	N/A
CTD Deck Unit	11P19858-0768	N/A
Slip Ring Assembly	1.406	N/A
CTD Pressure Unit	53980	8/1/07
Pump (primary)	051646	4/17/08
Pump (secondary)	051626	4/17/08
Temperature (primary)	031457	6/18/08
Temperature (secondary)	03P2299	6/18/08
Conductivity (primary)	040926	8/21/08
Conductivity (secondary)	041799	7/9/08
Dissolved Oxygen (primary casts 1-23)	161	6/19/08
Dissolved Oxygen (primary casts 24-103,105-160)	158	25/7/08
Dissolved Oxygen (primary cast 104)	139	2/5/08
Dissolved Oxygen (secondary)	155	7/1/08
Altimeter	42434	N/A
Bottom Contact Sensor	#1	N/A
Fluorometer	AFLD-009	2/14/08
Transmissometer	CST-831DR	4/9/08
PAR	4469	2/1/08

Table 1: Serial numbers and calibration dates for the CTD components. These temperature, conductivity, and dissolved oxygen sensors are being returned to Sea-Bird for calibration.

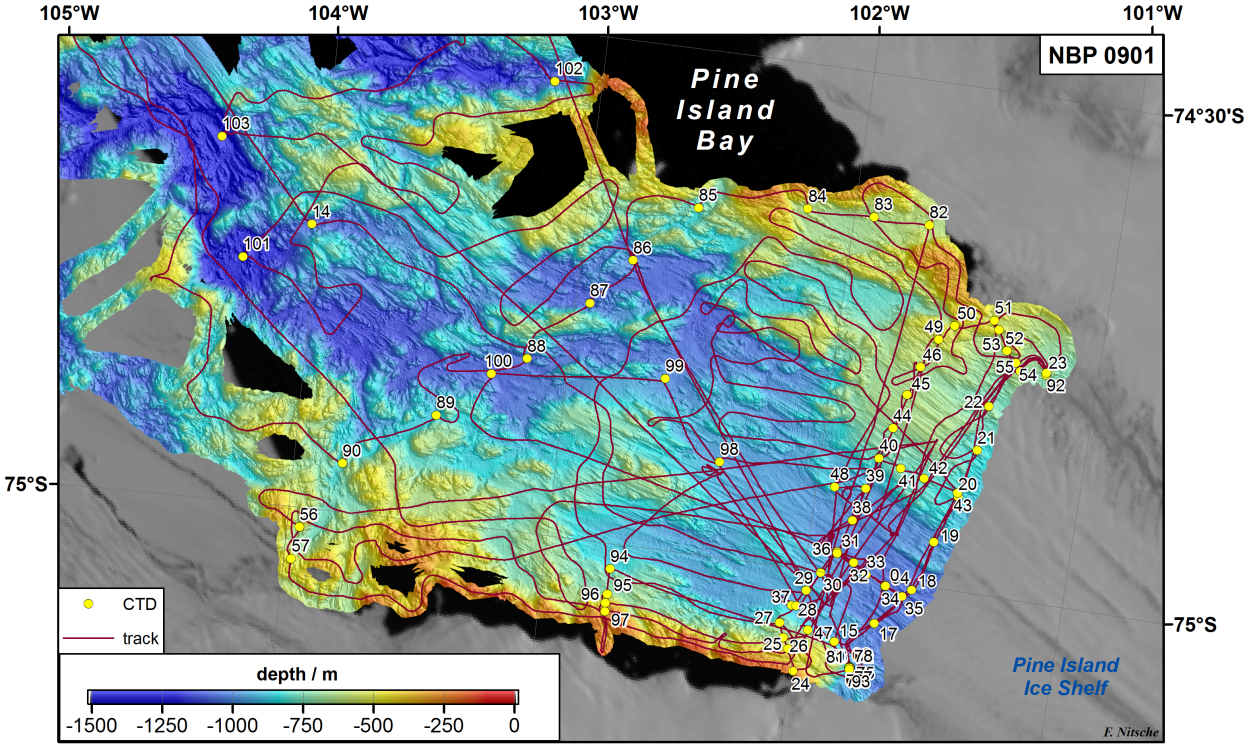

Figure 2: NBP0901 CTD station locations (yellow dots) in the Pine Island Bay with cruise track.

Figure 3: A CTD being lowered into water in front of Pine Island Glacier. Rosette of gray Niskin bottles is visible inside white frame. Image © Maria Stenzel, 2009

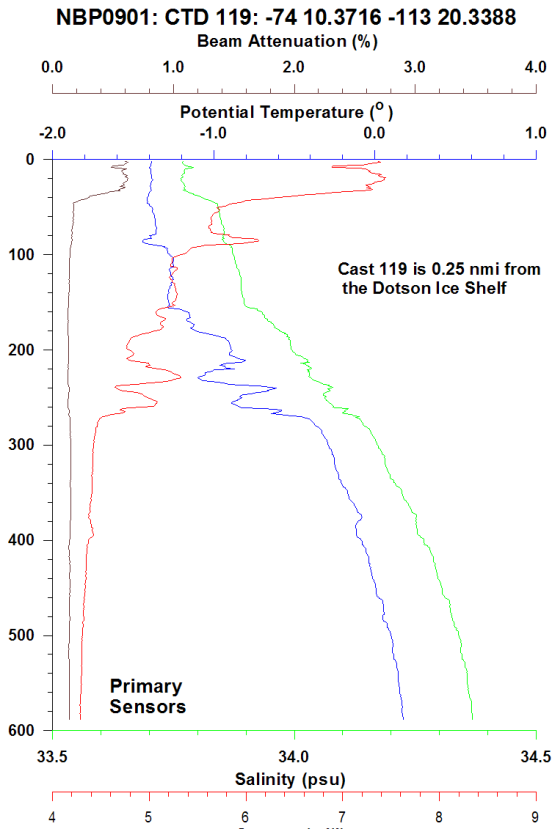

Figure 4: Profiles of temperature (blue), salinity (green), dissolved oxygen (red), and beam attenuation from the transmissometer (brown) for CTD cast 119, which was collected 0.25 nmi from front of the Dotson Ice Shelf.

was removed for the final CTD, since it is only rated to 2000 m and the CTD went to 4500 dbar. CTD casts were typically made to within 10 m of the bottom using both a Benthos PSA-916 altimeter and a SBE bottom contact with a 10 m line to determine distance off the seafloor. Exceptions are casts 1 and 2, which only went to 2000 m in much deeper water, cast 159, which went to 1200 m in 4500 m water, and yo-yo casts 63-81. The CTD was lowered at 20 m/minute from the surface to 50 m, 30 m/minute from 50 m to 100 m, and 50 m/minute below100 m. It was raised at 50-60 m/minute. Sea ice conditions or distance to ice shelves and any nearby icebergs were recorded on the CTD log, when applicable.

The same temperature, conductivity, and secondary dissolved oxygen sensors were used for all casts. The primary dissolved oxygen sensor was switched after cast 23, when it was determined to have high frequency noise and an offset from the calibration samples taken with the rosette. Additionally, a different primary dissolved oxygen sensor was used for cast 104 due to serial number confusion. Serial numbers and calibration dates for all CTD components are given in 1.

Data was acquired using Sea-Bird's SeaSave version 7.14 software on a PC running Windows XP. The software has been integrated with the Palmer's NEMA 1 Hz GPS to provide a position for each CTD scan. Generally, the system performed well, although modulo errors occurred due to faulty scan lengths. The faulty scan lengths are believed to originate during transmission through the wire. The modulo errors may indicate low insulation in the conducting wire. These errors were resolved by redoing the end termination on the cable. The CTD wire was terminated at least 4 times in order to reduce modulo errors, generally only removing short portions of the wire. Mechanical terminations are known to have been done before casts

1, 7, 104, and 159. At least one additional electronic termination occurred roughly before cast 9, but the date/time was not noted. In the original termination, the incorrect mechanical connector was used. This connector did not have a slot, which allows the electrical connection wire to easily exit the device without interference from the cable supporting the rosette frame. As a result, the electrical connection wire became pinched and a retermination was necessary (before cast 7). At this time, the mechanical connection was switched with one allowing the electrical connection wire without interference. A slip ring was changed before cast 93 and changed back after it did not reduce modulo errors. The cast number for the return of the original slip ring is unknown, as is the serial number of the replacement. It was necessary to restart one cast as 34b, midway in the downcast, when the software failed mid-cast. Additionally, due to operator error, cast 2 was done twice, since data was not archived the first time. The second cast for 2 is denoted 2b. Near the Getz Ice Shelf during a time of cold, southerly, katabatic winds, there were problems with icing in the sensors for cast 153. The CTD was brought on board and the sensors and pumps flushed, which cleared up the problem. Subsequent deployments under these conditions immersed the CTD rapidly, cutback on the rinsing of the sensors and rosette, and increased the Baltic room temperature. The problem did not reoccur. The PAR sensor was found to be unplugged following cast 98 and was subsequently reconnected to the fish when the disconnect was identified. The use of audio tapes as a backup has ceased in RPSC CTD proceedure. On NBP0901, screen prints were made as a backup for each cast of both the surface 200 m and the entire downcast for each station and saved in the CTD Log. Ken Mankoff developed digitization software that would convert these screen prints to profiles, if need be. This capability was not needed, after implementation of the screen saves as part of the CTD procedure.

Processing was performed immediately upon completion of the CTD using Sea-Bird's SBE Version 7.14e processing software using a modified version of the Huber et al. batch file, which can be found on the cruise data DVD. Both raw and processed data were then promptly copied to both a backup disk and the data disc available for general use. Random spikes occurred in the data throughout the cruise, particularly in pressure, temperature and conductivity. These spikes were removed in processing using wild edit. Plots of the processed potential temperature, salinity, dissolved oxygen, and density were generated for each cast by Robin Robertson and used to identify spiking in the different quantities. Air surface pressure on deck differed by -0.8 to -1.0 dbar between the start and end of each cast, showing shallower pressures on the up-cast. Although there were variations in this surface pressure difference, there was not an identifiable trend throughout the set of casts. Dissolved oxygen exhibited the usual hysterisis. Some drift occurred in the salinity and dissolved oxygen sensors and is discussed in their respective sections. When the switch of primary dissolved oxygen sensor was done after cast 23, correct calibration coefficients were entered, but the sensor serial number and date were not changed. This situation persisted until cast 104, before which the sensor was changed and calibration coefficients were modified accordingly. The primary dissolved oxygen for cast 104 is deemed to be in need of recalibration and is unsuitable for use. The sensor was again changed after cast 104 and all the relevant data (calibration coefficients, sensor number and dates) updated. From cast 105 on, all information is correct. Casts 24-103 have the wrong date and serial number for the primary dissolved oxygen sensor in the config files.

A 24 hour yo-yo deployment of the CTD was performed at the southern notch of the Pine Island Glacier (PIG), in order to evaluate the structure and variability of the outflow from the PIG. A CTD descent was started on the hour for the yo-yo casts, 58-81. The fourth cast, cast 61, was 15 minutes late starting its descent. The first 5 casts went to 900 m. The remaining yo-yo casts, 63-81, reached only to 800 m, as the deeper water column showed little change between casts 58 and 62. For the yo-yo casts, an ascent rate of 60 m/minute was used. The rosette was typically brought on board after each cast in order to charge the LADCP battery, download the LADCP data, and allow the winch operator to rest.

Water samples were collected using 10 liter "Bullister bottles" on the rosette for dissolved oxygen, salinity, oxygen isotopes, and total CO_2. Operation of the rosette was generally trouble-free other than the occasional failed release or open valve, as noted in the Bottle Logs. Samples for dissolved oxygen and salinity were collected for sensor monitoring and offset adjustment as needed. These samples were analyzed on board. Refer to the respective sections for further information. Samples for oxygen isotopes, and total CO_2 will be returned to the U.S for analyses. Four bottles of water from 10 m were also provided to the DynaLife group from many of the CTD casts directly before TMC casts.

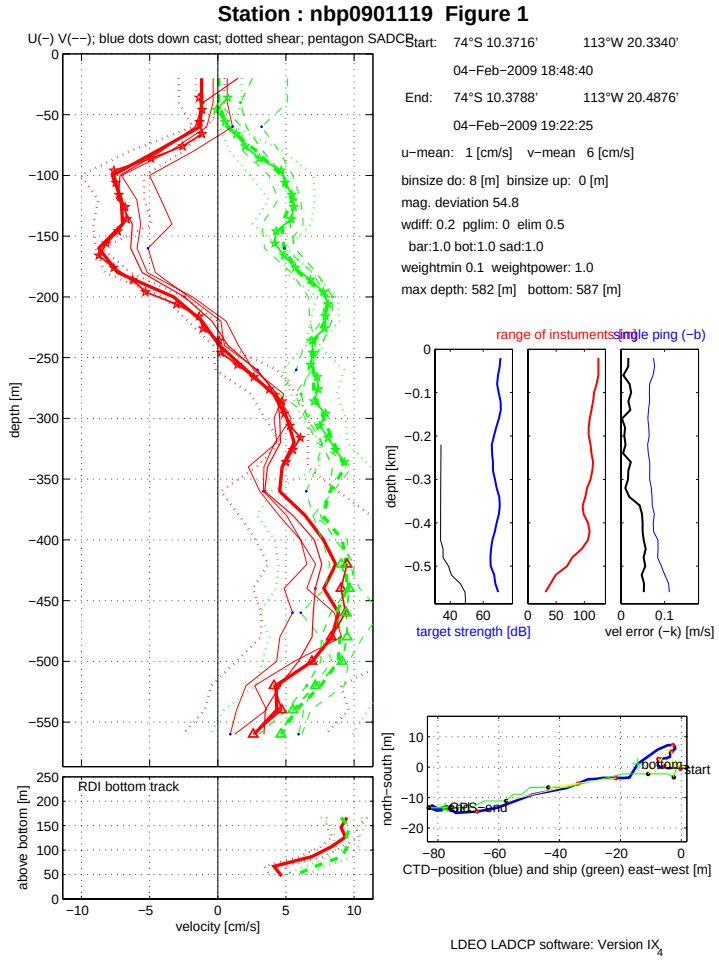

Figure 5: Example of a LADCP profile corresponding to the CTD cast profiles in Figure CTD-1. The East-West velocity (U solid line) changes direction roughly at 250 m and the North-South velocity (V dashed line) shows multiple layers in Northward direction away from the Dotson Ice Shelf cavity.

Most of the CTD casts were shallow, less than 1000 m. The shallow casts did not require many samples to define the water column. Typically, 3-8 samples for dissolved oxygen and salinity were taken per cast. At times, all bottles were fired in order to verify the mechanisms still functioned properly. Samples were typically taken at 10 m (below the ship's draft ∼5-6 m), 10 m above the bottom, the temperature extrema (defined as minimum and maximum), and in homogeneous oxygen/salinity layers for 'calibration'. Water was also collected at depths of interest for oxygen isotope samples.

The CTD's revealed that the water column in front of the ice shelves is layered, despite its weak stratification. The water column typically had two layers, an upper layer heavily influenced by melt water exiting from the ice shelves and a lower layer primarily composed of Circumpolar Deep Water (CDW). A profile collected in 0.25 nmi in front of the Dotson Ice Shelf showed a surface mixed layer (SML) extending to ∼38 m, in which temperature, salinity, dissolved oxygen, and beam attenuation (as determined by the transmissometer) are relatively uniform. In the SML, dissolved oxygen and temperature were well correlated. The upper layer fell below the SML from roughly 100 to 300 m and was both complex and active. In it, dissolved oxygen switched to be anti-correlated with temperature, as is typical in the deep ocean. The upper layer itself was composed of layers of 10-100 m height and strong intrusions. An example layer can be seen in Figure 4 between ∼95 and 160 m. Strong intrusions are evident between 200-270 m. Significant changes occurred in the upper layer between the down- and up-casts (not shown). These changes could have been induced by a dynamic water column changing between the down- and up-casts, by a small scale spatial variations in the water column with the CTD sampling from different water types, or by a degraded up-cast record. The depth of the upper layer varied within the Amundsen Sea, with a deeper upper layer (100-450 m) in front of the PIG compared to 100-300 m in front of the Dotson. It is plausible that the upper layer thickness is related to the draft of the ice shelf, although the ice shelf drafts are not well enough known for this to be definitively determined. Below the upper layer, generally a transition layer occurred in the region of the pycnocline. The lower layer typically extended from below this transition layer to the bottom, here ∼400-590 m. It was less active and showed a gradient of temperature and salinity increasing with depth

and dissolved oxygen decreasing with depth. The maximum temperatures and salinities occurred near the bottom in this layer. And small steps occasionally occurred in its upper portion.

The CTD operations were carried out by Robin Robertson, Katie Leonard, Chris Little, and Ken Mankoff with the CTD operated by RPSC personnel George Aukon and Greg Watson. Thanks are due to RPSC marine technicians Mike Lewis, Robert Zimmerman, Jullie Jackson, and Amy Schaub for their outstanding deployment of the CTD and rosette and their prompt mechanical repairs. We also appreciate the excellent winch operations of a Ben Aaron, Ric Tamayo, and Louie Andrada. Raul Guerrero assisted with setting up both the sensors and processing.

2.2 LADCP

A 300kHz RDI Lowered Acoustic Doppler Current Profiler (LADCP) was attached on the CTD rosette frame facing down. It was deployed on each CTD cast to provide a profile of the horizontal velocities with depth. Only a single LADCP head (SN 754) was used. Typically, the LADCP battery was charged every 3 casts, with the charging requiring between 20 min and an hour. The charging time needed depends on the charge remaining in the battery. It is possible that more time might be requred if the battery voltage was lower.

The LADCP operated well, without any problems due to broken beams. There are two CTD casts without LACDP profiles. On cast 1, the LADCP cover was not removed, with the result that there was no valid data. On cast 116, the instrument was not properly started due to operator error. Local times instead of GMT times were saved for LADCP profiles 2-36. The times both in the files and on the printed graphs in the CTD Log book are incorrect. The LADCP computer was shifted to GMT after cast 36 and the processing scripts modified to correct the time for incorporation of CTD and shipboard ADCP (SADCP) data. There were no problems with lack of scatterers in deep water, even on cast 160, which reached 4497 dbar. It should be noted that LADCP profile 2 goes with CTD cast 2b, not the non-existent CTD 2.

LADCP data was processed in Matlab using Andreas' Thurnherr's version IX.5 of the processing code, process_cast. Note the plots indicate version IX4, but the processing software says IX5. The processing incorporated processed CTD and SADCP data to provide navigation data and constrain the LADCP velocity profile, reducing errors. The SADCP was an RDI 150 kHz narrowband instrument. The maximum range of this instrument is 300 m, but valid data typically ceased between 250-280 m. Profile plots of the processed velocities for each LADCP profile are included in the CTD Log book. Only six LADCP profiles experienced processing errors. Three of these are casts 1, 2, and 116 as noted above. A shear solution was determined for profile 2. Three profiles showed pressure spikes in scans. These were casts 150, 151, and 153, which had 20, 20, and 22 pressure spikes in 2 scans, respectively. Their processing reports are included in the CTD Log book.

During the yo-yo casts (58-81), the LADCP was charged for 15-20 minutes after each cast, after cast 66. Monitoring of the LADCP battery voltage showed this to be sufficient to maintain the batter voltage of 50 V. Before cast 66 of the yo-yo, the LADCP was charged only once, after cast 60. Profiles 58, 61, and 64 each have multiple casts within the original raw data file, with 3 casts each in 58 and 61 and 2 casts in 64. A Matlab script, split_yoyo, was written to split the original raw files into separate raw files for each of the casts. This script is specific for these casts, although it could be generalized. When using split_yoyo, it is necessary to run it twice. The first time, the data is plotted and the user must identify the scan number for separation of the casts. It is relatively easy to identify scans when the LADCP is aboard the ship by the relatively constant zero velocity values. Any scan number within that period is valid for the split. This has been done for these three cases with multiple profiles and the scan numbers hardcoded into the script split_yoyo. In the future, if a general script is desired, the hardcoding of these scan numbers and the file names need to be modified. Note the three original raw files were renamed with an underline between the first and last cast numbers, ie. the original LADCP profile 58 raw file with three casts is named 058_60dn000.000, as opposed to its original name 058dn000.000. The new file of that name has only the raw data corresponding to cast 58 in it. This was done in order to allow processing of this data without further modification of the processing software.

In front of the Dotson Ice Shelf, the East-West velocity was aligned roughly along the front of the ice shelf cavity and the North-South velocity in/out of the cavity. For the corresponding LADCP profiles for CTD cast 119 (Figure 4), the North-South velocity (V, green line in Figure 5) was positive, indicating outflow from the cavity, from below the SML (50 m) to the bottom. The North-South velocity did fluctuate with depth, but did not indicate clear layers. However, the East-West velocities (U, red line) changed direction at around 250 m, indicating two layers, as in the CTD structure. Below 400 m, corresponding to the lower layer of the CTD, U was relatively uniform at ∼8 cm/s and V uniform at ∼9 cm/s. The result was a northeasterly flow of the lower layer. This indicates exiting CDW after transit of the ice shelf cavity. The upper layer behavior is more complex. Between 100-160 m, roughly the depth of the large step or layer in CTD 119, the East-West velocity was constant at ∼7-8 cm/s and the V velocity ∼5-6 cm/s. This portion of the upper layer, depths 100-160 m, appears to be flowing WNW roughly at a 30o with the front of the ice shelf. Below this layer, stronger U velocities occur in a 40 m layer from ∼160-200 m, which corresponds to two ∼20 m layers in temperature. At depths of 200-260 m, U velocities are small and change direction and V velocities weaken. Strong intrusions occur in this depth range of weaker velocities. The weaker velocities may enable water to interleave more easily, increasing intrusions. It is likely the interleaving water masses originated from the ice shelf cavity south of this site and a water mass north of this site, since the V velocities are stronger for this depth range. In the transition layer, ∼300 to 400 m, U velocities generally increased in magnitude and V velocities fluctuated between 7 and 9 cm/s. A series of peaks at roughly 75 m intervals were apparent in the V velocities between 100 and 300 m depth. There were no apparent correlations between this series of velocity peaks and the temperature or salinity profiles of the CTD.

The LADCP operations were carried out by Robin Robertson, Katie Leonard, Chris Little, and Ken Mankoff. Raul Guerrero assisted with installation of the LADCP and battery charging.

2.3 Dissolved Oxygen

Katherine Leonard, Chris Little, Ken Mankoff

Two SBE 43 dissolved oxygen sensors are a standard part of the CTD sensor array. SBE 43 sensors have an accuracy of 2 percent of saturation, and a stability of 2 percent per 1000 hours. Titrated values by the Winkler method are also necessary to 'calibrate' the CTD oxygen sensors, i.e., to correct for sensor bias, drift and potential offsets. During NBP0901, 407 oxygen samples were collected for Winkler titration from 126 CTD stations, plus an electronically undocumented cast at the site of station two. The Langdon amperometric titrator was used to determine dissolved oxygen concentrations in whole bottle samples of approximately 140 mL of seawater collected from the CTD rosette. In addition to those 407 samples, at least 30 blanks and 125 standards were also determined using the automated titrator system.

Three liters of KIO_3 standard were prepared and shipped south by C. Langdon in September 2008, of which 1.725 L were used in running standards and blanks during the course of the cruise. The titrations also consumed close to one liter each of MnCl and NaOH-NaI solutions for pickling samples, 5-molar H_2SO_4, and Na-Thiosulfate titrant. Approximately 100mL of each of these chemicals remained at the end of the cruise, but dispensing that liquid into water samples would have required different equipment than was available in the NBP's Langdon titrator system. Adequate supplies were unavailable on board with which to prepare new pickling chemicals, and the titrant stocked in dry form on board the NBP is the pentahydrate rather than the preferred anhydrous variety.

Fewer than half the projected number of seawater samples were collected and analysed for dissolved oxygen content during NBP09-01, due to constraints imposed by an insufficient supply of pickling chemicals. However, through careful management, cautious sampling strategies, and analysts' nimbleness in spill-avoidance, the available reagents were stretched to allow sample collection through the final station of the cruise. The titration work, principally conducted by C. Little, proceeded smoothly, with occasional unexceptional hiccoughs due to ship motion bouncing the magnetic stir-bars and air bubbles in the Na-Thio in the micro burette and titrant lines. Sampling (principally by Little and Mankoff, with help from Leonard and Robertson during the pm and am shifts respectively) immediately followed each cast, from the deepest niskins first,

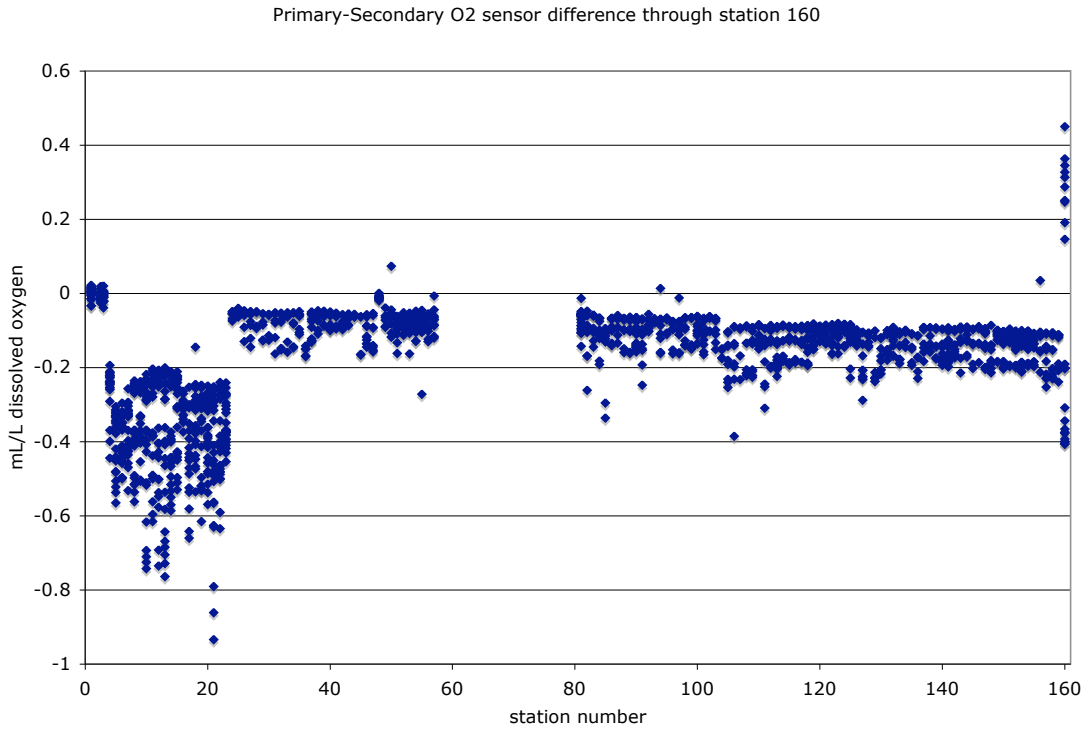

Figure 6: Ox1 minus Ox2 sensor values versus CTD station number. Note significant errors between CTD stations 4 to 23, and 160.

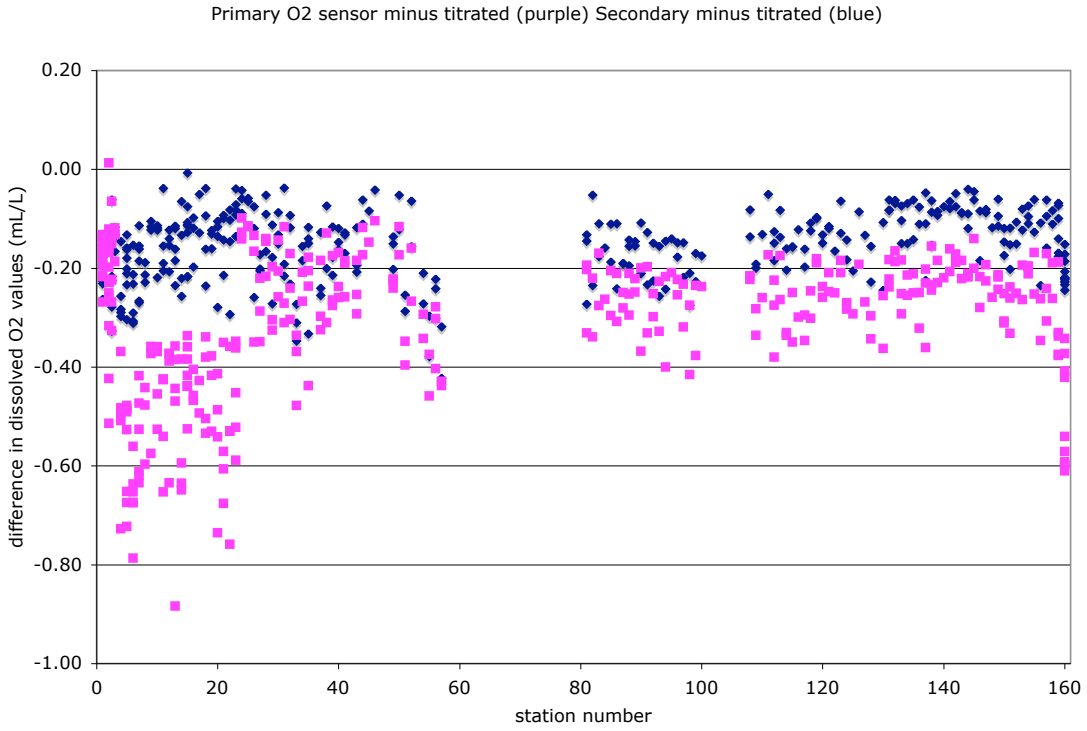

Figure 7: Titrated dissolved oxygen values minus Ox1 and Ox2 sensor values versus CTD station number. Outliers have been removed.

with dissolved oxygen preceding any other water collection, so the seawater samples collected were generally of very high quality. However, bubbles injected into the flasks by the pickling chemical dispensers, particularly the NaOH-NaI were a persistent problem throughout the cruise. Samples frequently sat for longer than 24 hours between collection and titration, during which time there was a strong tendency for bubbles to develop in the sample flasks.

Pre-cruise stable blank determinations took many runs to achieve, while post-cruise blanks were slightly offset to a higher value, likely due to degradation of the chemicals in the months since they were prepared. Standard determinations showed normal variation and expected values, but were probably underperformed in the effort to conserve chemicals. The new oxygen flasks' volumes were determined in August 2008, prior to shipment south. One flask, #439, appears to have been given an incorrect volume of 53ml, rather than the approximately140mL typical of the others. It was inadvertently used twice, once during station 2A, and once during station 160. There is no electronic data with which to compare the derived value for station 2A, but at station 160, a duplicate sample was collected from the same bottle. Using the oxygen content determined for the duplicate, and assuming zero error, the volume of bottle 439 would be 141.150 mL.

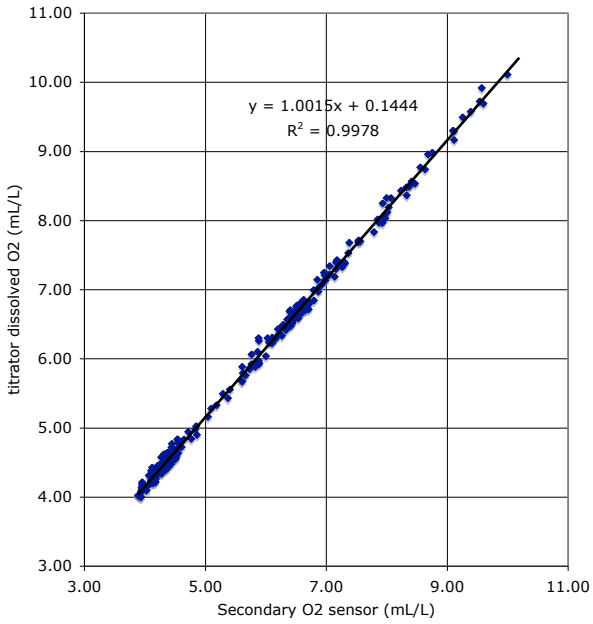

Figure 8: Titrated dissolved oxygen content versus Ox2 sensor values. Outliers (more than one standard deviation beyond the average for the outlier-free dataset) have been removed, and linear regression is shown on the chart.

The primary and secondary oxygen sensors on the CTD were in excellent agreement at the beginning of the cruise (casts 1-3 showed an average difference of 0.01 ± 0.01 mL/L at locations where bottles were tripped), then the primary sensor appears to have failed between casts three and four. The average difference between the sensors at bottle depths for casts 4-23 was 0.37 ± 0.13 mL/L. There was some reluctance to replace it, given the well-functioning secondary sensor, but following cast 24, the primary sensor was replaced. There appears to have been some slight degradation of the primary sensor over the remainder of the cruise, as evidenced by very slight increasing steps in the difference between the two sensors shown in figure 6. These steps appear to have occurred between casts 83-84, 103-105 (coinciding with the different sensor used during cast 104, noted in the CTD section of this report), and 125-126. Between casts 24 and 159, the average difference between the two sensors at bottle depths was 0.11 ± 0.06 mL/L. Cast 160 shows significantly different down and up cast values for both the primary and secondary dissolved oxygen sensors, and the secondary sensor appears to have experienced some significant distress at depth, perhaps because this was a 4600m station, the only one on which the CTD was lowered below 2000m. The sensor difference at bottle-closing depths during that cast averaged 0.31 ± 0.10 mL/L. Duplicate titrated values from 6 levels should be adequate to determine which of the four recorded profiles of dissolved oxygen content from this cast was correct.

The titrated values showed significant noise with respect to the primary dissolved O_2 sensor, but most were well-correlated with the secondary sensor, prior to cast 160, as shown in figure 7. Initial averages and standard deviations were calculated for the full dataset of titrated values, then 54 titrated values (including all samples from casts 42, 53, and 160) were rejected from the dataset due to their greater-than-average deviation from the mean offset. The large deviations between titrated and sensor values for the rejected samples were likely due to aging of the samples between sampling and titration. The average difference between the remaining titrated and same-depth secondary sensor values was -0.15 ± 0.07 mL/L for casts

through 159. The primary sensor used during most of the cruise (casts 24-160, skipping 104) was offset -0.25 ± 0.09 mL/L from the titrated values through cast 159. All of the O_2 sensors used during this cruise will be returned to SeaBird for calibration. In the interim, the secondary sensor looks to be the better choice for post cruise data processing, as shown in figure 8.

2.4 Salinity Determination (Autosal) and CTD temperature/conductivity Sensor behavior

Raul Guerrero and Ken Mankoff

In order to monitor the performance of the CTD conductivity sensors, 506 salinity samples were analyzed during the cruise using SN 61-670 Autosal salinometer. Only one salinometer was available onboard, and it performed within factory specifications. Laboratory room temperature control was excellent, remaining mostly between 0.2 and 1°C below the Autosal temperature setting of 24°C. Data from the Autosal was captured using the ACI 2000 hardware/software package. On each "run", an average of two boxes (48 samples collected over 10 to 12 stations) were measured by Raul Guerrero and Ken Mankoff. The standardization was performed at the beginning of each "run" using P149-Oct.2007 IAPSO standard seawater, and a control of drift was done at the end of the run, using a new vial from batch P149 from October 2007 or P148 (one year older). Differences in readings among these vials were not observed when run together. A total of 25 vials (18 P149 and 7 P148) were used on 11 runs. The Autosal was stable throughout the cruise and little or no restandardization was required between the runs (as may be seen in Table 3). Opening vials on runs 3 and 9 (stations 16 to 31 and 128 to 139 respectively) were standardized around 0.00010 CoRatio units down and on runs 4 and 10 the adjusted value were back up, indicating probably a bad vial on the former runs. The rosette salinity comparison to CTD salinities seems to show this variation, which in Sa units represents -0.0015, falling within the precision of the Autosal. Consequently, any shifts do to bad vials were not applied. Standardization readings throughout the cruise are shown in table 3.

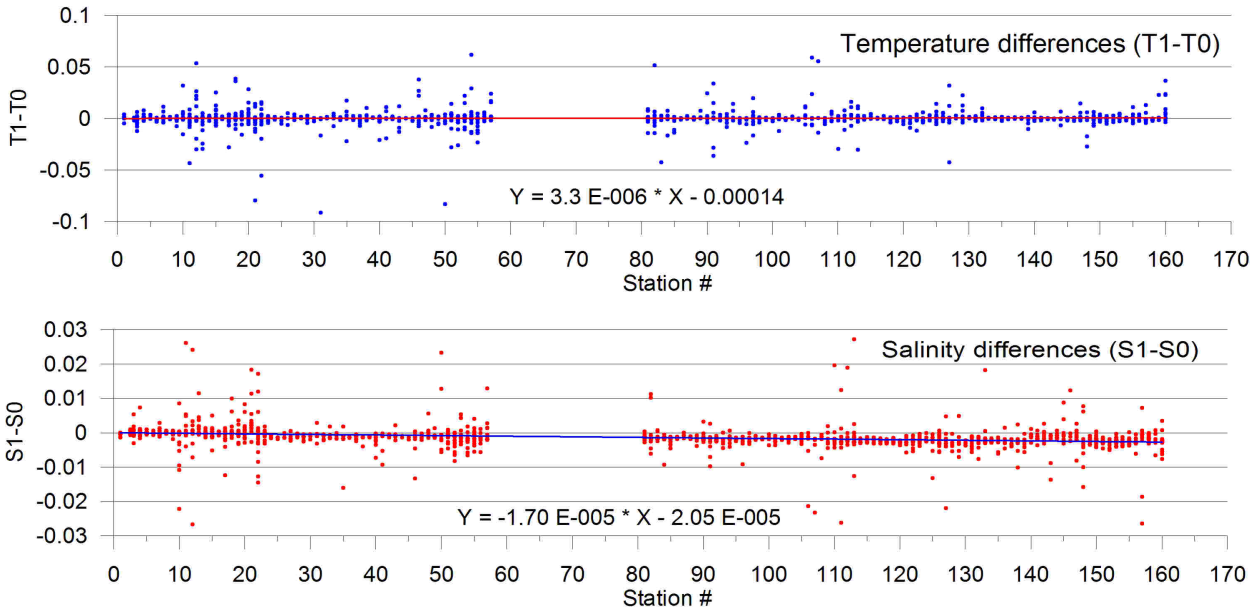

Figure 9: Temperature and Salinity differences between Primary and secondary CTD sensors (Sec. minus Pri.) versus Sta #.

In order to check functioning of the CTD and test water tightness of bottles, twenty samples were drawn from 1000 m depth on a test station performed early on the cruise (station 1). Even though depth reached was not ideal for inter-calibration, salinity values from all 20 bottles felt between -.007 and +.003 difference to CTD

Run	Test	1	2	3	4	5	6	7	8	9	10	11
Stby.	6088	6088	6086	6075	6085	6086	6088	6091	6088	6078	6089	6088
Stats.		1-5	6-15	16-31	32-55	56-91	92-101	102-117	118-127	128-139	140-152	153-160

Table 2: Salinometer "standby" reading throughout the cruise. Very good stability was observed between runs as little or no re-standardizing was needed.

Sa readings, with a mean error of -0.0004 for primary and -0.0001 for secondary and standard deviations of 0.0026 and 0.0025 respectively. Differences among primary and secondary (Sec-Pri) sensors throughout the cruise were found to be almost zero for temperature and a drift from 0 (at sta 1) to -.003 (at sta 160) for calculated salinity (see fig 9 and table 2)

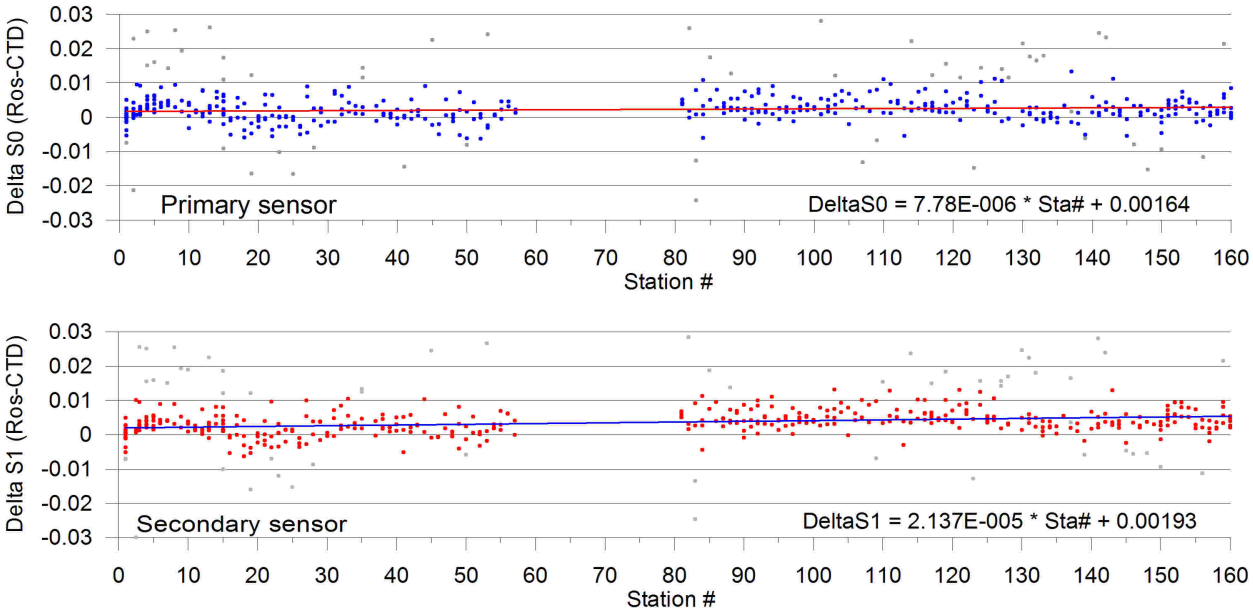

Figure 10: Salinity difference, DeltaS (rosette minus CTD), versus Station # for primary and secondary conductivity sensors. Grey points were considered outliers and discarded for the final error estimations.

Sensor	Liner fit vs sta#	Sta1	Sta160
Te	Y = 3.3 E-006 * X - 0.00014	0.0001	0.0007
Sa	Y = -1.70 E-005 * X - 2.05 E-005	0.0000	-0.0027

Table 3: Fits versus Station number of difference between Primary and Secondary sensors, for temperature and calculated salinity.

Errors in salinity resulting from the primary and secondary conductivity sensors were tracked throughout the 160 stations (Fig. 10). Salinity errors, denoted as DeltaS, are reported as the rosette salinity minus the CTD sensor salinity.

The drift, observed in fig 9, among CTD calculated salinity is mainly observed in the secondary sensor (fig 10). Primary sensor shows smaller slope with the same sign (growing with time).

Fig 11 shows DeltaS0 and DeltaS1 versus Pressure. It shows a lack of calibration point below 1200 m as most of the CTD profiles were in shallower waters (over 90%). There seems to be weak pressure dependence, not analyzed in this report. Larger spreading on deltas are located above 600 m depth.

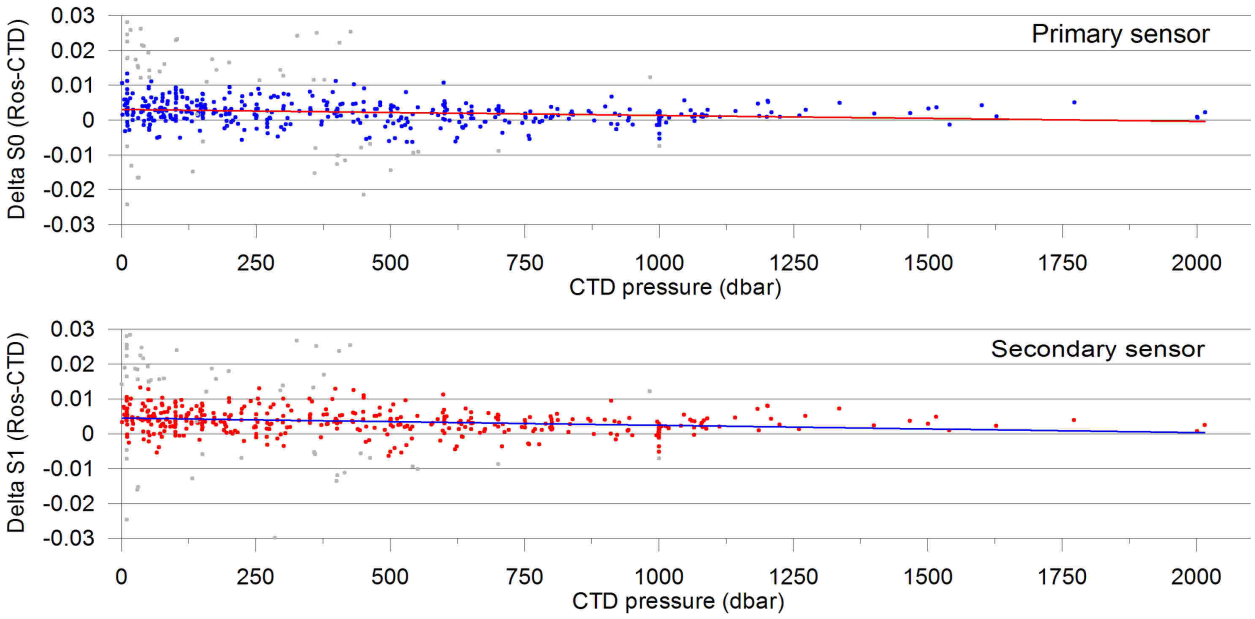

Figure 11: DeltaS versus CTD Pressure, for primary and secondary sensors showing a pressure dependency. This pressure effects were not considered in the preliminary sensor versus sta# error calculations. Grey color points were those considered outliers on the fittings versus Sta. #

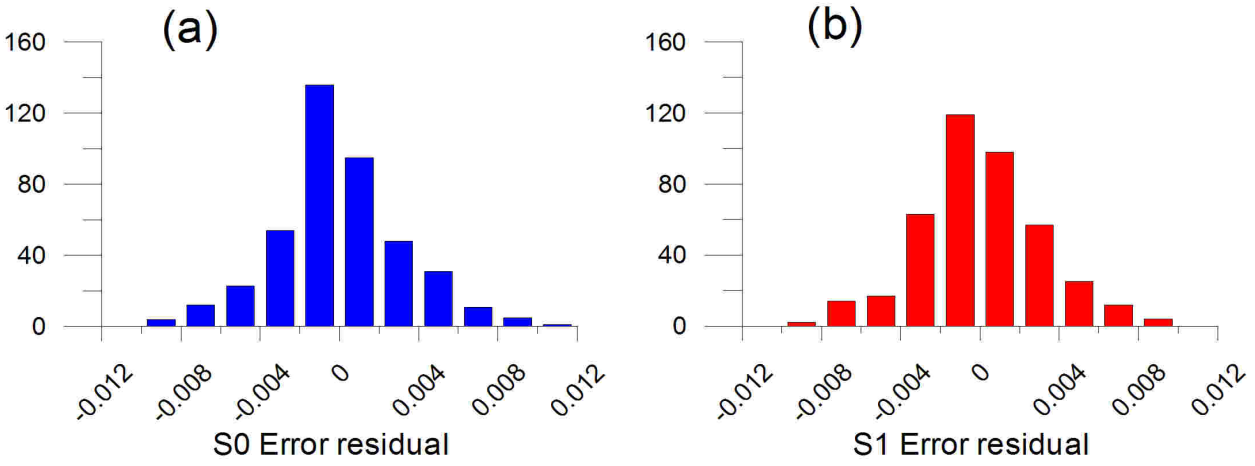

Figure 12: Residual histograms for: (a) primary sensor and (b) secondary sensor. The standard deviations reported in Table 3, for S0 and S1 residuals were 0.0032 and 0.0031, respectively.

In order to estimate the accuracy of the comparisons between RosSalts and CTDsalts two linear fits of DeltaS0 and DeltaS1 vs Sta# were performed. Fit1 allowed identifying and flagging outliers that were two standard deviations away from the fit. Fit2 was applied to the calculate residuals and gave a final overall accuracy of the preliminary errors. The fitting coefficients and the residual standard deviation for both sensors are presented in Table 4. This table also shows the number of RosSal values that felt over 2 standard deviations from the fits, considered not good for calibration.

Sensor	Fit	Res St Dev	# points	discarded	% used
Pri	DeltaS0 = 7.78E-006 * Sta# + 0.00164	0.0032	420	89	78.8
Sec	Y = 2.137E-005 * X + 0.00193	0.0031	411	86	79.1

Table 4: Fitting of DeltaS values as a function of Sta#, standard deviations of residuals are presented for primary and secondary sensor. Also the percentage of point used for the fittings.

The accuracy in these preliminary error estimations are reflected in the standard deviations of the residuals, being 0.0032 for primary and 0.0031 for secondary sensors respectively. The residual histograms are presented in fig. 12. These standard deviations should be lessreduce if an adjustment of the error is previously performed as function of Pressure.

Errors reported here on salinity have been estimated with the only objective being the evaluation of the behavior of the Conductivity sensors throughout the cruise. Most points marked here as outliers can probably be related to niskin leakage and/or contamination, and unstable layers not suitable for calibration.

Associated Bottle Data Files A Microsoft Excel spreadsheet file was generated with bottle information coming from the rosette niskin measurements performed onboard (Salinity and Oxygen) and from CTD instruments at the corresponding niskin firing levels. CTD instrument values are extracted by the SBE software modules "datcnv" and "rossum", which average over 2 seconds or 48 scans around the tripping of the niskin. An Excel file, named 'Bottle_NBP0901.xls' (spread sheet 'nbp0901001.btl') contains the integrated bottle information. All rosette salinities (SaRos) and corresponding error calculations have been included in the bottle files (columns Y to AM). Values with a residual larger than 2 standard deviations from the fits are labeled 'outliers'. Other associated bottle files are:

- NBP0901001.bl thru NBP0901160.bl are output bottle files from SBE data processing.
- NBP0901A thru NBP0901K.dat are ACI 2000 software output files from Autosal runs (Autosal folder)
- NBP0901A thru NBP0901K.xls are excel files used to average salt readings (Bottle folder)
- Salbottles.xls is an excel file that compiles all the final salts by run.

Note: CTD salinity entries for primary sensor on station 2 were punched in from the CTD log sheet. Data was not archived on this station (see CTD report) but salinity bottles were taken and measured.

3 Autosub III Operations

Adrian Jenkins (BAS), Pierre Dutrieux (BAS), Steve McPhail (NOCS), James Perrett (NOCS), Andy Webb (NOCS), Dave White (NOCS)

3.1 Introduction

The UK component of NBP0901 was funded by the Natural Environment Research Council (NERC) and was undertaken by personnel from the British Antarctic Survey (BAS) and the National Oceanography

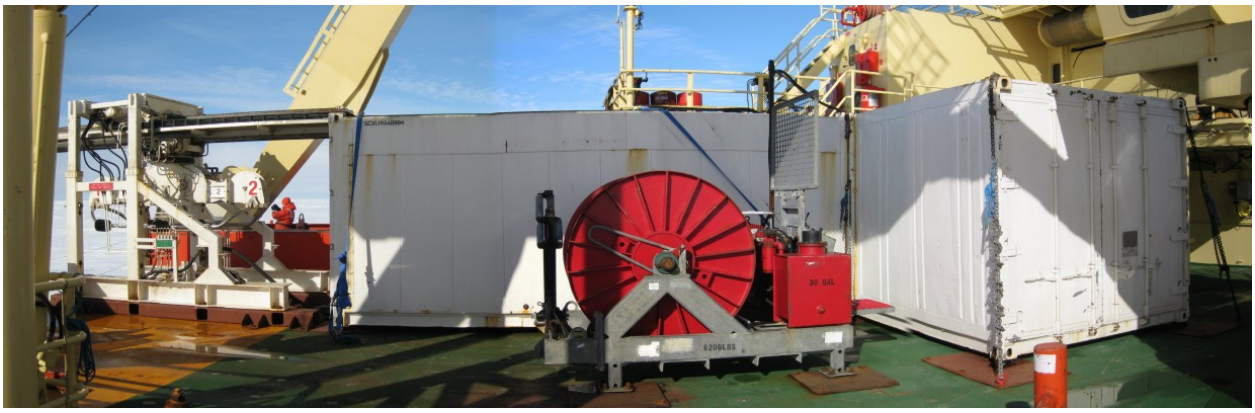

Figure 13: Side view of the Autosub containers.

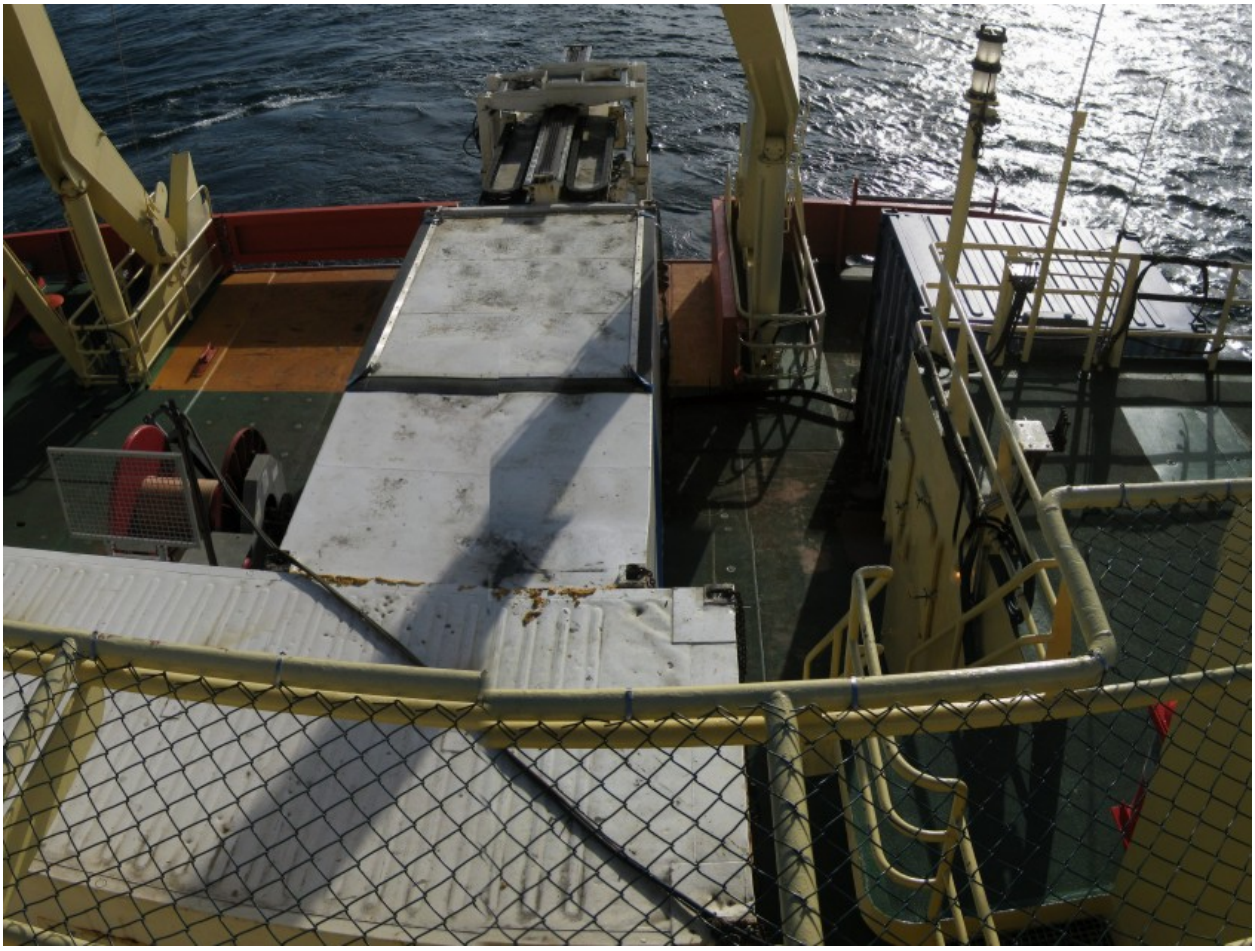

Figure 14: Plan view of Autosub containers on the N B Palmer Aft deck.

Centre, Southampton (NOCS). The work involved the deployment of NERC's autonomous underwater vehicle (Autosub-III) on six missions beneath the floating extension of Pine Island Glacier (PIG), to study how warm Circumpolar Deep Water (CDW) gets beneath the glacier and how it determines the rate at which the glacier melts. The specific aims of the project were to: map the seabed beneath the glacier; map the underside of the glacier; and determine where and how heat is transferred from the inflowing CDW to the outflowing

ice-ocean boundary layer. To do this Autosub-III was equipped with the following instrumentation: Seabird 9+ CTD, with dual conductivity and temperature sensors plus a SBE43 dissolved oxygen sensor and Wetlabs transmissometer; Simrad EM2000 multi-beam echosounder; upward-looking RDI 300 kHz ADCP; downward-looking RDI 150 kHz ADCP. Unusually light sea ice conditions allowed the ship to access Pine Island Bay during the early stages of the cruise and provide the perfect conditions for autosub deployment. A total of eight missions, including two test missions in open water and six science missions beneath the glacier were run during the two-week period from 17th to 30th January 2009. Total track length was 887 km (taking 167 hours) of which 510 km (taking 94 hours) were beneath the glacier.

Figure 15: Acoustic fish being deployed from starboard 'A' frame.

3.2 Preparation and Mobilisation in Punta Arenas

Autosub mobilisation began in Punta Arenas in December 08 prior to cruise NBP0901. The Autosub gantry places very large vertical deck loads and required a custom made deck/gantry interface plate, designed at NOCS but constructed in Punta, to reduce the loads to an acceptable level. The launch and recovery gantry was bolted to the deck matrix via the adaptor plate. The container/garage assembly was secured in place and the Autosub vehicle secured within the garage container set up.

We had problems with some of our wooden equipment not meeting Chilean requirements for heat treatment. Our acoustic fish bases, weights box, and railway sleepers (used for blocking up the Autosub chocks) were destroyed, the replacements being made from locally sourced wood.

Following discussion with Raytheon employees the aft garage roof was lowered and container doors refitted for the crossing to the Amundsen Sea (this turned out to be essential, since the aft deck of the Palmer becomes awash to a depth of 0.5 m, even in moderate seas).

Figure 16: Autosub being fended off.

The deployment and recovery gantry for Autosub was run from our own hydraulic pump (HPU) mounted in a 10 foot container, mounted adjacent to the main containers on the port quarter. This was powered from the ship's 480VAC 60Hz three phase power, providing up to 100 Amps, with an earth connected to the ship's earth. The two main containers were joined to make the garage and workshop with a fabric roller door and heating to keep the vehicle batteries warm. The workshop containers were supplied with 208VAC three phase, up to 60A, with a neutral and an earth.

Installation of acoustic equipment into the aft winch control room was completed, the mission control computers were set up in the main dry lab and aerial systems were installed.

On arrival at Pine Island Bay the aft container was reconfigured for Autosub operations. Figures 13 & 14 show views of the gantry and Autosub's purpose-made containers on the aft deck.

3.3 Acoustic operations

Autosub carries three independent acoustic communications devices, in addition to the acoustic measuring devices.

Emergency beacon

The emergency beacon transmits a 4.5 kHz narrow-band chirp to communicate over a long range. It was used on all missions to track the sub on its outward leg under the glacier. The transducer is deployed by

Figure 17: Using small boat for recovery.

hand, via a sheave mounted on the ship's rail, to a depth of about 80m (100m of cable, from the exit point of the work space). The deck unit and controlling laptop (Toshiba) were housed in the aft control cabin. The laptop was used to run the NOCS "beaconview" program. Initial electrical noise problems were traced to a fault in the sea cable producing a ground loop fault. After repair (see fault log) good ranges were obtained, limited only by the acoustic noise from the ship.

LinkQuest digital telemetry system

Autosub carries a LinkQuest Tracklink modem and transponder, which is used to track and command the sub when underwater, and to receive a limited subset of digital data. The LinkQuest worked well at ranges of up to 2-3km, although the tracking display, which was repeated on a monitor on the bridge, was only available in head-up mode.

ORE LXT acoustic transponder

This transponder (also known as the "dumb" transponder) is used for tracking, as a backup for the LinkQuest. The LXT worked well, tracking the sub to a similar range as the LinkQuest.

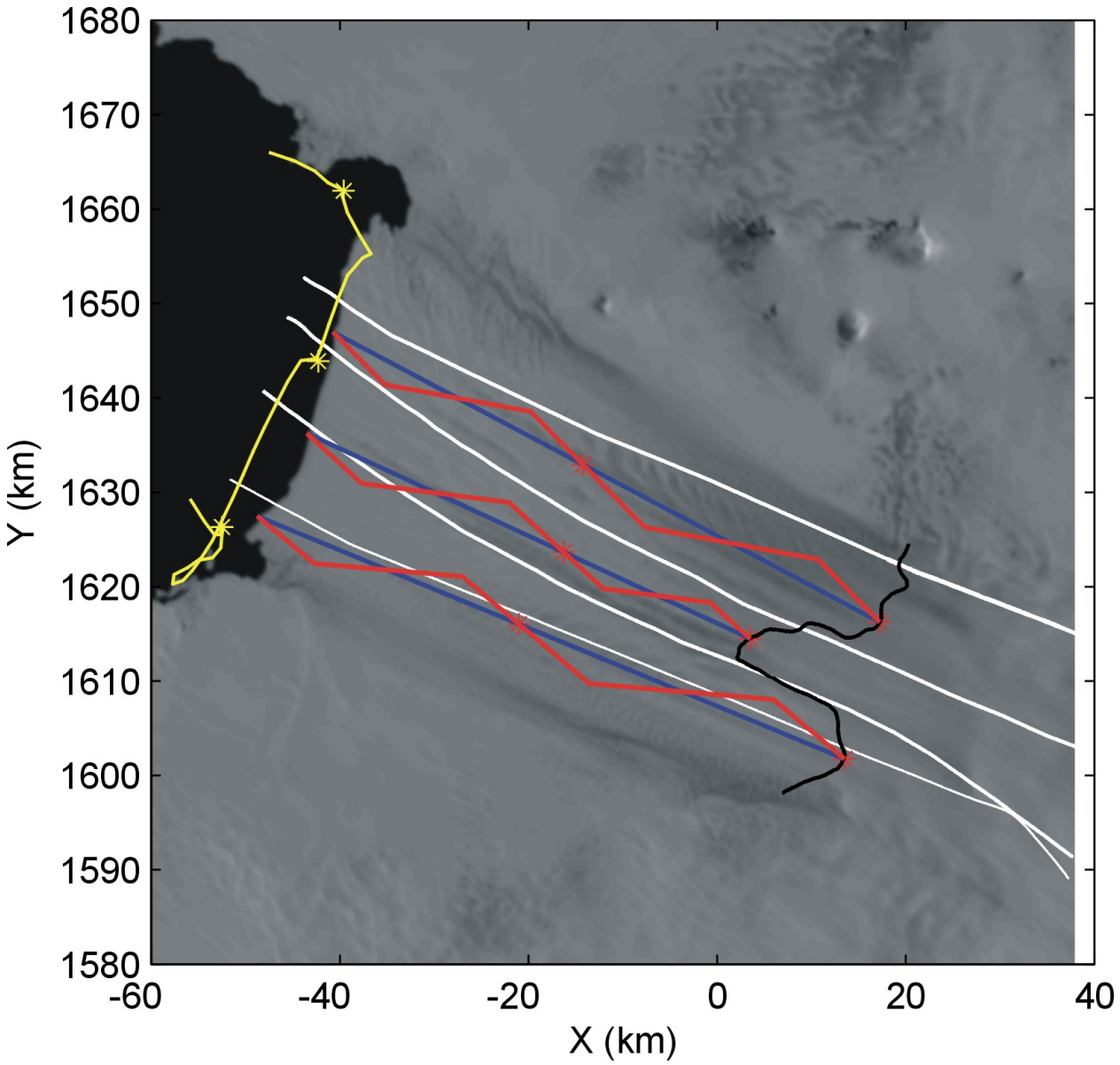

Figure 18: Planned mission tracks beneath PIG, with inbound legs shown in blue and outbound in red. Red stars indicate the turning points for both short and long missions. The white lines indicate the four longitudinal radar profiles that were the main source of ice draft estimates. The 1996 grounding line is shown in black, and the NBP9402 cruise track in yellow. Axes are labelled with the projection coordinates of the image. The standard parallel for this projection is 70^oS, so 1 km on the image represents 1.0135 km on the ground.

Acoustic Tow Fish

With the exception of the emergency beacon receiver array, all the ship-borne acoustic transducers are mounted on the tow fish. This is a 380 kg towed body that was deployed to a depth of 12m from the starboard A-frame (Figure 15). It was suspended using the 5/16" wire on the lower waterfall winch (SWL 3 tons), the fish's own cable being paid out by hand and made fast once the fish was at depth.

From our experience, the Nathaniel B. Palmer appears to be an acoustically noisy ship. Even with all the

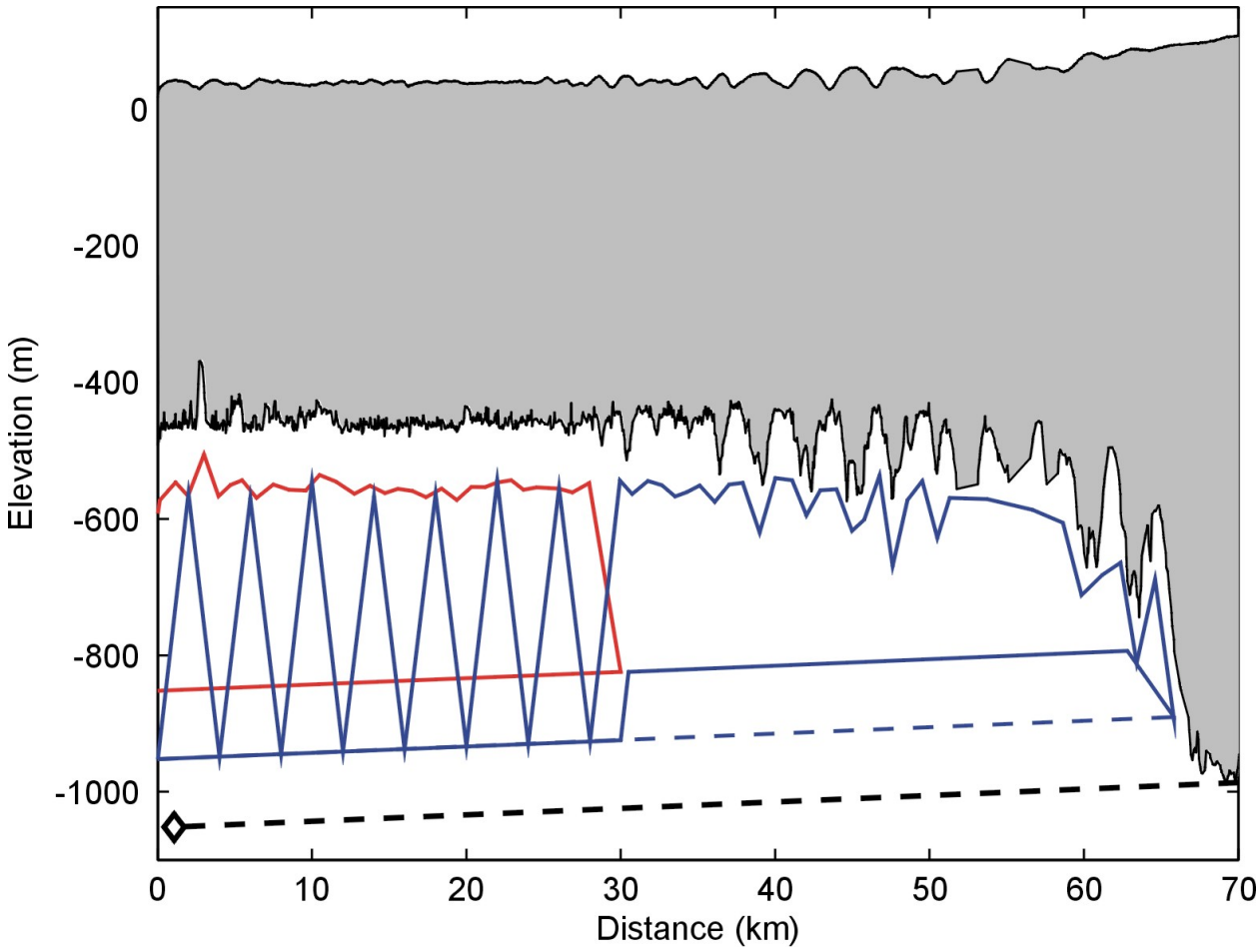

Figure 19: Planned mission profiles beneath PIG, with short missions shown in red and long missions in blue. The ice thickness profile is taken from the southernmost radar flightline of the four shown in Figure 6, starting near X=50 km, Y=1630 km. The bold, dashed line joins the two points of known seabed depth at the ice front and the grounding line.

ship's sonars switched off, ranges on the Autosub LinkQuest rarely exceeded 3 km, or less than half that achieved on the RRS *Discovery*, RRS *James Cook*, and the MV *Terschelling*. The emergency beacon was clearly audible to a range of 10km, and could be detected intermittently in quiet weather (particularly with the ships propulsion system disengaged) up to 20km away.

3.4 Recovery operations

On the first recovery we kept with the method we had developed over the preceding years. This requires a small float, jettisoned from Autosub, to be grappled. The float is connected by a light line to heavy lift lines, held within the Autosub vehicle, which are pulled aboard and coupled to the Autosub gantry. Autosub is then winched aboard.

R/V Nathaniel B Palmer is a twin screw, direct drive, fixed RPM, variable pitch ice breaker. During the first recovery it was found that the cut away counter and the huge suction generated from the main propellers would draw the Autosub under the stern. This was only averted by the fact that the ship has a very low freeboard enabling the use of boat hooks (Figure 16).

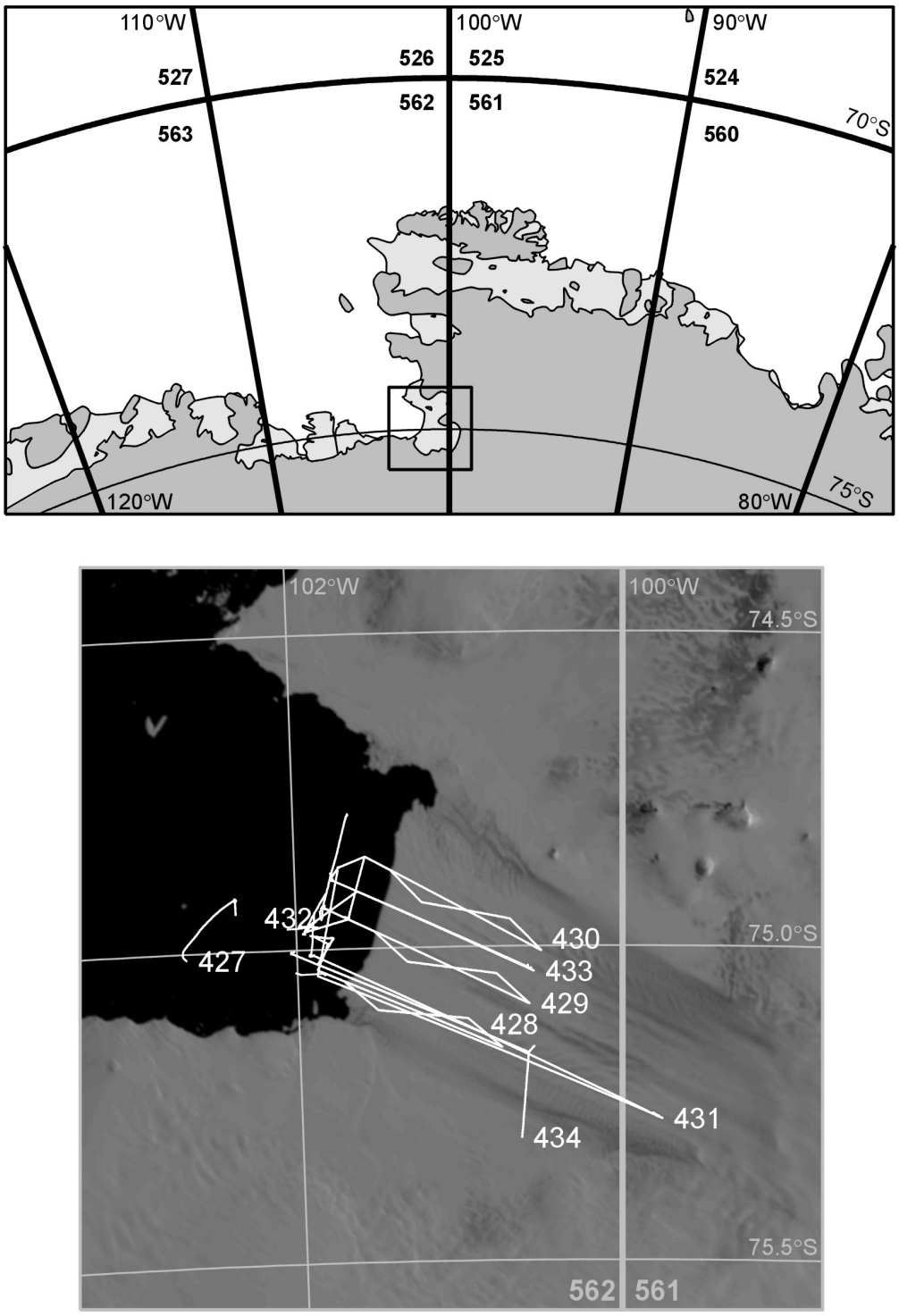

Figure 20: Autosub-III missions completed in PIB during NBP0901. Missions 427 and 432 were test missions run at the start of operations and following repairs to the damage sustained on mission 431.

A meeting was called, and after discussion with officers, ship technicians and the Autosub team, a decision was made to use a method the Autosub team had not used in the past. The method required the use of a small boat to act as a drogue and to keep the Autosub vehicle under control while the recovery operation

was under way (Figure 17). This method was refined over the next couple of recoveries, with the use of the Autosub recovery (Jack) float being abandoned in favour of a direct pick up by the small boat. It became a practical, slick and more importantly safe method of recovery. The small boat was used in winds of up to 25kts with a wave height of about 0.6m (2 feet). The use of a small boat would limit the operational window, but with the work site being within a bay and sea being damped by ice, sea conditions were never a problem.

3.5 Autosub missions

Outline plans for six science missions beneath the ice shelf, including three that penetrated 30 km into the outer cavity and three that penetrated the full 60 km to the grounding line, had been approved by NOCS prior to the cruise. Final planning of waypoints and profiles was guided by ice thickness data, from airborne radar sounding, the bulk of which was collected in early 2006, and seabed soundings from NBP0402, refined with multi-beam data collected during the course of NBP0901. We also made extensive use of a Modis visible image (Figure 18), collected in late December 2008. Where the ice is grounded, the combination of ice thickness and surface elevation from the radar observations gives the depth of the bed. We therefore had knowledge of the seabed depth along the grounding line at the inner edge of the cavity. Depths there are similar to those at the ice front (800 to 1000 m) so we assumed that the bed would be fairly flat.

Planned tracks and profiles for the six missions are shown in Figures 18 and 19. The three shorter missions were intended to track the seabed at 200 m altitude on the way to the turning point, approximately 30 km from the ice front, then ascend to track the ice base at 100 m clearance on the way out. A global minimum depth of 500 m was set to prevent Autosub tracking up into hollows in the ice shelf base, while the zig-zag course on the way out was designed to sample a wider range of basal features with the multi-beam echo-sounder, which was oriented up for these missions. The original plan was then to run three further missions that extended these tracks by approximately 30 km into cavity. It was intended that the actual turning point would be determined by Autosub's detection of minimum headroom, set at approximately 200 m of water (i.e. about 100 m clearance above and below). For the inbound leg of the longer missions Autosub would track the seabed at 100 m altitude, then track the ice base at 100 m clearance, so obtaining multi-beam images of the ice base, as far as the 30 km point reached on the shorter missions. From this point out the sub would undulate between bounds set by minimum clearance of the ice base and seabed or global minimum and maximum depths, whichever were encountered first.

The three shorter missions (M428-430) were successfully completed as above. Further discussions about the longer missions led to the abandonment of the zig-zag course for the first part of the return leg, as far as the point reached on the shorter missions. It was felt unwise to have multiple waypoints programmed for the inner part of the cavity, where we were uncertain about the turning point. It was quite possible that the sub would detect minimum headroom at a point further out than one of these waypoints and then attempt for a second time to go further into the cavity to reach its next waypoint. Finding the route blocked would then trigger a mission abort.

The first of the longer missions (M431) showed the dangers of tracking an irregular ice base without a minimum depth protection (the global minimum of 500 m, required for the outer part of the cavity, gave no protection on the inner part), as the sub followed a course similar to the hypothetical one in Figure 16. The triggering of multiple collision avoidances (one of which was not actually avoided) led to the mission being aborted, and a rethink for the final two missions. For these we planned only seabed tracking with an altitude of 100 m in the inner cavity, and since we could not image the ice shelf base, switched the orientation of the multi-beam echo-sounder so that we could gather seabed imagery. The fifth mission (M433) was also aborted when minimum headroom was detected earlier in the mission than we had anticipated and the sub turned to find its path to the next waypoint blocked by an ice keel. The sixth and final mission (M434) track was then further amended to access the inner cavity by a known safe route, then explore to the south and the north (Figure 17). Beyond the known safe area we planned only bottom tracking, although we ran at two altitudes (100 and 200 m) to the south, where we knew that the 500 m minimum depth would keep

the sub safe from the major irregularities of the ice base. This mission went according to plan, except that the sub detected minimum headroom very early on the northern leg. From the start of the straight leg back to the ice front Autosub followed an undulating course, collecting data on the water column between the ice base and seabed.

Mission tracks, as executed are shown in Figure 17 and a summary of each is given in Table 5. Included here are the test missions, run at the start of operations and following the repairs necessitated by the collision on M431, and the preliminary open water tracks run at the start of each mission as part of the risk mitigation strategy.

#	Start time, pos, duration, km	Plan	Comments and Faults
427	19/1/2009 1341 GMT S: 74:59.48 W: 101:48.23 6.8 hrs 38 km.	Test Mission to 850 m depth.	None critical. Motor appeared to stop and restart intermittently - fixed for M428. T1 on CTD appeared intermittent - connectors cleaned and cable replaced for M428. Hotel Ground Fault reading high - investigation showed that source was related to the grounded CTD chassis but no fault found.
428	19/1/2009 2035 GMT S: 74:59.48 W: 101:48.23 18.4 hrs 101 km	Sub Ice shelf Mission. Started with short (2 hr) test mission, followed by data retrieval and checking. Then AUV run under the ice shelf. 30 km at 200 m const altitude, then turn and 100 m up altitude.	Mission completed as planned. Good multibeam, CTD, O2, & Transmission data. Poor ADCP up profiling range noted.
429	23/1/2009 1544 GMT S: 74 55.9 W: 101 50.7 1 + 3+ 17 hr 113 km	2nd run under the PIG. 30 km in. 200 m altitude in, and 100 m distance off the ice shelf coming out.	First attempt at mission was unsuccessful because shortly after vehicle dived the down ADCP misinterpreted a scattering layer at approximately 500m as the seabed, causing the vehicle to go to a safe waypoint due to insufficient depth. To overcome this, we reduced the maximum ADCP range to 440m. Second attempt was unsuccessful as we were unable to communicate acoustically with the AUV due to a faulty crimp joint in the acoustic fish cable. Final mission was successful and completed as planned.
430	23/1/2009 1544 S: 74:57.18 W: 101:40.77 19 hr 107 km	3rd under ice shelf mission. 30 km in. 200 m altitude in, and 100 m distance off the ice shelf coming out.	Battery changed before mission. Mission completed as planned.
431	24/1/2009 1345 GMT S: 74:52.21 W: 101:43.86 34.5 hr 183 km	4th under ice shelf mission for Palmer 0901. First 60 km mission. Run 60km in at 100m altitude, turn when got to far waypoint or collision avoided and then run back at 120m up altitude to 30 km point, then profile for the remainder.	Mission terminated early due to the emergency exception being called (failed collision avoidance). Consequently, the AUV carried out no profiling on the way out. The vehicle had, however reached 55km under the ice shelf. Vehicle nose section damaged by collision with ice. Port CTD plumbing damaged. Linkquest transducer bulkhead connector damaged (the telemetry system was working properly on recovery).

continued on next page

continued from previous page

#	Start time, pos, duration, km	Plan	Comments and Faults
432	27/1/2009 2212 GMT S: 74:57.71 W: 101:55.26 3.4 hrs 18 km	EM2000 set looking downwards. 4 hour test mission.	Battery changed before mission. No problems noted.
433	28/1/2009 0432 GMT S: 74:57.71 W: 101:55.26 30.5 hrs 160km	Approximately 55km under ice shelf at 100 m altitude. Turn on minimum headroom setting. Profile out the last 30 km. EM2000 looking down.	Vehicle turned around due to limited headroom as expected, but further limited headroom situations on the return caused collision avoidance behaviour leading to a run back to the safe waypoint. Hence no profiling was carried out.
434	30/1/2009 0955 GMT S: 75:0.29 W: 102:2.08 33.7 hrs 167 km	45km under the ice, turn south for 10km at 200m altitude then return to turn point at 100m altitude, then go north for 10km at 100m altitude, return to turn point at 200m then return to safe way point profiling from 500 to 900m depth.	Battery changed before mission. Completed successfully, although the vehicle turned back early during its northern leg after detecting a deep ice keel.

Table 5: Summary of All Autosub-III Missions on N B Palmer 0901

4 Moorings

Stan Jacobs, Scott Worrilow, and Raul Guerrero

Three types of long-term mooring deployments were carried out during 0901, along with two mooring retrievals. Most of the O-274 moorings (14) were extended versions of the simple 'Bottom Landers' set out by R Guerrero and F Nitsche during an early 2006 Polarstern cruise, in conjunction with our previous Amundsen Sea project. Five of those were recovered during NBP07-02 and the 6th site was revisited on this cruise. Its release did not respond and dragging was not considered feasible because of that silence, substantial sea ice cover and an iceberg over the mooring site. Examples of the 14 new moorings are shown in Fig 21. The majority of these were set near ice shelf fronts in the southern Amundsen and near the continental shelf break (Fig 22) in water depths ranging from ∼600 to 1260 m (Table 6). Mooring heights above bottom were limited by the need to stay below deep iceberg drafts, which we estimated to be ∼400 m.

These bottom-anchored moorings were all deployed anchor first, as several were located in areas of >30% sea ice cover and/or where the bottom topography was rough or sloping. Each line included at least one Nortek Aquadopp or Alec AEM USB current meter and Seabird Microcat (SBE-37), plus two or more Seabird temperature sensors (SBE-39). Single ORE releases, shallow CARTs or deep 8242s, were rigged above 100-200 lb concrete block bottom weights. Nine inch and 12" trawl floats and a Novatech beacon at the top completed each mooring, with all instruments mounted on 5/16" Samson Tenex line. Deployments were engineered by S Worrilow and R Guerrero, assisted by RSP MTs and others, including ECO personnel

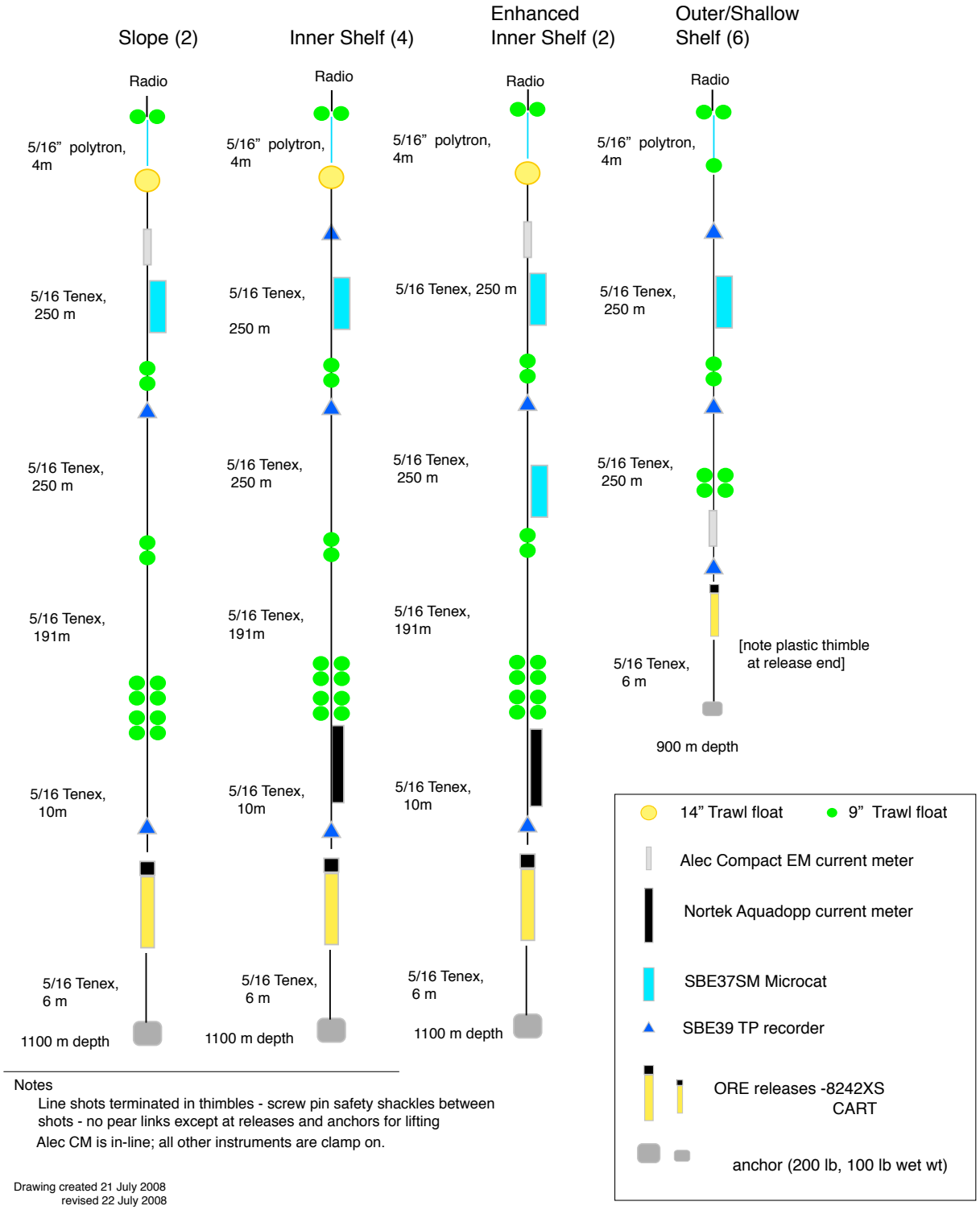

Figure 21: B Huber mooring schematics for the 14-site 'BSR' array deployed on the Amundsen Sea continental shelf and slope during NBP09-01.

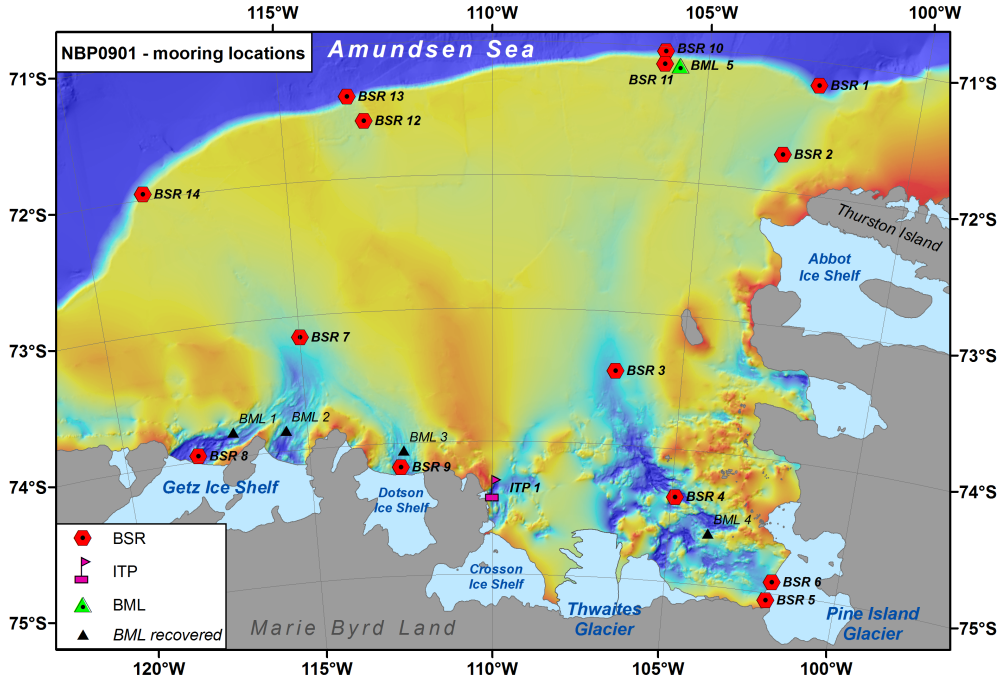

Figure 22: F Nitsche site map showing the locations of BSR and ITP moorings set from the NBP in early 2009, and BML moorings set from Polarstern in early 2006. BML 1-4 were recovered in early 2007.

Figure 23: ITP mooring deployment photo showing tripod, ITP, and ice hole. Image © Maria Stenzel, 2009

at the helm.

The high iceberg production and retention rates in the eastern Amundsen restricts the use of this type of mooring to the study of deep water variability, since much of the meltwater produced by the ice shelves and icebergs appears to be in the upper 400m. Most instruments were located high on the moorings in an attempt to capture changes in the lower pycnocline and deep water volume on the shelf. To monitor change in the upper water column requires a different approach, and led this year to the deployment of an 'Ice Tethered Profiler' of the type recently used with considerable success by Toole, Timmermans and Krishfield in the Arctic. Indeed, the ITP we used is the one they first deployed in the Arctic and was refurbished by that WHOI group for this project.

While Arctic ITPs drift with the pack there and are rarely recovered, a drifting ITP on the Amundsen continental shelf is likely to ground on one of its many shoals. We thus sought fast ice that seemed likely to stay fast for at least a year, in the greater Pine Island Bay region where both the deep water and shallower layers could be monitored over time. Options were limited during 0901, the overall ice cover being on the light side. The location we settled on (Table 6) was about 6 km south of a fast ice edge that extended east from Bear Peninsula (Island). An ice edge has been encountered in that location twice previously, but it was much farther south in 2006 and 2007. Both the ice and snow cover at the ITP site were less than anticipated, but we delayed deployment to as late in the cruise as possible, and were beginning to see new ice formation a few days later. The work went smoothly, in good weather and less time than planned, with the instrument set to profile daily over the upper 750 m of a water column >1300 m-deep (Fig. 23). The ITP did not initially 'call home' as soon as expected, occasioning a return trip to the site, but by the time it was reached good-quality profiles were being received at the WHOI end of its Iridium link. Some mid-profile degradation in salinity has since occurred, perhaps due to biofouling of the pump (M-L Timmermans, pc).

The third mooring type consisted of a McLane Moored Profiler (MMP) and ASL Ice Profiler (AIP) anchored in 4600 m well northwest of the Amundsen continental shelf (66 27 S, 129 28.2 W) for project O-261. Although the weather was deteriorating at the time of deployment, the work went well on an anchor-last operation. Unfortunately, the top buoy, meant to end up at 75 m, appeared at the surface during a subsequent triangulation run. This necessitated recovery, since its AIP would not function there and its buoy would likely work the wire and profiler to excess and then be enveloped in the sea ice. Release and recovery were successful, but its line came up tangled and apparently stretched (the latter perhaps the underlying problem), and the lack of spare line precluded redeployment.

Mooring #	Latitude S	Longitude W	Depth (m)	Date y/m/d	CTD #
BSR 1	71 10.539	102 24.498	1094	9/1/13	5
BSR 2	71 43.351	103 03.147	744	9/1/14	7
BSR 3	73 26.767	106 44.561	902	9/1/16	11
BSR 4	74 21.637	104 53.346	1259	9/1/16	13
BSR 5	75 03.356	101 59.024	800	9/1/22	47
BSR 6	74 54.861	101 52.695	950	9/1/22	48
BSR 7	73 09.657	114 59.187	750	9/2/03	113
BSR 8	73 57.744	118 01.087	1242	9/2/03	117
BSR 9	74 11.060	112 31.014	1048	9/2/05	125
BSR 10	71 02.159	105 59.948	1047	9/2/10	134
BSR 11	71 07.847	106 00.114	520	9/2/10	135
BSR 12	71 34.565	113 02.508	611	9/2/12	142
BSR 13	71 23.276	113 23.961	1073	9/2/12	144
BSR 14	71 57.537	118 27.781	602	9/2/15	157
ITP 1	74 21.265	109 58.285	1340	9/2/05	126
BML 5	71 08.21	105 39.97	540	6/3/18	302-1

Table 6: Coordinates, water depths, dates and accompanying CTD stations for most of the moorings shown in Fig. 22.

5 Sea Ice Studies

Ted Maksym, Sharon Stammerjohn

5.1 Motivation and Objectives

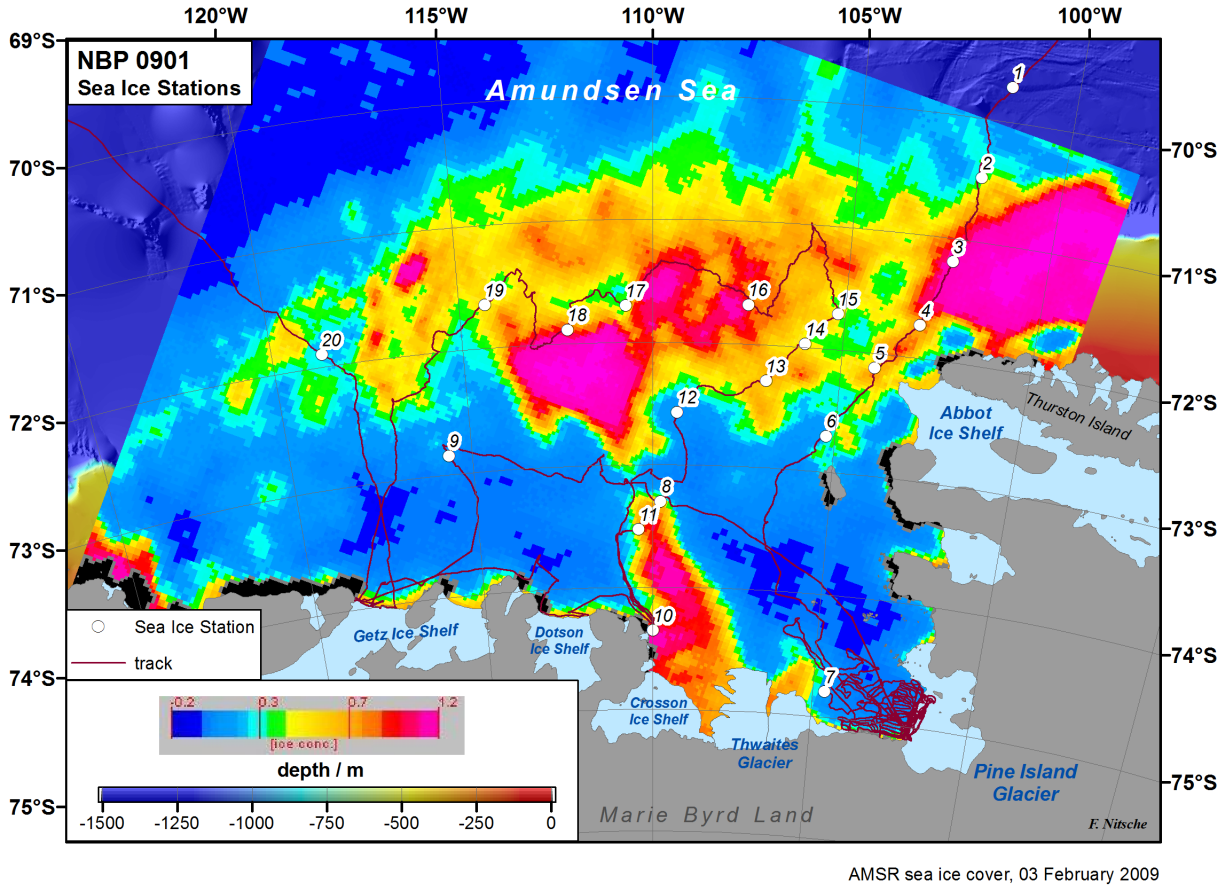

Figure 24: Station map showing locations of 20 sea ice stations. An AMSR-E image of sea ice concentration from February 3 is shown for context. Note, the southbound leg (made during Jan 10 to 15) followed a low sea ice concentration zone, which by February 3 became covered by sea ice advected in from north of the Thurston Island area. Also, the last sea ice station (#20) was covered by higher concentration sea ice than is pictured for February 3. (Map by Frank Nitsche.)

Circumpolar sea ice extent in the Southern Ocean has modestly increased over the satellite observational period (1970s to present). Lurking behind that circumpolar average however are large increases in sea ice extent in the Ross Sea sector, where the ice season has lengthened by almost 2 months over 1979-2007. In contrast, sea ice extent in the AP-Bellinghausen-Amundsen Sea region has decreased, and at a faster rate, as revealed by a shortening of the sea ice season by up to 3 months, though over an ocean area that is little more than half the size of the Ross Sea sector.

In the Amundsen Sea the largest area of sea ice change lies offshore of the shelf break, centered on 69-70^{o}S, 107-110^{o}W, where sea ice duration became 83 days shorter over 1979-2007 (i.e., similar to sea ice changes upstream in the southern Bellingshausen). Smaller areas of change have occurred in Pine Island Bay (34 days shorter) and in the vicinity of the Dotson (91 days shorter) and Getz (63 days shorter) Ice Shelves.

Seasonal sea ice changes in the Amundsen Sea appear to be more pronounced in spring, when the wind-driven sea ice retreat can be up to 80 days earlier (whereas changes in the Bellingshausen Sea are more pronounced in autumn). An early retreat in the Amundsen Sea is usually followed by a later advance, though the magnitude of the advance anomaly is usually half that of the retreat anomaly (e.g. 40 versus 80 days, respectively).

Within this backdrop of Southern Ocean sea ice change, little is known about the snow and sea ice thickness distributions, the processes that control it, or the role that snow and summer surface melt processes play in the persistence of the sea ice cover. This is particularly true in the Amundsen and western Bellingshausen Seas which have until now been largely unsampled. Yet this region has some of the highest snow accumulation rates in the Antarctic. This deep snow cover plays a complex role in the sea ice mass balance through melt and refreezing and conversion of snow to ice through sea water flooding. These processes have implications for how summer sea ice will respond to climate change, play a vital role in the structuring of sea ice ecosystems in porous gap layers in the ice, and complicate satellite retrievals of snow and ice thickness. A major aim of sea ice activities on NBP0901 was to better understand how these processes control sea ice mass balance.

Within this context, sea ice studies on NBP0901 focused on assessing the properties of summer sea ice in the Amundsen Sea (extent, thickness, growth/melt history, snow fraction, deformation and drift). Below in Section 5.2 we give an overview of our sampling approach and discuss general findings. In Section 5.3 we give a more detailed description of methodology of our three main activities - shipboard observations of ice conditions, a sea ice sampling program, and deployment of instrumentation in the ice. In this section, we also describe the various caveats of our approach, with emphasis on how it might be modified and improved for future missions.

5.2 Overview of Sampling Approach and Initial Findings

During NBP0901 we made 197 underway hourly observations during approximately 13 full days in sea ice, held 20 sea ice stations and collected 92 meters of sea ice cores. Our stations and samples were distributed along north-south and east-west transects in the region of the summer pack ice (Figure 24). The total amount of ice core retrieved for structural analysis alone exceeded 52 m - comparable to totals obtained on dedicated sea ice cruises, but a record relative to total length of the sea ice team (3.6m). This is of particular significance, as sea ice physical properties have not been previously examined here. In all, the number of summer sea ice cores taken in the data-sparse Amundsen Sea has been more than doubled. We also deployed 3 sea ice mass balance buoys which continue to dutifully phone home to tell us where they are and that they're doing fine. These will for the first time allow continuous monitoring of multiyear snow and sea ice surface processes throughout the year. Combined with structural information from the ice cores and process modelling, these data will help us understand the role these processes play in evolution of the sea ice cover and how these processes might modulate the response of sea ice to climate variability.

Mean sea ice thickness of cores collected was 159 cm and ranged from 29 to 469 cm, while mean sea ice thickness of the level ice observed while underway was 164 cm. However, both approaches (discrete sea ice sampling and underway observations) were biased towards thinner ice, e.g. the ice team avoided sampling ridges while the ship avoided navigating in heavy pack ice (e.g. Figure 25). (These caveats are discussed more fully in Section 5.3.) We note however that the majority of floes sampled were flooded and deformed, and 9% of the surface ice area observed underway was ridged (yielding an estimated ridged thickness of 228 cm).

By week 6 (Feb 10 to 16), signs of autumn came with the appearance of grease ice and nilas within the ice pack. Ice that survived the summer was either thick multiyear ice advected from the western Bellingshausen north of Thurston Island, or heavily deformed first year ice that generally predominated the summer pack ice. Overall, the modest thickness of level ice (averaging less than two meters) was consistent with the very low ice extent that occurred in the summer of 2007.

Overall, there are two features which appear to play an important role in the persistence of summer sea ice

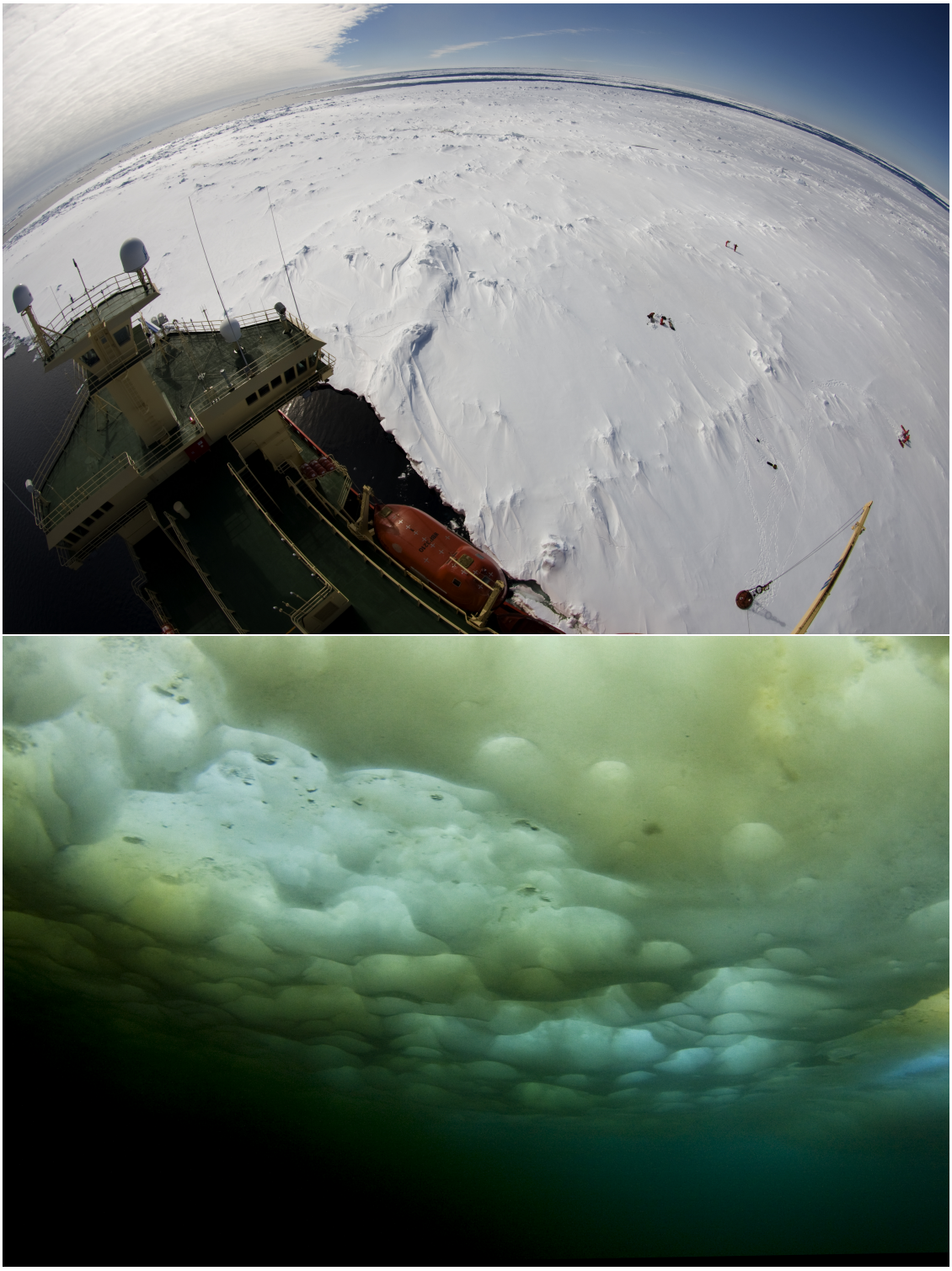

Figure 25: (top) A representative photo of a sea ice station showing moderate surface deformation and ridging with site selection in areas of surface level ice. (bottom) A representative photo of the under ice environment typical of summer sea ice, showing bottom melt features and biomass. (Photos ©Maria Stenzel.)

in the Amundsen Sea - (1) the confinement of drift ice by the Thwaites iceberg tongue, and (2) the import of thick multiyear ice from north of Thurston Island. The Thurston Island region is particularly interesting as it is a highly persistent region of perennial ice that appears to be maintained by a combination of high snowfall and an unusually stable water column. Recent changes in ice extent and duration there may also have implications for the ice cover downstream in the Amundsen Sea.

Generally, the underway sea ice observations qualitatively reflect the regional differences mentioned above. For example, average level (and ridged) sea ice thickness on our north-south transit (from the ice-covered outer continental shelf south to open water in Pine Island Bay, Jan 12 to Jan 16), was 182 (and 253) cm. Average level (ridged) sea ice thickness on the subsequent northward but more westward transit (from the fast ice in Crosson Bay back to the outer continental shelf, Feb 5 to Feb 9), was 172 (246) cm. Continuing further west along the outer shelf (Feb 10 to Feb 15), average level (ridged) sea ice thickness was 141 (201) cm. Thicker and more heavily ridged sea ice to the east is consistent with the probable import of multiyear ice from the Thurston Island region, while thinner, less deformed sea ice further to the west (110-120W) indicated a predominance of local sea ice production.

Preliminary analysis of samples taken suggests that the properties of Amundsen summer sea ice may have more in common with previous observations in the Ross Sea than the Bellingshausen. Superimposed ice from snowmelt formed a relatively thin layer on most floes, and seawater flooding of the surface was observed at most sites. Well-defined surface gap layers - important sea ice habitats - have been relatively infrequent. This is likely due to the high degree of deformation and surface flooding observed. Overall, this appears to be consistent with a predominantly first-year summer sea ice cover.

Snow depth averaged 47 cm. On the southward transect into Pine Island Bay the snow was warm and melting, but by the time the pack ice was re-entered temperatures had cooled and the snow had begun to freeze. Snow was predominantly icy and fresh even close to the slush/ice surface, suggesting there had been at least moderate snow melt. However, snow crystal structure and the lack of thick layers of superimposed ice suggest surface melt may have been modest. Average snow density was 400 kg m^3.

The flooding observed at most sites resulted in up to 39 cm of slush on top of the ice. In those cases where there was significant positive freeboard a thin layer of superimposed ice, formed from snowmelt, was present. In many cases, the location of the ice surface was unclear as the surface ice beneath the slush was often soft and poorly consolidated. A thin (5 cm) layer of ice was often found "perched" above the slush layer similar to previous observations in the Ross Sea in summer. This was either superimposed ice or snow ice. As

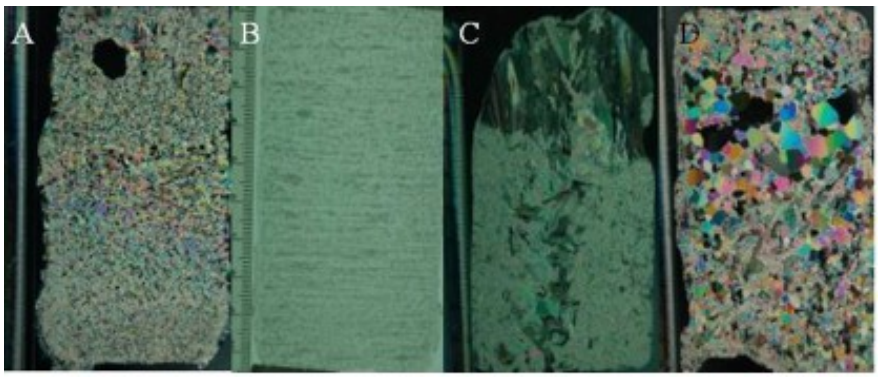

Figure 26: Examples of thin and thick sections illustrating key processes. (A) Thin section of the upper part of an ice core above a gap layer from ice station 6. The very fine-grained granular structure (< 1mm) is likely snow ice. (B) Thick section of a consolidated gap layer showing horizontal bands of bubbles. This suggests that the gap layer is snow ice. (C) Bottom section of a core from station 17 with platelet-like structure embedded in frazil and congelation layers. This is likely a refrozen void suggesting the ice was multiyear. (D) Thin section of buried superimposed ice formed from snowmelt from a multiyear ice core. (Photos by Ted Maksym.)

mentioned, clearly defined gap layers were observed less frequently than for summer sea ice in the Weddell and Bellingshausen Seas, although evidence for high primary productivity in the upper portion of ice cores suggest that similar features (i.e., favourable growth habitats) were present but that perhaps the gap layers were now mostly semi-consolidated.

Ice cores were composed primarily of granular ice (e.g. Figure 26). Clear evidence for thick layers ($>$ 10 cm) of snow ice were observed in a limited number of ice cores. All but one core showed clear evidence for deformational thickening. While congelation ice was observed in most cores, in only one case was a continuous, undeformed layer greater than 20 cm observed. Superimposed ice crystals were frequently observed, but clear layers with large polygonal grains (suggestive of substantial snow melt) averaged only a few centimeters thick.

While much of the ice is expected to be first-year based on very light ice conditions observed in the Amundsen and Bellingshausen Seas the previous summer, this was difficult to confirm, even from surface appearance (i.e angular ridges). In several cores initially thought to be from floes less than a year old refrozen melt features were found. It is unlikely that large voids formed during this summer would have refrozen, indicating that this occurred at the end of the previous summer. This further suggests that much of the multiyear ice in the Amundsen Sea may be advected in from the Western Bellingshausen.

Taken together, these observations suggest the following preliminary assessment of the summer ice regime:

- Initial ice formation in the Amundsen Sea was primarily through frazil/pancake ice formation.
- Ice deformation is the primary means of thickening for ice that survives into the summer.
- Surface snowmelt is relatively minor, particularly compared to previous observations in the southeastern Bellingshausen Sea.
- Snow ice formation is modest prior to summer. However, by the end of summer flooding is widespread and snow remains deep, so snow ice formation can be expected to cause significant thickening of multiyear ice.

Summer sea ice thinning and retreat is then controlled primarily by ice drift variability and disposition of solar energy in the ocean. A key question is how change or variability in snow accumulation or summer surface melt processes might affect ice thickness and modulate sea ice response to climate variability. Data collected by the ice mass balance buoys described below is expected to help answer this question.

5.3 Methods and Caveats

ASPeCt Ice Observations and Automated Camera System

Hourly observations of sea ice conditions were carried out while the ship was operating in ice using the standard Antarctic Sea Ice Processes and Climate (ASPeCt) protocol (Worby, 1999). The hourly observations relied heavily on a handful of intrepid volunteers, whom the ice team would like to gratefully acknowledge (in alphabetical order): Pierre Dutrieux, Adrian Jenkins, Katie Leonard, Chris Little, Ken Mankoff, Frank Nitsche, Robin Robertson. Though we attempted to engage more volunteers by giving an overview of the ASPeCt protocols at the beginning of the cruise, we suspect that the level of detail required by the protocol, as well as the ambiguity regarding ice types, daunted most would-be volunteers. We therefore emphasized that the most important estimates to make were (in order of importance): ice thickness, ice concentration, snow thickness, followed by ridged areal coverage, ridge sail height and ice type. Unfortunately, obtaining good estimates of snow and ice thickness when transiting through open summer pack ice is difficult, since the passing of the ship does not tend to turn over the floes but instead pushes them aside, (that is, when the ship actually ventures into the pack ice). More often than not, the ship preferred navigating the leads, so most estimates of ice thickness were made without the aid of the 'bouncing ball'. Other known difficulties are estimating ridge sail height from a 20 meter high bridge. (We thus encouraged observers to occasionally venture down to the main deck to re-calibrate their view of sail height from near-ground level.)

An automated camera system provided by Steve Ackley was installed on NBP0901 to provide a digital archive of the underway sea ice observations. One camera was mounted on an outside railing 1 deck above the bridge (outside the ice tower) with an oblique view of the area just aft of starboard. Another camera was mounted on the 01 starboard railing, pointing down over the bouncing ball. The former view will be digitally ortho-rectified by Ackley's UTSA group (led by Blake Weissling) to provide quantitative estimates of sea ice concentration. The latter 'bouncing ball' view was intended to archive ice thickness, but given the lack of over-turned floes in summer pack ice, its archive will be of limited use. Also, as first-time installers and users of the camera system, we encountered some difficulties. The 01 'EisCam' was not functioning for most of the initial southward transect through ice (likely a wiring issue), and some hourly video feeds were lost due to software glitches. Despite these problems, we managed to archive most of the oblique views, and we look forward to seeing post-processed results by Ackley/UTSA.

Snow and Sea Ice Sampling

Floe Selection and Deployment Sampling of sea ice and snow was carried out at a total of 20 ice stations. This was facilitated by the "near optimal" ice conditions that were encountered. The lack of ice in Pine Island Bay and north of the Getz and Dodson ice shelves permitted timely completion of Autosub and oceanographic work in these areas, and the light conditions in the main pack ice to the north kept transit time between stations relatively low. This allowed more time for sea work than originally anticipated, while north of the polynyas there was sufficient ice along most of the cruise track that a suitable floe could be found for sampling along-track. In a few cases the ship was diverted into heavier ice for a few miles - primarily to find sites suitable for deployment of instrumentation.

Because of operational constraints and the thick and heavily deformed ice, sampling was generally confined to ice in areas of low to moderate concentration ($< 70\%$), or within a few tens of miles of the ice edge. This may introduce a potential bias in the observations to favour areas where melting conditions were more prevalent than in the inner pack. There is no reason to suspect a bias in ice type or snow conditions, however. The cruise track allowed sampling along both the southern and northern edges of the Amundsen pack, as well as transits through both the eastern and western sides of the pack and forays deeper into the cental pack, so that the sampling strategy is likely to have captured the overall variability in ice conditions in the region. The possible exception is an area of persistent heavy ice North of the Thwaites iceberg tongue, centered at roughly 72.5 ^{o}S and 111 ^{o}W.

Although the number of ice floes occupied more than doubles the previous total for sampling summer sea ice physical properties in the Amundsen, the dataset is fairly small for a robust statistical characterization of the pack. Focus was therefore placed on resolving processes that control the summer evolution of sea ice, such as flooding and snow ice formation, snow melt and superimposed ice formation, and internal ice melt and the formation of gap layers.

Sampling strategy was therefore not to select floes at random as is typical of dedicated sea ice cruises, but rather floes were chosen to best span the range of ice conditions, while focussing on level pans within thicker, older (and moderately deformed) ice floes (Figure 25Top). Despite the surface appearance of level ice at many of our sampling sites, the underside was often quite a different story (Figure 25Bottom) as revealed by the photographic prowess of Maria Stenzel with logistical prowess from Zim Zimmerman, Julie Jackson, Amy Schaub and Mike Lewis.

Heavily deformed sites were avoided to best facilitate interpretation of growth conditions and comparison with models. In the outer pack ice region, this was impossible as almost all floes were heavily deformed. At these sites, sampling was carried out away from ridged areas as best as possible. Fast ice sites were preferentially sampled since these offer the best opportunity for model comparison, as the history of the ice is most readily determined via satellite imagery and deformation is least likely.

Most floes selected were a few hundred meters or more across to facilitate station keeping as close-packed ice was rare. Once a suitable floe had been selected the ship would either position alongside the floe for

deployment by personnel basket via the aft crane, or bow in about one-half ship length for deployment via the forward crane. For the first several stations the aft crane was used, but this was then switched to forward deployment for most of the remaining stations since this was usually quicker and easier to keep station. While cracking of floes aft of the forward crane was common, the ice was usually soft so cracks rarely propagated far forward of the bow. The bridge took particular care in parking the ship, and as a result we never had to reseat the ship after deployment.

Three to four people and sampling equipment were deployed at a time using the personnel basket. A typical ice station that included a snow pit and two ice cores of 2-3 meters in length took 2-3 hours on the ice. Floe selection, ship positioning, and deployment on the ice typically took an hour or more. Including time spent diverting off the ship track to find suitable ice on a few occasions, total ship time devoted to sea ice work is estimated to be about twice the actual on ice time.

Once on the ice, a representative area of level ice and snow was chosen for sampling. In most cases, this was within 50-100 meters of the ship. The major exceptions were sampling in conjunction with deployment of ice mass balance buoys (IMBs) where sites were selected as far from the ice edge as was practical.

Ice Coring At the sampling site snow was cleared from the ice surface and ice cores were taken with a 7.5 cm bore Kovacs ice corer. In most cases, two complete cores were taken at the same site - one for salinity and one for structure. The only exception was on station 5, a thick multiyear ice site where deep snow and soft, wet ice made it difficult to retrieve the deeper parts of the core. Here only the top two meters were retrieved for salinity, and just over five meters were retrieved for structure. Most cores were retrieved using a gas-powered motor mounted on the corer. This proved to be efficient and retrieved good-quality cores in most cases. Difficulties were encountered mainly when ice shavings or snow built up in the hole. This could be avoided if shavings are continually cleared while drilling and snow pits are well cleared when deep snow is present. For soft ice, particularly for the surface section where gap layers were often present, coring was done by hand to minimize breakage (or when we desired a bit of exercise).

As the salinity core was retrieved, each section was cut with a handsaw into 10 cm sections and placed immediately into 2 quart plastic buckets to minimize brine loss from the often very soft and porous ice. Temperature was measured for each section using a digital thermometer inserted into drilled holes in the ice. These samples were later analyzed onboard for salinity and chlorophyll content and samples drawn for δ^{18}O.

A second core was taken and placed into polyethelyene bags and cooled on the ice with saline ice packs to begin freezing the cores before their onboard placement in a freezer container in the ship's hold for structural analysis. In many cases, the gap-layer ice was unconsolidated and slushy and not suitable for structural analysis. In these cases the ice was placed in plastic buckets for later analysis of salinity and δ^{18}O. When the ice was flooded, there was often a perched ledge of ice at the base of the snowpack. If the slush beneath this ledge was well-consolidated, the entire thickness was retained for structural analysis. If not, the core was taken from the consolidated ice surface and the ledge was sampled separately.

After coring, the ice thickness was measured with a thickness tape and the freeboard noted. Positions and thicknesses of any gaps in the ice were noted when possible.

As mentioned above, at several sites, the photographer, aided by the MTs and/or idle scientists, drilled a 5 inch auger hole near the coring site to take photographs of the underside of the ice using an underwater housing mounted on a long, extendable pole. Many of the photographs were very enlightening and informative about the under-ice topography. It would be worthwhile in the future to use a simple cheap camera (that is, when professional photographers are not available) with a remote shutter release to take under-ice images at all coring or drilling sites.

Snow sampling Snow properties were examined either at a site adjacent to the coring site if the snow was fairly homogeneous, or in the same pit. The snow stratigraphy was examined for crystal structure, the

presence of ice layers and wicked brine. Temperatures within the snow were determined at 5-10 cm intervals with a handheld digital thermometer with a thermistor probe. Snow densities were determined using either a 100 cm^3 rectangular sampler with 3 cm resolution, or a 250 cm^3 wedge sampler with 10 cm resolution, depending on snow thickness and hardness; deep snow was more coarsely sampled. When the entire snow column stratigraphy was not sampled, at least each stratigraphic layer was sampled. Density was determined on the ice using an Ohaus CT600 portable balance. Samples were then placed in plastic bags to be melted onboard for salinity and δ^{18}O. At flooded sites, the slush was filtered through a 250 μm mesh for analysis of the brine on board. Complete slush samples were also taken where possible without drainage of brine.

Shipboard Analysis Salinity core samples were allowed to melt in plastic buckets in the dark. During periods of intensive sea ice sampling some samples were stored in the freezer in Ziploc bags and melted in buckets later. Salinity was measured using an Orion 115 conductivity meter. Between 15 and 30 ml of the melt water were then sealed in either Nalgene HDPE bottles or polypropylene centrifuge tubes (when we ran out of bottles) sealed with Parafilm. These samples will be analyzed at UC Santa Cruz for δ^{18}O. Melted snow samples were also measured for salinity and bottled for later δ^{18}O analysis.

Up to 250 ml of the remaining water was filtered onto 47 mm glass fibre filters and frozen immediately at -20^{o}C in centrifuge tubes for later chlorophyll analysis. When convenient, chlorophyll samples were run in batches using a Turner designs 10AU fluorometer. Samples were first dissolved in 7 ml of acetone for 24-36 hours in the dark at 4^{o}C. Samples were diluted as necessary in acetone and a measurement was taken to determine Fo. Two drops of 1.2M HCl were added to each sample and a second measurement was taken for Fa. The biologists onboard were very helpful with advice, equipment, calibration of the fluorometer, and assisting in calculation of pigment concentrations.

Analysis of ice core structure involved cutting of thick and thin sections and photographing of pore and crystal structure. The time spent during Autosub operations in ice-free Pine Island Bay allowed the opportunity to try a number of techniques for cutting thin sections. In order to best preserve the microstructure for micro- and macro- photography, a double-microtoming technique was chosen. First, the core was cut in sections of up to 20 cm and the halved lengthways with a bandsaw. These were sanded smooth and then fixed to glass plates with a bead of fresh water. The plates were warmed slightly to achieve a good seal. A thick section ($<$ 3 mm thick) was then cut on the bandsaw and smoothed on a Bright series 8000 sledge microtome. The ice was then flipped on the plate and resealed, taking care to achieve a good seal with minimal melting. The sections were then thinned to between 0.5 mm and 1.5 mm depending on crystal size and fragility of the ice. A total of 137 thin sections were made. A custom stage was made for the microtome, but it was difficult to level accurately, which complicated the double-microtoming process.

Sections were photographed under polarized and transmitted light to determine structure (e.g. Figure 26), density, and void distribution. Macro photography was done using a Nikon D50 digital camera with either a 18-55 mm zoom or a 105 mm macro lens. Selected portions of the cores were photographed using a Nikon 5500 Digital camera mounted on a Leica Wild M3C microscope at between 6.4X and 40X. Based on the observed structure, half the core was sectioned and melted for a second determination of salinity and later δ^{18}O analysis. The remaining half of the core was retained for later thin sectioning back in the UK. Some sections will be sent to a colleague at Dartmouth College to examine three-dimensional pore structure using x-ray tomography.

After leaving Pine Island Bay, there was insufficient time to continue extensive processing. For the remaining cores, thick sections 2.5-5 mm thick were cut unmounted. It was found that these could be adequately smoothed by hand to eliminate saw marks in the photographs. These were photographed only for large-scale analysis. Selected sections of the remaining half-cores will be thin sectioned in the UK.

Ice core analysis was carried out in a 20 ft freezer container kept in the ship's hold. This provided more space than the old walk-in freezer (now the Autosal room) and was fairly stable for photography even in rough weather. A few problems did occur. First, the defrost cycling for much of the cruise would occasionally warm the freezer to greater than -10^{o}C. This seemed to fix itself towards the end of the cruise. Temperature

variations meant that the first half of the ice was processed at about -15^{o}C, with some sections a few degrees warmer. The latter half was typically at about -18^{o}C. Unfortunately, temperature variations were not noted during photography.

Ship vibration also hampered photography. Vibration was minimized by mounting the light table and camera stand on foam and holding the lens steady. A camera stand that dampened vibrations in the light table, camera, and lens would be helpful. The light table provided by Raytheon was old, dim, and brightness varied, particularly when cold.

The digital camera for the microscope was old, slow, and rather finicky. It was difficult to focus. A lens mount for a digital SLR camera would be useful.

5.4 Ice Mass Balance Buoy and Drifter Deployments

Instrumentation available for deployment on the ice included four GPS drifers (PI Ackley), one CRREL ice mass balance buoy (IMB, PI Ackley), and 3 mini-IMBs provided by the Scottish Association for Marine Science in collaboration with BAS.

The four GPS drifters were initially intended for IPY SIMBA project (NBP0709). However, deck tests at the beginning of that cruise revealed transmission problems presumably due to a cold-temperature sensitivity. Those units were returned to the manufacturer (Trident Sensors) for testing and possible replacement or refurbishment. Four of those repaired/replaced units were made available for deployment on NBP0901. Unfortunately however our deck tests revealed that 2 of the 4 drifters continued to have chronic transmission problems, while the other 2 appeared to reliably transmit on the helo deck even during a cold temperature snap where temperatures decreased to -19 to -20 degC. We therefore decided to deploy the 2 operational drifters, only to discover that 1 of the 2 also succumbed to transmission problems. We therefore were successful in deploying only 1 working ice drifter. The 2 chronic drifters will be returned once again to the manufacturer for further testing.

A CRREL IMB (lead PI Ackley) was deployed on the fast ice in front of the Crosson Ice Shelf, alongside an WHOI ice-tethered profiler (ITP). The CRREL IMB consists of a 4.5 meter thermistor string (sectioned into 1.5 meter lengths), with thermistors spaced 10 cm apart for a total of 45. Additional sensors are mounted on two PVC masts, one extending mostly underwater, supporting an upward looking sounder, mounted at about 1.5 meters below the bottom ice surface, for measuring changes in distance to bottom ice surface and a SeaBird SBE39 for measuring temperature, conductivity and pressure. The other PVC mast supported a downward looking sounder, mounted at about 2 meters above the snow surface, for measuring changes in distance to top snow surface. The two sounders combined yield estimates of ice mass balance changes. The surface mast also supports an air temperature probe housed inside a gill plate. All masts and thermistor strings are white to decrease heat absorption during sunlit days. Each sensor is hooked to a data logger enclosed in a protective white box, which also houses a barometric pressure sensor, the GPS antennae/receiver and Argos transmitter. To date, the CRREL IMB is reliably transmitting all data, though there are indications that the surface air temperature probe is not functioning properly. Fortuantely, the thermistor change extends approximate 1.35 meters above the snow surface, thus providing additional surface air temperature readings.

The deployment site for the CRREL IMB was on fast ice north of Crosson Ice Shelf at about 3 miles south of the fast ice edge and in the near vicinity (within 15 meters) of the WHOI ITP. The deployment site consisted of fairly level ice, averaging at about 50 cm thickness, located southward of an area that was moderately ridged. Given the 50 cm ice thickness, we decided to overlap the 3rd thermistor section with the other two sections that were in series. This allows 5 cm temperature resolution through the ice-snow-air layers (i.e., from -50 cm to +80 cm relative to the ice surface).

In addition to the CRREL IMB, two SAMS IMBs also were deployed. The SAMS IMBS are designed as a low-cost, easily deployable alternative to a full IMB, with the future potential for deployment of a large

enough number to be able to regionally charcterize ice growth and melt processes. The design consists of a single wire of addressable digital temperature sensors with 1/16 of a degree resolution. Each string consists of 144 sensors with a 4 cm spacing mounted on a thin flexible PCB that was weatherproofed in heatshrink. Each has a surface mounted resistor that heats the sensor when a voltage is applied, allowing the thermal response of the sensor to be monitored. This "hot-wire anemometer" mode will in principle allow discrimination of the medium that the sensor is in (i.e. snow, ice, air or water) and hence determination of snow and ice thickness without the need for acoustic sounders. A particularly advantageous feature of this system is the potential to continuously monitor surface processes such as flooding, snow ice formation, and snow melt. These processes are a particular focus of the sea ice program.

Data is recorded using a Persistor CF2 logger and transmitted via Iridium modem. To reduce power consumption and data transmission costs, temperatures are recorded 4 X daily, and a heating cycle is applied once per day. Power is supplied by 80 alkaline D-cell batteries. All components other than the sensor chain are enclosed in a 1550 Pelicase (20 cm x 35 cm x 50 cm).

This is the first deployment of these systems in the Antarctic. Modifications from the design used in the Arctic include a longer chain to accommodate thick ice and snow and finer sensor spacing to resolve surface processes.

To deploy the IMBs, 2 meters of the sensor chain were cable tied to a 2" diameter ABS pipe to support the sensors in the snow and air. This was fixed in the field via a threaded joint to a second pipe that was secured in a 2" auger hole in the ice. The remaining sensors were run along the ice surface to a hole 40 cm away and dropped through a drill hole through the ice.

Two systems were deployed. A third failed during testing on the helo-deck due to failures in both the sensor driver module and the Persistor logger. The cause of the first failure is unclear, but it is probable that a short damaged the logger. The first system was deployed at ice station 11 on the Northwest side of the Thwaites iceberg tongue. This site was chosen as it was well protected by icebergs and fast ice to the east so had a fair chance of surviving into the winter. High Resolution ASAR data was provided by BAS under the auspices of the European Polarview project was particularly useful in locating the site and finding a route through the iceberg tongue. The IMB was deployed in 2.7 m of sea ice about 1/2 mile from the fast ice edge.

At this site, the snow was removed in blocks prior to drilling and then replaced around the snow mast. This prevented wetting of the snow, but it is likely that there were air gaps between sensors and replaced snow so that detection of snow in the heating cycle is difficult. The second IMB was deployed at ice station 13 on a roughly 500 m floe in the middle of the pack ice band. The ice was 2.0 m at this site. Rather than clear the snow, holes were carefully drilled through both the snow and ice. Crushed snow was packed in the gaps around the sensors to ensure good contact. Both sites were flooded. Deployment of each station took about 2 hours.

Initial analysis of the data show that the different layers can be resolved, but the thermal response of snow and air are only slightly different. This may be because the response is detected using the temperature rise after a one minute heating cycle. This may not be sufficient time for the heat to flow through the heat shrink on the sensor chain and deeply into the snow. It may be better to transmit temperature information at several points during a cooling cycle, similar to what is done with needle probe measurements of thermal conductivity. Further testing of alternative potting methods to reduce thermal mass of the chain would be worthwhile.

5.5 Remote Sensing Support

High-resolution satellite data has proved indispensible on previous cruises to support navigation through ice and to find suitable ice floes for sampling and instrumentation deployment. Useful satellite data available on NBP0901 consisted of near-real time acquisition of visible OLS (0.55 km resolution) and SSM/I passive microwave (12-25 km resolution), and visible band AVHRR (1.1 km resolution) using the Terrascan system.

Infrared was less useful because of low variability in surface temperature in summer.

This was supplemented by imagery provided through the European Polarview program. This is a multinational program designed to provide a variety of products to ships operating in ice-covered waters. Several national Antarctic programs use a variety of data routinely aboard ships where large-bandwidth data transmission is available.

AMSR-E, Quikscat POL, and reduced resolution ENVISAT ASAR 3-day composites were provided by Roberto Saldo at Denmark Technical University. Pre-arranged acquisition of wide swath ASAR was facilitated by Andrew Fleming at BAS, who sent high resolution sub-images upon request to the NBP. ASAR imagery proved extremely helpful in identifying areas of both pack and fast ice suitable for deployment of instrumentation. It was indispensible in finding fast ice in the Western Pine Island Bay, and aided in locating a fast ice site for one of the BAS IMBs and the ITP/IMB site. However, it was severely limited when the ship was operating outside of INMARSAT range. File size restrictions on email - even on special accounts - severely limited image quality. It would be worth pursuing having a separate system for staging imagery to be sent via Iridium. It is also worth implementing a means for downloading imagery over the web via Iridium. This has been done successfully on other ships. The advantage is that imagery can be browsed at low resolution at the Antarctic Polarview node website, and subregions may be downloaded at high resolution.

Visible OLS was useful when weather was clear, which occurred several times during the cruise. Quikscat was of little use. It often is useful in delineating the full extent of sea ice, but it seemed to consistently overestimate ice extent.

Perhaps the most used sources of imagery were passive microwave from SSM/I or AMSR-E. Qualitatively, both did a fairly good job at detecting sea ice extent, with errors usually smaller than expected for this time of year. There are some caveats regarding its use for navigational purposes, however:

The Terrascan system onboard provided ice extent using a number of algorithms, with often quite different results. Some of these appear to use a 15% cutoff as implemented on the NBP (such as the Artist algorithm), while others do not (such as SeaLion and Bootstrap). Some of the Algorithms provide a higher resolution product (SeaLion and Artist), but do so by using the 89 GHz Channel. This is much more subject to weather effects than the other channels and so can produce large errors in ice concentration. While the bootstrap product is lower resolution, it appeared to be less affected by spurious day-to-day variations in ice concentration. This can be confusing to those less familiar with this type of data.

During NBP0901, satellite ice concentration varied considerably in the pack ice north of the coastal polynyas during late January - early February. This is likely due to surface emissivity variations associated with melt-freeze cycles and weather. Again, the Bootstrap algorithm performed better at the cost of lower resolution.

There appear to be issues with the F15 satellite. This showed very little ice compared to others on many occasions.

AMSR-E provides a more reliable ice concentration than the SSM/I products at equivalent resolution (SeaLion and Artist), but is still subject to some of the same problems with surface emissivity variation. However, as this is not available via Terrascan, it was often 1-2 days late.

5.6 References

Haas, C., D.N. Thomas and J. Bareiss (2001), Surface properties an processes of perennial Antarctic sea ice in summer, J. Glaciology, 47, 613-25

Worby, A.P. and I. Allison (1999), A technique for making ship-based observations of Antarctic sea ice thickness and characteristics. Part I. Observational techniques and results. Antarct. CRC Res. Rep. 14, 1-23.

6 Seafloor Mapping

Frank Nitsche, Kathleen Gavahan

6.1 Objective

A large portion of the bathymetry of the continental margin around Antarctica is still unmapped. In the Amundsen Sea, scientific questions concerning warm water entering the shelf and collecting in deep inner shelf troughs depend on the local and regional bathymetry. Detailed bathymetry data were also needed to determine depth and location of CTD and mooring sites as well as for planning Autosub operations. Improving the existing bathymetry of the Amundsen Sea continental shelf also better defines existing troughs and supports reconstruction of past ice flow on the continental shelf.

We have thus been running the swath-mapping system throughout NBP0901 The main mapping team consisted of Kathleen Gavahan (Raytheon) and Frank Nitsche (LDEO) and was supported by several others, especially Ken Mankoff, Adrian Jenkins, Robin Robertson, Chris Little, Stan Jacobs, Andy Webb, Pierre Dutrieux, and Sharon Stammerjohn, who helped edit raw multibeam files.

6.2 System Description and Operation

The main equipment used for seafloor mapping on this cruise was the Simrad EM-120 swath-mapping system. It operates at a 12 kHz main frequency and receives up to 191 beams from angles up to 65^o to each side of the ship, providing a resolution of $\sim 1.5^o$ of the seafloor and a coverage of $\sim$4 times the water depth. To adjust for changes in sound velocity, CTD and XBT data were used to update to the local conditions throughout the cruise.

The raw data are recorded digitally and displayed in real-time. Once a day the raw data were processed and edited manually for outliers and false bottom returns using the mb-system 5 software package. The final data are stored in MBsystem format 57 and will be archived at the Antarctic Multibeam Synthesis Database (http://www.marine-geo.org/antarctic/).

In addition to the swath-mapping system we almost continuously ran a sub-bottom profiler to provide independent depth measurements. Sub-bottom data can also be used to determine sediment sample locations. At the start of the cruise a Knudsen 320B echosounder with 3.5 kHz main operating frequency was used. From January 16th 2009 we used the Ocean Data Equipment Corporation Bathy 2000 echosounder and sub-bottom profiler. The Bathy 2000 transmits a chirp signal of 3.5 to 4 kHz. It determines the bottom and images the uppermost subbottom sediment layers down to a few 10s of meters depending on sediment character. The data were archived digitally in the Bathy2000 variant of the SEGY-format.

Additional bathymetry data of previous NB Palmer , JC Ross, Polarstern, and Oden cruises provided extra guidance and helped to avoid accidental duplication of existing tracks.

6.3 System Performance and Problems

Throughout the cruise, both the EM-120 swath-bathymetry and the Bathy2000 echosounder operated normally under most conditions, but had problems with receiving good data in sea ice. The Bathy2000 was only disturbed by heavy pack ice but the EM-120 multibeam had problems with heavy pack ice and certain types of newly formed ice such as grease ice and nilas. The ice gets under the ship, blocking signals coming to and from the transducers, producing bad data even in easy and calm conditions. We rarely encountered such ice conditions during NBP0901, but a larger issue was the drastic drop in data quality in rough seas.

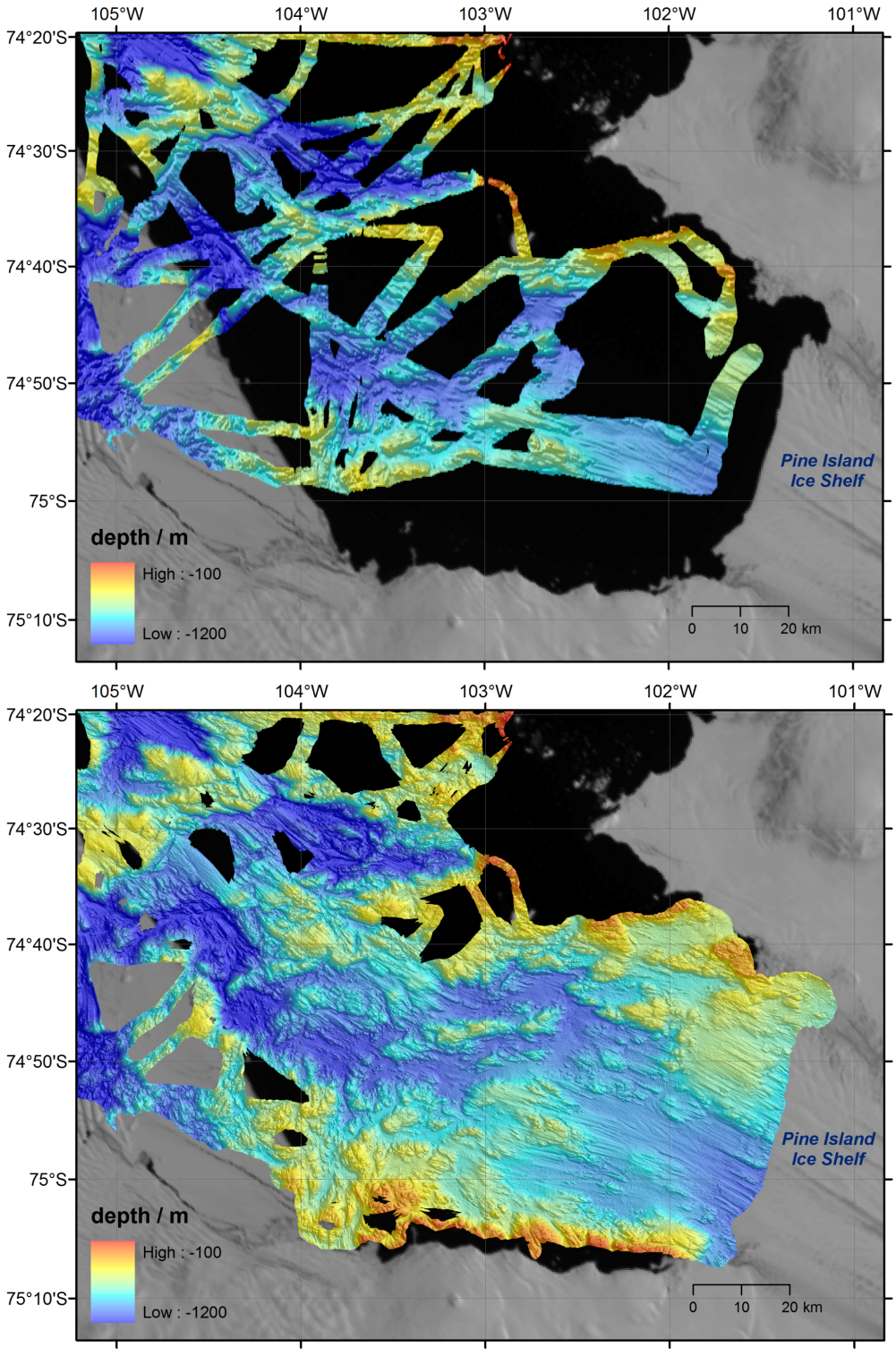

Figure 27: Sun-illuminated bathymetry of the inner Pine Island Shelf before (top) and after (bottom) the mapping of NBP0901. Background is a MODIS from NSIDC (December 2008).

Due to the location of the transducers it is likely that they are effected by air bubbles generated by the waves and ship-sea interactions.

The SeaSurveyAdvanced display software allows real-time display of new and pre-existing multibeam data, an essential tool for route and station planning as well as for ship navigation. The additional helmsman display on the bridge allows the mates to steer a course designed to ensure maximum coverage by not duplicating pre-existing data from the NBP, BAS, and AWI. Occasionally there were problems with this software and/or its computer due to age and software. An upgrade or replacement in the near future is highly recommended.

6.4 Results: Swath-Bathymetry

During this cruise we collected and processed 11912 km of multi-beam swath data (540857 pings, 103303687 beams (soundings) representing ~11.9 GigaBytes of data.

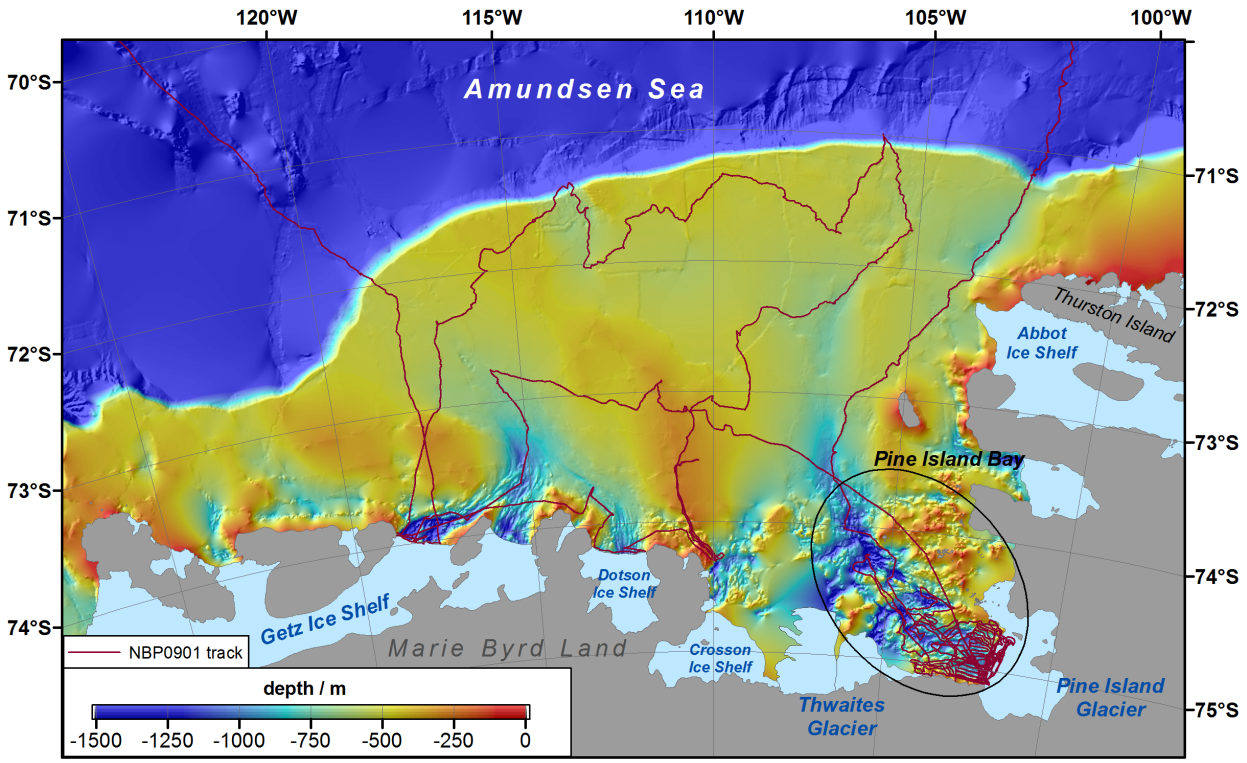

Figure 28: Preliminary version of the updated Amundsen Sea bathymetry compilation.

Most of the newly acquired bathymetry data cover previously uncharted areas, adding significantly to our understanding of the regional bathymetry.

Work is needed to reconcile significant swath-map differences between various ships, probably due to varied assumptions about sound velocity. In addition, some earlier MB data have not been ping-edited completely.

Pine Island Bay

As result of Autosub operations under the Pine Island Ice Shelf the NB Palmer spent ~two weeks in this area and mapped the Pine Island Bay seafloor in some detail. Systematically adding to existing data resulted

in a comprehensive bathymetry image of the area, as shown in figure 27 that shows the morphology of the seafloor right in front of the ice shelf in great detail. Much of the remaining unmapped area is shallow and includes small islands, or access was blocked by sea ice and icebergs.

Updated Amundsen Grid

The new bathymetry data collected during this cruise will be used to update the existing bathymetry compilation of the Amundsen Sea (Nitsche et al 2007). Beside the Pine Island Bay trough, improvements of the overall bathymetry image were made along most of the cruise track, especially in the outer shelf region, and the central ridge separating the Pine Island-Thwaites trough system from the Getz trough system (Fig. 28).

6.5 Results: Sub-Bottom Profiling

During the cruise the Bathy2000 sub-bottom data were mostly used as an additional source for bathymetric depth information. We did not perform a systematic analysis of the sub-bottom data during the cruise, but they are digitally available and will aid the interpretation of morphological features identified in the swath-bathymetry mapping.

Nitsche, F.O., Jacobs, S., Larter, R.D. and Gohl, K., 2007. Bathymetry of the Amundsen Sea Continental Shelf: Implications for Geology, Oceanography, and Glaciology. Geochemistry, Geophysics, Geosystems, 8: Q10009, doi:10.1029/2007GC001694.

7 Onboard numerical modeling

Chris Little

A modified version of the Hallberg Isopycnal Model (HIM) was used to aid the interpretation of oceanographic processes under the Pine Island Ice Shelf (PIIS). An idealized ice shelf shape based on earlier studies was gradually modified to represent PIIS. Although only the most "realistic" model run is presented, those findings highlighted here are relatively insensitive to details of cavity shape and oceanic forcing. The numerical domain employed in this simulation was 80x100 km, discretized on a 1 km horizontal grid. The ocean consists of 10 isopyncal layers coupled to a bulk mixed layer; the depth of the "mixed" layer is determined by a turbulent kinetic energy budget. Ice-ocean fluxes through a viscous sub-layer parameterization are governed by mixed layer temperature, salinity, and flow speed.

7.1 Bathymetry and Ice Thickness

The water column thickness – depth of ocean floor minus the depth of the ice shelf base, if present – for this simulation is shown in figure 29. Bathymetry was derived from multibeam maps of Pine Island Bay and from "BEDMAP" where bathymetric data were unavailable (i.e. underneath PIIS). The model's ice shelf draft was derived from BEDMAP ice thickness data assuming a constant ice density (0.917 kg m^{-3}); the grounding line is located where the floating ice thickness is less than the bedrock depth. The lack of bathymetry and ice thickness data in the "northern lobe" of PIIS makes its role in the sub-ice shelf circulation difficult to determine.

Higher resolution datasets show evidence that PIIS is heavily crevassed, and previous studies indicate that sub-ice topography influences flow. To illuminate the effect of inverted basal channels of different dimensions,

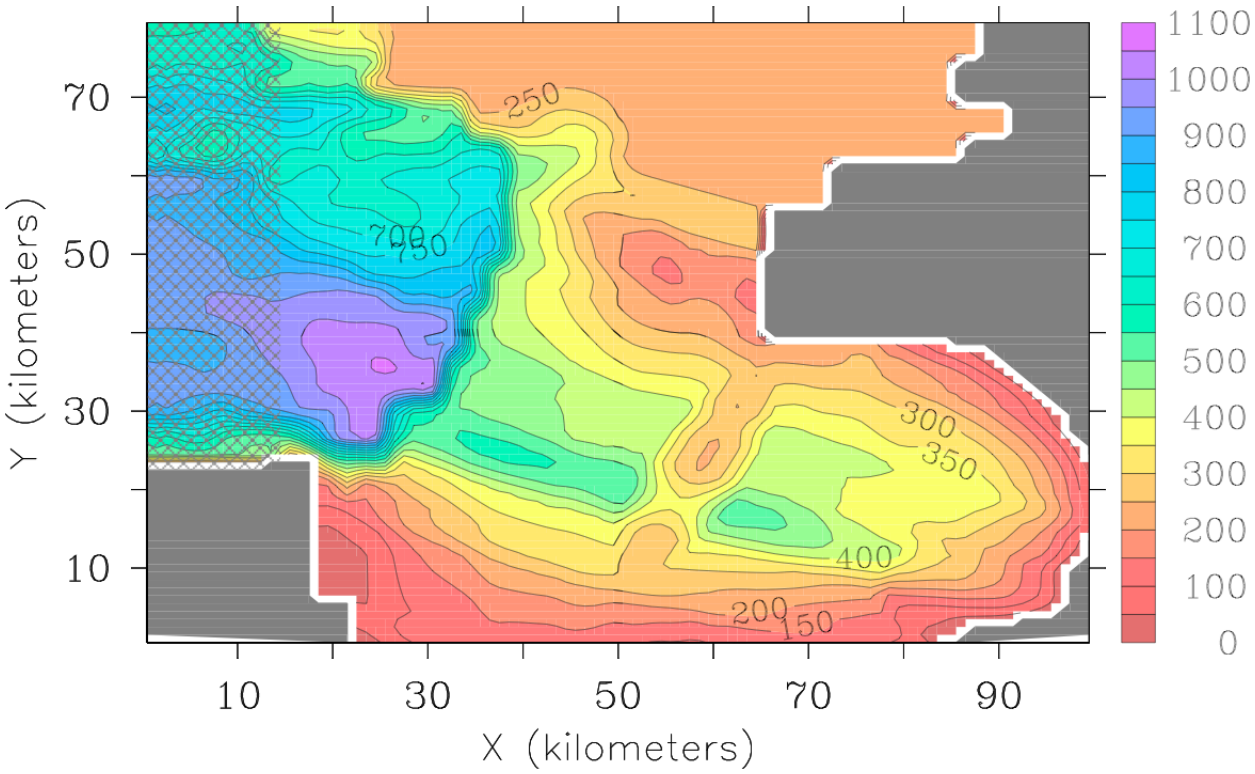

Figure 29: Water column thickness (m) over the model domain.

the ice shelf draft was altered by an increment that varied sinusoidally transverse to the longitudinal axis of the ice shelf. This alteration modified the ice shelf draft (contours in figure 30) by up to ∼100 meters.

7.2 Model Forcing

The model simulation was initialized with a meridionally uniform temperature and salinity profile corresponding to NBP09-01 CTD 14. Flow was initiated and maintained by buoyancy fluxes at the ice-ocean interface. No winds or tides were prescribed. During the simulation, the hydrography was restored to the initial conditions in the western 15 km. The model was integrated for 20 days, at which point the kinetic energy of the flow stabilized. The strong restoring may have limited accurate representation of the location of inflow as well as ice front hydrography. When more computational resources are available, that sensitivity will be explored.

7.3 Preliminary Results

Given our still limited knowledge of ice shelf basal topography, sub-shelf bathymetry, and forcing, model results are primarily qualitative. However, there is encouraging agreement between the observed and modeled ocean circulation and melting patterns. In figure 30, heightened melt rates occur in three distinct locations driven by differing dynamics: near the deepest parts of the ice shelf grounding line, near the ice shelf front, and in inverted channels at the ice shelf base.

The depth integrated flow illustrated in figure 30 obscures vertically sheared currents underneath the ice shelf. Heat used for melting is derived primarily from the densest, warmest waters respresented in the simulation (CDW); virtually all heat entrained into the mixed layer occurs within 10 km of the grounding

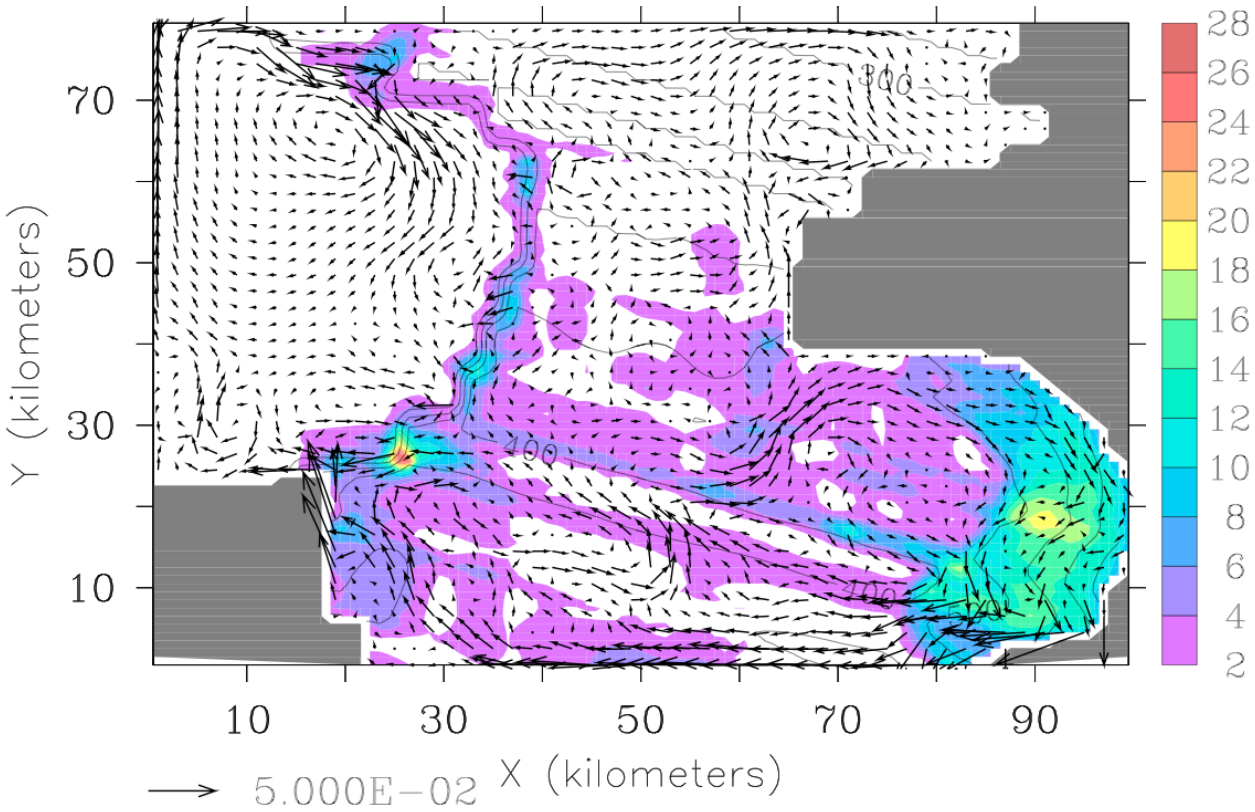

Figure 30: Ice shelf basal melt rates (m yr^{-1}, shading), depth-averaged velocity (m s^{-1}, vectors), and ice shelf draft (m, contours).

line. In the model, sub ice channels appear to play a major role in determining where glacial meltwater exits the cavity, but their effect on the overall and regional basal melting rate is less clear.

Meltwater-enriched seawater is exported in well-defined cores of outflow, separated in depth and location along the ice front. Lighter, colder water escapes the cavities via sub-ice channels, while a denser, warmer meltwater plume is forced towards the southern boundary, detaching from the ice shelf at approximately 500m. A vertical cross section of zonal velocity at the ice shelf front (figure 31) shows meltwater-enriched currents (both inflowing and outflowing, with outflow heavily influenced by channel location) at mid-depth and near the sea surface. Alternating bands of weak inflow and outflow characterize cross ice-front flow at depth.

Observations and other model simulations indicating that the majority of meltwater exits in a narrow band near the southern edge of PIIS are strongly supported by this simulation. Flow from underneath the ice shelf is sufficient to break the imposed stratification near the southern boundary, where CDW-derived meltwater mixtures upwell, warming the water column above the level of the ice shelf draft. Many other features of the model output also show promising agreement with oceanic and satellite-derived observations but require further analysis. Autosub and CTD-derived ice shelf thickness, bathymetry, small-scale roughness, and hydrography measurements will allow for better model validation. The general nature of these results may be applicable to other ice shelves in the Amundsen.

The presence of a numerical model stimulated many conversations about sub-ice shelf circulation, as well as the limits and opportunities for modeling ocean-ice interactions, particularly in light of newly collected Autosub data. Background information about numerical models and highlights from onboard discussions were summarized in an onboard "science talk".

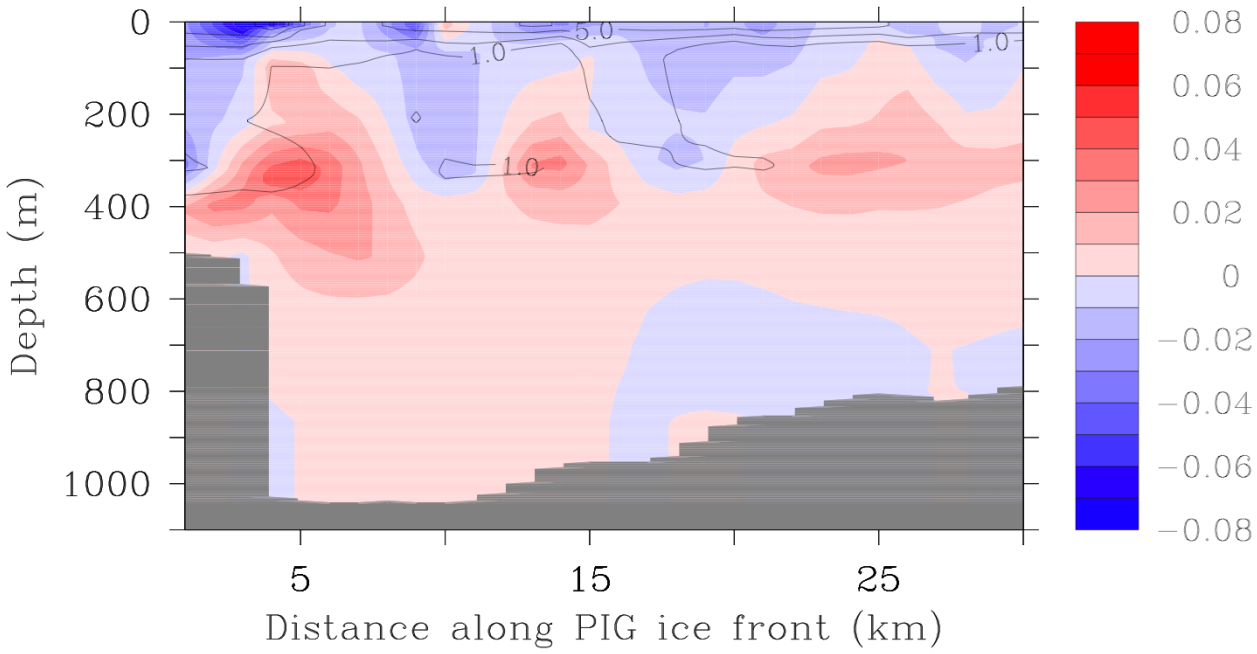

Figure 31: A south-to-north cross section along the ice shelf front. Velocity (m s^{-1}, shading, blue indicates flow out of the cavity) and meltwater concentration (per mille, contours) 1 km seaward of the model's ice shelf front.

8 DynaLiFe, Shedding a Dynamic Light on Iron Limitation in the Southern Ocean

The Southern Ocean plays an important role in the global carbon cycle, due to its large size and unique physiochemical characteristics. Approximately 25% of total anthropogenic CO_2 uptake by the oceans takes place in the Southern Ocean, mainly via primary production by phytoplankton. However, changes in the Antarctic climate may impact phytoplankton primary productivity and hence, the carbon export by the Southern Ocean. Primary production in the Southern Ocean is dominated by two phytoplankton groups that bloom in distinct locations and times: diatoms dominate blooms in shallow mixed layers, whereas the colony forming *Phaeocystis antarctica* (Prymnesiophyceae) dominates blooms in the more deeply mixed, open regions. Understanding what controls the dynamics of these two phytoplankton taxa is essential because they dominate virtually all polar waters, they have vastly different nutrient utilization characteristics, and both support very different marine food webs. In addition, this understanding is needed to recognize the potential impact of climate change on the Antarctic phytoplankton community and predict their role in the carbon export in the future. The Amundsen polynya and Pine Island Bay polynya are areas with the highest phytoplankton primary productivity in the Southern Ocean as estimated from satellite imagery (Arrigo and Van Dijken 2003) and are therefore vital areas to study phytoplankton primary productivity and carbon uptake *in situ*.

Previous experiments in our laboratory suggest that taxon-specific differences in photoacclimation contribute to the observed distribution. However, photoacclimation does not seem to be the only factor that controls the phytoplankton distribution. Iron (Fe) limitation of the algal communities in the Southern Ocean is now well documented. Moreover, much of the Fe is bound to organic complexes, so-called ligands. Ligands can increase solubility of Fe, but the effect on biological availability is unclear. In addition, phytoplankton Fe demand varies as a function of irradiance. Thus, the Fe needs of phytoplankton can change dependent on their light environment with great Fe requirements necessary to maintain growth in deeply mixed water columns and less Fe required by phytoplankton found in shallowly mixed water columns.

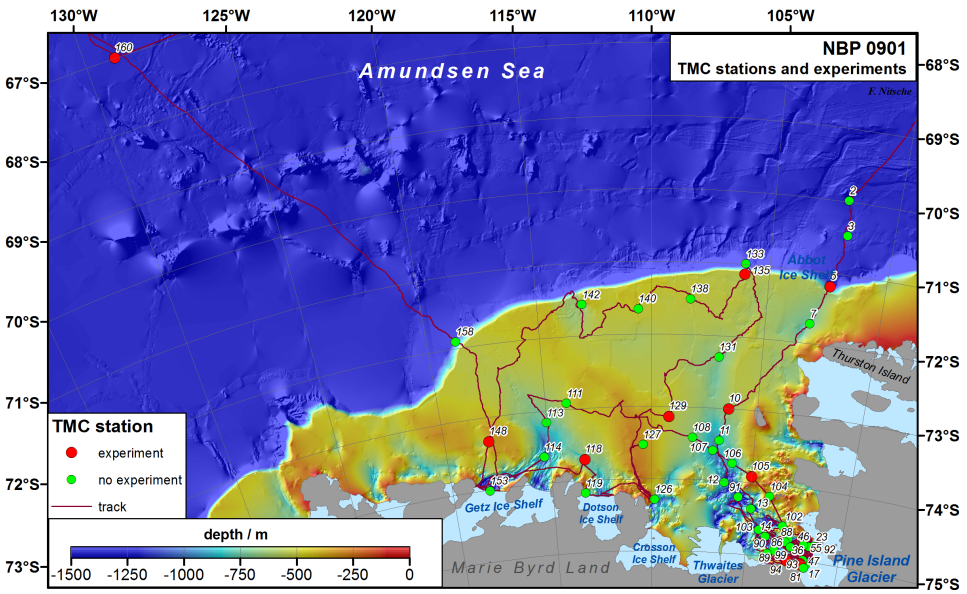

Figure 32: TMC stations sampled by the DynaLiFe project during the NBP0901 cruise. Red stations represent the start of a Fe/ligand bioassay experiment, whereas green stations represent a profile of 6 surface depths (Thanks to F. Nitsche for the cruise track figure).

The main hypothesis of the proposed research is: The interaction between Fe limitation and dynamic irradiance governs phytoplankton distributions in the Southern Ocean. For the NBP0901 cruise, five research questions were investigated in different natural phytoplankton assemblages at various stages of a phytoplankton bloom:

1. What is the carbon uptake physiology of the phytoplankton?
2. What are the photosynthesis versus irradiance characteristics of the phytoplankton?
3. What is the extent of damage caused by photoinhibition when phytoplankton reside near the surface?
4. What are characteristics and quantities of dissolved Fe and Fe bound to natural ligands?
5. Is Fe bound to artificial ligands accessible to phytoplankton?

8.1 Sampling Strategy

On the NBP0901 cruise, stations were sampled to obtain a suite of different natural phytoplankton assemblages at various stages of a phytoplankton bloom (Figure 32). Stations can be divided into sea-ice and open water stations. Preliminary analysis showed that sea-ice stations were mainly dominated by diatoms, whereas open water stations were mainly dominated by *Phaeocystis antarctica*. Open water stations can be divided into polynya stations and stations influenced by melt water driven upwelling in the vicinity of glaciers. Polynya stations were visited in both Pine Island Bay and the Amundsen Polynya. Glacier stations were mainly situated near the mouth of the Pine Island Glacier (PIG), and additionally, stations in front of the Getz, Dotson and Crosson glacier were sampled.

Table 7 shows the TMC casts at different CTD stations, and subsequent experiments and analysis by the DynaLiFe team. Trace metal clean (TMC) sampling of a profile (P) of the upper 300m of the water column was done using clean GoFlo bottles provided by the Royal NIOZ on a kevlar wire, using messengers to close the bottles. Sample depths were typically 10, 25, 50, 100, 200, and 300 m. To obtain large quantities of TMC surface water to do biological experiments, a TMC frame (Royal NIOZ) was used holding the six GoFlo bottles. The water depth for these casts using the frame (F) was typically 10 m. For all stations,

phytoplankton from the upper 200m water depths was collected on GF/F filters for analysis of Chl *a* (on board), pigment composition by HPLC, elemental composition (CHN), and particulate organic phosphorus (POP). Filtered seawater was collected from all depths and stored at -20^{o}C for late analysis of nutrients (Silicate, Nitrate, Ammonium, Phosphate). In addition to the TMC sampling, water samples from the surface (10m) were obtained from the regular CTD, to study carbon uptake by natural phytoplankton assemblages (see section below).

CTD	TMC	C uptake parameters			Photoinhibition		Fe analysis		Ligand	Fe/ligand
Station	cast	eCA	M M	Iso	PE-curve	exp	DFe	TFe	analysis	exp
2	none				10, 25	10, 25				
3	P	10	10	10	10		P	P	P	
5	F	10	10	10	10	10	10	10	10 (U, 0.2um)	Exp 1
7	P				10, 20	10, 20	P		P	
10	F	10	10	10	10	10	10	10	10 (U, 0.2um)	Exp 2
11	P				10, 40	10, 40	P			
12	none									
13	P	10	10	10	10, 20	10, 20	P		P	
14	P				10, 50	10, 50	P			
16	P	10	10		10		P	P	P	
17	P				10	10, 25	P			
23	P						P	P	300	
36	P	10	10	10	10	10, 25	P			
37	F	10	10	10	10	10	10	10	10 (SF, U, 0.2um)	Exp 3
46	P	10	10	10	10, 50	10, 50	P			
47	F	10	10	10	10	10	10	10	10 (U, 0.2um)	Exp 4
55	P		10				P	P	P	
81	P		10				P		P	
86	P	10		10	10		P			
88	P				10		P			
89	P				10	10, 50	P			
90	P				10		P			
91	P	10	10	10	10, 25	10, 25	P		P	
92	P		10				P		P (4)*	
93	P		10				P			
94	F				10	10	10	10	10 (SF, U, 0.2um)	Exp 5
99	P	10	10	10	10, 25	10, 25	P			
102	P	10	10	10	10	10, 25	P	P	P	
103	P				10		P			
104	P				10, 20	10, 20	P	P		
105	F, P	10	10	10	10	10	P	P	10 (SF, U, 0.2um)	Exp 6
106	P		10	10	10, 25		P	P	P(4)	
107	P				8, 25		P	P	P(4)	
108	P	10	10		10		P	P		
111	P	10	10	10	10		P			
113	P				10		P		P(4)	
114	P	10	10	10	10		P		P(4)	
118	F				10	10	10	10	10 (U, 0.2um)	Exp 7
119	P	10	10	10	10	10, 25	P		P(4)	

continued on next page

continued from previous page

CTD	TMC	C uptake parameters			Photoinhibition		Fe analysis		Ligand	Fe/ligand
Station	cast	eCA	M M	Iso	PE-curve	exp	DFe	TFe	analysis	exp
126	P	10		10	10		P			
127	P	10	10	10	10, 25	10, 25	P			
129	F	10	10	10	10, 10+L	10	10	P	10 (SF, U, 0.2um)	Exp 8
131	P	10	10	10	10	10, 25	P	P		
133	P	10	10	10	10	10, 50	P	P		
135	F				10	10	10	10	10 (U, 0.2um)	Exp 9
138	P	10	10	10	10		P			
140	P	10	10	10	10, 10+L	10, 25	P			
142	P	10	10	10	10		P	P		
148	F, P	10	10	10	10, 10+L	10	P	P	10 (SF, U, 0.2um)	Exp 10
153	P	10	10	10	10	10	P			
158	F, P	10	10	10	10, 10+L	10	P	P	10 (U, 0.2um)	Exp 11
160	F, P	10	10	10	10	10	P	P		Exp 12

Table 7: CTD stations and water depths of experiments and analyses by the DynaLiFe project during the NBP0901 cruise. See text for an explanation of the different analyses.
P = TMC profile of 6 waterdepths , 10, 25, 50, 100, 200, 300m
F = frame, 80L of TMC water at 10m
P(4)* = 50, 100, 200, 300m
P(4) = 25, 50, 100, 300m
SF = size fractionation
U = unfiltered water
10+L = PE-curve with the addition of lincomycin

8.2 Work at Sea

Characteristics of carbon uptake by natural phytoplankton assemblages

Christopher Payne and Philippe Tortell (not on board)

While carbon (C) acquisition has been relatively well characterized in laboratory cultures of phytoplankton, little information is available on the C uptake physiology of natural phytoplankton assemblages. During this cruise we measured several aspects of C uptake physiology using both membrane-inlet mass spectrometry (MIMS) and radioactive C (^{14}C) assimilation experiments. For all these experiments, phytoplankton collected from the surface ocean waters were concentrated by gravity filtration and resuspended into seawater buffers.

Extracellular carbonic anhydrase (eCA) activity Carbonic anhydrase is an enzyme which catalyzes the inter-conversion between the dominant forms of C in seawater, HCO_3^- and CO_2. We measured the rates of eCA in phytoplankton concentrates by adding $^{13}C^{18}O_2$ and monitoring the rates of change of masses 45, 47 and 49 using the MIMS. eCA rates varied from background (physical exchange only, no biology) in upwelling areas near the PIG to 30 times background at diatom-dominated off-shelf stations (1 & 160). eCA rates at ice stations and at the *Phaeocystis*-dominated polynya stations were highly variable.

Michaelis-Menten Kinetics We assessed the C uptake affinity of these same natural phytoplankton assemblages by measuring the rate of ^{14}C fixation in concentrated samples with increasing amounts of total DIC (dissolved inorganic carbon) over a short time-course experiment (10 minutes). By fitting a Michaelis-Menten type hyperbola to the data (Fig. 33) we are able to determine the half-saturation constant for C

uptake (K_m) as well as the maximum C uptake rate (V_{max}). In ice and polynya stations, half-saturation constants ranged from 234 mM to 1541 mM with lower values at high-productivity, low-pCO_2 stations. Upwelling stations near the Pine Island Glacier stood apart from all other stations, with very low $V_{max}$and very high K_m(754 mM to 3656 mM).

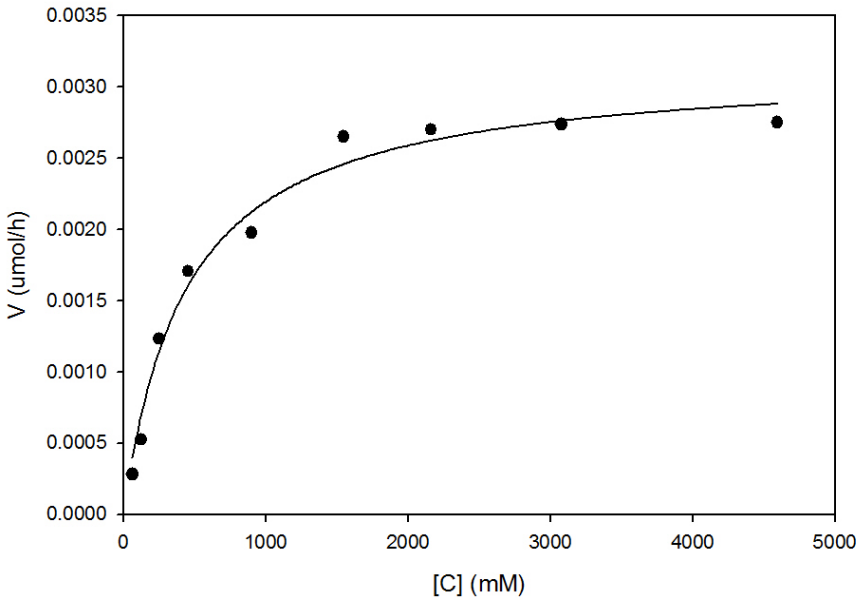

Figure 33: Phytoplankton carbon uptake rate as a function of total dissolved inorganic carbon for station 102, a *Phaeocystis*-dominated station in the Pine Island Polynya.

Isotope Disequilibrium We used the isotope disequilibrium technique to determine the relative fraction of HCO_3^- and CO_2 uptake in concentrated cell suspensions, and the relative activity of extracellular carbonic anhydrase (eCA). Essentially, short-term cellular ^{14}C fixation is monitored during a transient disequilibrium between $^{14}CO_2$ and $H^{14}CO_3^-$ in solution. A pH 7.0 ^{14}C spike is added to the concentrated cell suspensions (pH 8.5) to initiate ^{14}C uptake. Subsamples are withdrawn from the cuvette with a pipette and transferred at short intervals into scintillation vials containing 6 N HCl, thereby terminating C uptake. This procedure is then repeated with the addition of dextran-bound sulfanilamide (DBS), an eCA inhibitor. By quantifying the curvature of the uptake curves as the ^{14}C equilibrates to pH 8.5 we are able to determine the relative amount of HCO_3^- uptake (f, fraction of total C uptake), as well as eCA activity (Fig 34). This measure of eCA activity is indirect but completely independent from the eCA activity measured using the MIMS and can therefore be used as confirmation of rates measured using the MIMS.

These experiments revealed that HCO_3^- transport is the dominant mechanism of inorganic C uptake in all areas studied (f ranged from 0.83 to 0.95). The relative importance of HCO_3^- use was not related to phytoplankton biomass, productivity, or ambient CO_2 concentrations at individual sampling stations. eCA rates measured ranged from 0.0061 (uncatalyzed rate constant, indicating no external CA activity) up to 0.03. As for f, no pattern was observed with eCA activity and either phytoplankton biomass or ambient CO_2 concentrations. eCA rates measured by isotope disequilibrium were correlated to those measured by MIMS.

Diatoms and *Phaeocystis Antarctica* (the 2 main phytoplankton types found during this cruise) may have very different C uptake affinities and mechanisms, thus further analyses back in the laboratory (phytoplankton cell counts and HPLC pigment measurements) will be useful in teasing apart the variability measured during this cruise.

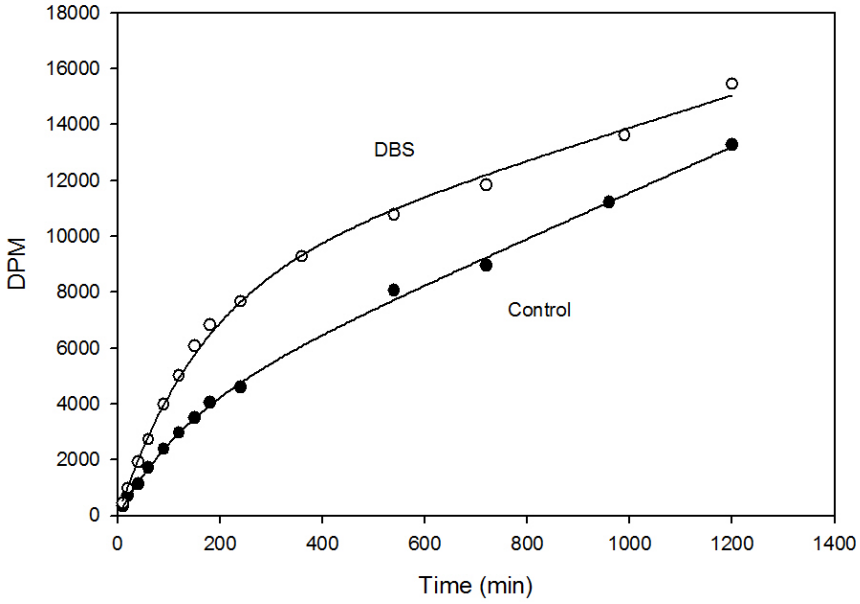

Figure 34: Isotope disequilibrium experiment from station 131, a diatom-dominated station in the ice. Filled circles represent an un-amended cell suspension and open circles represent the same cell suspension amended with DBS, an extracellular carbonic anhydrase inhibitor.

Photosynthesis vs. Irradiance characteristics

Gert L. van Dijken

During this cruise a total of 163 P-E curves (photosynthesis vs. irradiance) were made to study the characteristics photosynthesis by natural phytoplankton assemblages at different light levels. These are used to determine maximum photosynthetic rates, the light intensity to which the phytoplankton is adapted, light limited rates of photosynthesis and photoinhibition parameters.

For this 13-14 20 mL PET scintillation vials were filled with 10mL of seawater sampled with trace metal clean GoFlo bottles. Radiolabelled bicarbonate ($H^{14}CO_3$) was added (1 μCi/mL of seawater) before the vials were transferred into a photosynthetron where they were incubated for 2 hours at 2^{o}C under different light conditions, ranging from 2 to >600 μEin m^2 s^{-1}. After incubation samples were filtered over Whatman GFF filters under very low vacuum pressure (<50 mm Hg). The filter was returned into the thoroughly rinsed vial and 2 mL of MilliQ water and 100 μL of 6N HCl were subsequently added. The vials were gently shaken for at least 18 hours to drive off inorganic carbon. After neutralization with 100 μL 6N NaOH, 6 mL of scintillation cocktail was added. The samples were counted for 10 minutes on a liquid scintillation counter.

P-E curves were made at 45 stations (Table 7), whereas at 23 stations a second P-E curve was made where the filtration step was skipped. This was done to determine if fixed radiolabelled carbon was lost during filtration, possibly due to breakup of *P. antarctica* colonies or cell leakage. For this, instead of 10 mL seawater sample only 2 mL was used and no MilliQ water was added. Additionally, 10 mL, rather then 6 mL, scintillation cocktail was added. At 5 stations the inhibitor lincomycin (final concentration 0.6 * 10^{-3} mol L^{-1}) was added to study the effects of repair processes under high light conditions (see photoinhibition section below). 78 P-E curves were made for the different treatments of the Fe/ligand bioassay experiments.

Lastly, for each P-E curve an absorption spectrum of the phytoplankton pigments was made on a Perkin

Elmer UV/VIS Lambda 18 spectrophotometer with an integrating sphere (Labsphere RSA-PE-18). The spectrum will be used to quantify the amount of light absorbed during the photosynthetron incubation and subsequently calculate quantum yield of photosynthesis. Water samples were filtered over GFF filters. The filter was mounted in front of the integrating sphere and light absorption was measured from 300-800 nm. Detrital absorption was measured after extraction of sample in 80% methanol.

Photoinhibition in Antarctic phytoplankton

Anne-Carlijn Alderkamp

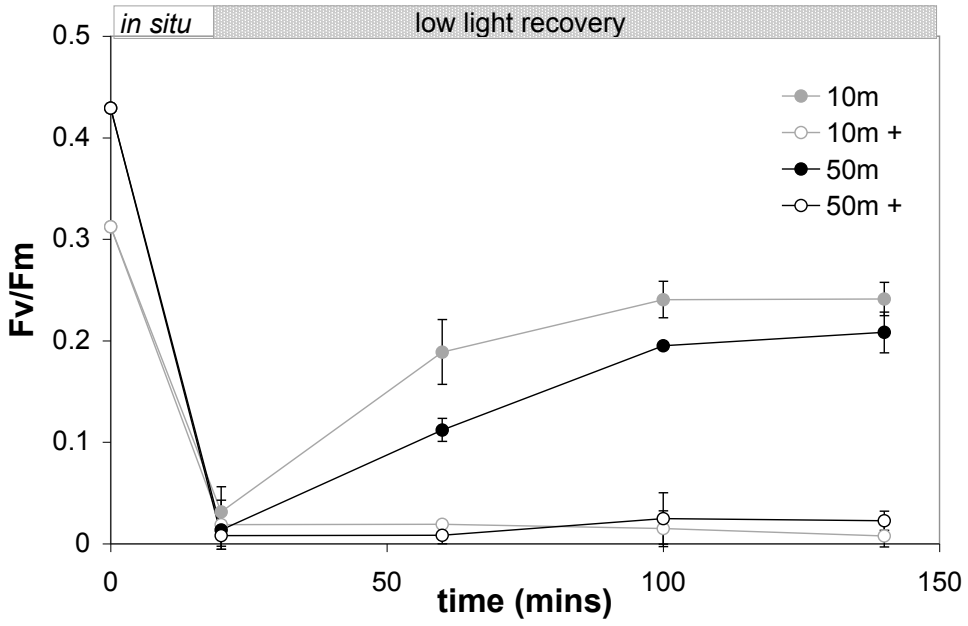

Figure 35: A typical example of photochemical efficiency of photosystem II (Fv:Fm) dynamics during a deck incubation followed by recovery under low light conditions. Means and standard deviations are shown for triplicate incubations of water collected at 10m and 50m depth, without and with (+) the addition of lincomycin, an inhibitor of repair of photosystem II.

Phytoplankton residing in the upper 100 meters of the water column receive a variable light climate due to seasonal and dial light cycles, changes in ice and cloud cover, and wind driven vertical mixing of the watercolumn. These alterations require acclimation of light harvesting and protective mechanisms to ensure maximum photosynthetic efficiency at low light levels and protection from photoinhibition at high light and UV levels. The objective of the NBP0901 cruise is to determine 1) if Antarctic phytoplankton experience photoinhibition when residing near the surface, 2) if photoinhibition is related to the depth of the mixed layer, and 3) the importance of repair of photodamage versus photoprotection.

Short term deck incubations were caried out at 31 stations in the Amundsen Sea, representing different natural phytoplankton assemblages at various stages of a phytoplankton bloom. The depth of the mixed layer was determined based on the CTD profile. Samples contaning *in situ* phytoplankton were collected from surface water and the chlorophyll maximum. The maximum photosynthetic efficiency of photosystem II (Fv:Fm) was analyzed with a PAM fluorometer. Samples were incubated for 20 mins at incident light levels in deck incubators. The decrease in photosynthetic efficiency of photosystem II (Fv:Fm) of the phytoplankton was determined by PAM fluorometer. Subsequently, recovery of photosynthetic efficiency was measured during incubation at in situ temperatures and low light levels. In parallel experiments, the repair

of photodamage was prevented by addition of 0.6 * 10−3 mol L^{-1} (final concentration) of the inhibitor lincomycin. Lincomycin inhibits transcription of chloroplast encoded proteins, such as the D1 protein, which is a crucial component of photosystem II and one of the first proteins to become damaged by high light.

Preliminary data A significant decrease in photosynthetic efficiency of photosystem II was observed after incubating *in situ* phytoplankton samples in deck incubators at incident light levels (Fig. 35), both for samples from the surface as well as the chlorophyll maximum. Part of the decrease in photosynthetic efficiency was reversible during 120 mins of recovery under low light conditions. The inhibition of repair by the addition of lincomycin did not affect the decrease in photosynthetic efficiency directly after exposure to surface irradiance, but reduced the recovery in almost all experiments. The addition of lincomycin in PE curves (G. van Dijken, see PE-curve section) confirmed significant photoinhibition at high light levels (> 300 μE m^{-2} s^{-1}) when repair was inhibited. Experiments conducted early in the morning, or at low incident light levels showed the least photoinhibition, which was rapidly reversed. Experiments conducted at higher light levels showed strong photoinhibition, that was not (completely) reversed during 120 mins of recovery. In these cases, lincomycin prevented recovery completely, as shown in Fig. 35.

Future work The microscopic analysis of phytoplankton slides, as well as the analysis of photo-synthetic and -protective pigments will be related to the characteristics of the mixed layer to help explain differences observed in the dynamics of photosynthetic efficiency in the experiments

Concentrations of dissolved iron in the Amundsen Sea

Patrick Laan

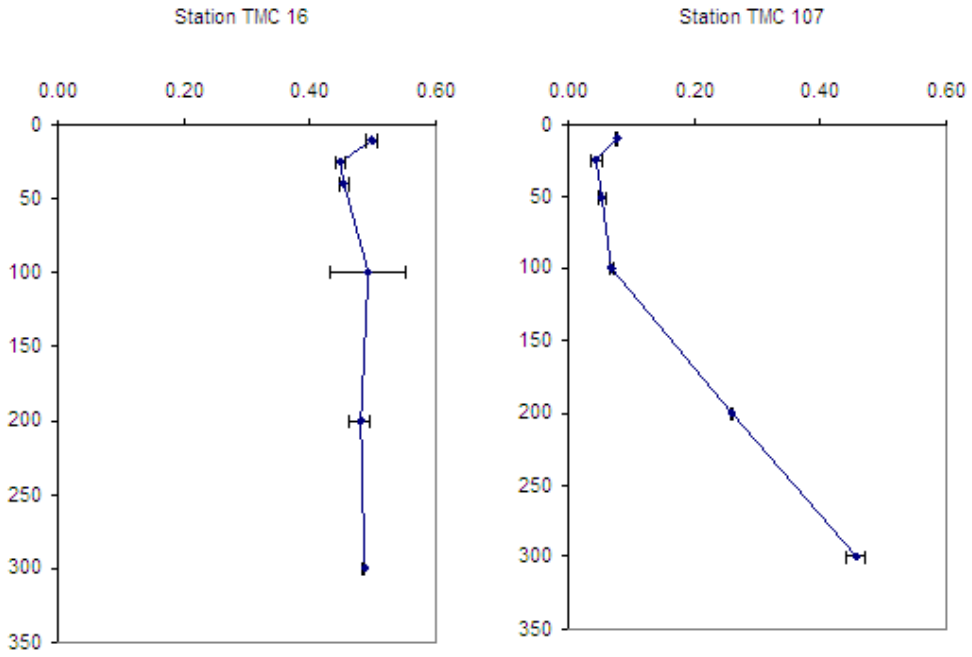

Figure 36: Depth profile of dissolved Fe concentrations from stations 16 (upwelling at the southern end of the PIG) and 107 (central Pine Island Polynya).

Dissolved iron (DFe) concentrations of 40 profile stations and 7 surface stations were measured directly on board by an automated Flow Injection Analysis (FIA) after a modified method of De Jong et al. 1998. In

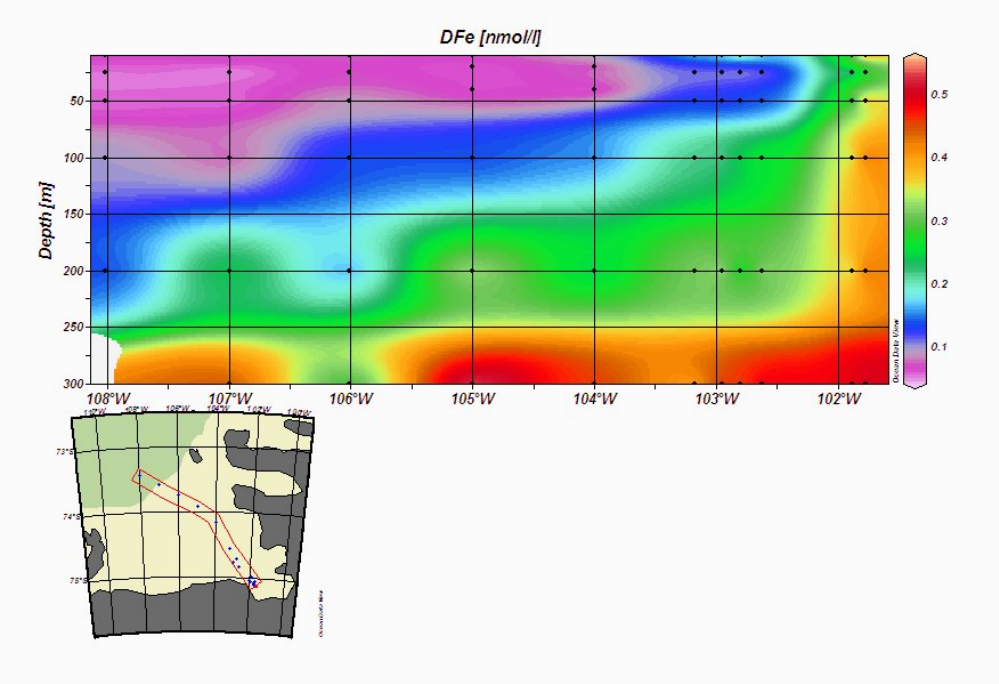

Figure 37: Section plot of dissolved Fe concentrations from the PIG area through the central Pine Island Polynya.

addition, unfiltered samples from 17 profiles and 7 surface stations were acidified and stored to determine the total Fe concentrations in the NIOZ laboratory after 6-12 months of dissolution (see table 7). Filtered (0.2μm) and acidified (pH 1.8) seawater was concentrated on a column containing aminodiacetid acid (IDA). This material binds only transition metals and not the interfering salts. After washing the column with ultra pure water, the column is eluted with diluted acid. After mixing with luminol, peroxide and ammonium, the oxidation of luminol with peroxide is catalyzed by iron and a blue light is produced and detected with a photon counter. The amount of iron is calculated using a standard calibration line, where a known amount of iron is added to low iron containing seawater. Using this calibration line a number of counts per nM iron is obtained. Samples were analyzed in duplicate sample bottles, each of which was measured in triplicate, and average DFe concentrations and standard deviation are given. Concentrations of DFe measured on the NBP0901 cruise ranged from 30 pM up to 0.7 nM. The standard deviation varied between 0% and 10% (the latter being exceptional), but was generally $< 5\%$ in samples with DFe concentrations higher than 0.1nM. Since samples containing less than 0.1nM DFe are near the detection limit of the system; the standard deviation of these measurements was sometimes high (<30%).

The average blank was determined at 0.024nM±0.010nM and was defined as a sample loaded for 10 seconds and measured daily. The average limit of detection, 0.009±0.008 was defined as 3*standard deviation of the mean blank and measured daily. To better understand the day to day variation duplicate sample bottles were measured at least 24h later. The differences between these measurements were rather large, in the order of 5-20%, while the largest differences were measured in samples with low DFe concentrations. To correct for this day to day variation a so-called lab standard sample was measured daily. All data will be corrected for the mean average of this value after the cruise and all data presented so far are uncorrected for this day to day variation. The consistency of the FIA system over the course of the day was verified using a drift standard. The drift was observed to be less than 7% and no corrections have been made for this drift. A certified SAFe standard (Johnson et al. 2007) for the long term consistency and absolute accuracy was measured at a regular basis.

Preliminary results The profile from station 16 clearly shows high iron input near the PIG (Fig. 36). DFe concentrations are high throughout the entire water column and indicate a constant input of DFe into the polynya. Profile 107, which is in the central Pine Island Polynya, shows much lower values throughout the first 300 meter which can be explained by the high phytoplankton abundance in the surface water. DFe concentrations during a transect from Pine Island Glacier (PIG) (101 S,30W) through the central Pine Island Polynya in north westwards direction clearly show the high DFe concentrations near the PIG and the rapid decrease of the DFe in the polynya, especially in waters shallower than 50m (Fig. 37). Extreme low DFe values in the central polynya correlate with the biological productive area as observed from the fluorometer data and Chl *a* measurements.

Physical and chemical speciation of iron in seawater

Charles-Edouard Thuroczy

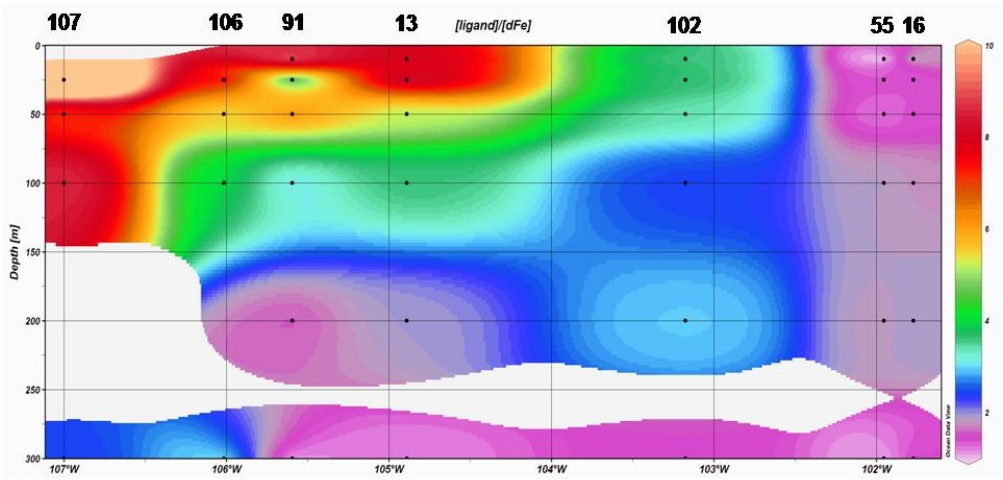

Figure 38: Section plot of the ratio of ligand/dFe concentrations from the PIG area through the central Pine Island Polynya. CTD station numbers are indicated above the graph.

The distribution and biological availability of Fe is strongly controlled by its physical-chemical speciation within seawater, where colloids and Fe-organic complexes are dominant factors. In order to study the distribution and the biological availability of Fe the natural Fe organic complexes were determined in the surface waters of the Amundsen Sea (300 m).

Methods Samples were collected using Go Flo bottles and filtered under ultra-clean conditions in flow benches (class 0). The concentration of iron binding ligands (organic compounds which strongly bind Fe) and their binding strength (conditional stability constant) were studied in 5 size classes here: unfiltered water, 0.2 μm filtered water, $<$ 1000 kDa (Stereapore, Mitsubishi-rayon Co. Ltd, Nishioka and al., 2000, 2005), $<$ 100 kDa and $<$ 10 kDa ultra-filtrated water (Sartorius, Vivaflow 50, Schlosser and Croot, 2008). The left-over fraction from the ultra filtrations (retentates) were also analyzed for dFe and ligand characteristics to ensure a mass balance calculation and validate the ultrafiltration method.

The dissolved iron concentrations in all the size fractions (and retentates) were measured (see dFe measurement section) using a chemo luminescence method (FIA) with acidified samples (pH 1.8). Total iron concentrations will be measured 6-12 months after the acidification of the unfiltered sample.

Ligand characteristics were determined by using a complexing ligand titration with addition of iron (between 0 and 10 nM of Fe added) in buffered seawater (mixed NH_3/NH_4OH borate buffer, 5 mM). The competing

ligand 'TAC' (2-(2-Thiazolylazo)-p-cresol) with a final concentration of 10 μM was used and the complex $(TAC)_2$-Fe was measured after equilibration (> 15 h) by cathodic stripping voltammetry (CSV) (Croot and Johansson, 2000). The electrical signal recorded with this method (nA) was converted to a concentration of $(TAC)_2$-Fe (nM). Subsequently, the ligand concentration and the binding strength were estimated using the non-linear regression of the Langmuir isotherm (Gerringa and al., 1995) and a newer "Leo" model currently built up (Gerringa et al , in prep). The voltammetric equipment consisted of a μAutolab potentiostat (Type II and III, Ecochemie, The Netherlands), a mercury drop electrode (model VA 663 from Metrohm). All equipment was protected against electrical noise by a current filter (Fortress 750, Best Power).

Sampling statistics 26 stations were sampled on this cruise (see table 7). These included 14 profiles and 5 stations where different size fractions were analyzed after 4 filtrations with different filter sizes (0.2 μm cut-off, 1000 kDa, 100 kDa and 10 kDa). In addition, 11 Fe/Ligand experiments were analyzed (see Fe/ligand experiment section). Special attention was given to determine the iron binding ligands before and after incubation with and without artificial ligands in these experiments, to look at the response of algae and the change of the ligand characteristics during the incubations.

Preliminary results An average ligand concentration of 0.789 nEq was found on the NBP0901 cruise, varying from 0.2 and 1.6 nEq of Fe. Highest ligand concentrations were found at 10 m depth followed by a minimum at 25 m. Concentrations increased with depth to become rather constant at 200 and 300 m. Low Fe binding strength of the ligands was found at 10 and 25 m in the polynya suggesting freshly produced ligands by organisms (phytoplankton or bacteria) or by a change in the ligand content and characteristics due to the biologic activity (the pool of strong binding ligands may be removed or used).

The ratio ligand/dissolved iron (Fig. 38) clearly shows differences between the surface water and deeper samples. Very high ratios (∼10) were found in the surface waters of the Pine Island polynya due to the low dissolved iron concentration and high ligand concentrations. In the deep water (200 and 300 m) of the polynya and the circumpolar deep water upwelling in front of the PIG the ligand/dissolved iron ratio was close to 1 indicating a saturation of the ligands by iron and the possibility for iron to be removed from the water column by precipitation.

Fe/Ligand Bioassay Experiments

Matthew M. Mills

Methods We conducted a total of 12 bioassay experiments investigating phytoplankton utilization of iron (Fe) and ligand bound Fe (Table 1). Trace metal clean techniques were used throughout the preparation and execution of the bioassay experiments. Surface seawater (60 L) was collected from ∼10 m using Go Flo bottles and used to randomly fill 2.0 L acid-washed polycarbonate bottles. Under a laminar flow hood located in a clean room, the bottles were amended with iron (Fe) and ligands, alone and in combination, to final concentrations of 4.0 nmole L^{-1}. Three different ligands were used; desferroxamine mysalate (DFB), phytic acid (PA), and -(-)gallocatechin (GA). In experiment 8 and 10, two additional treatments containing nitrogen were conducted. Treatments were thus; control (C), +Fe, +DFe, +PA, +GA, and +PA+Fe, +Ga+Fe, +NH_4NO_3, +NH_4NO_3+Fe. All treatments were conducted in triplicate. The bottles were then sealed with parafilm, placed in Ziplok bags, and set in on-deck incubators with circulating surface seawater for 4-5 days. The light level in the incubator was adjusted to 25% of incident irradiance. At termination of the experiments the control and +Fe treatments were sampled for dissolved Fe (dFe) concentrations (see dFe measurements section) and ligand measurements (binding strength and concentration, see speciation of iron in seawater section), while all treatments were sampled for the macronutrients NO_3^- and PO_4^{3-}, chlorophyll *a* (chl *a*) concentration, maximum photochemical efficiency of photosystem II (Fv:Fm), particulate organic carbon, nitrogen, and phosphorus, pigment analysis, and cell abundance. Subsamples from each treatment were pooled and $^{14}CO_2$ fixation was measured at increasing irradiance (photosynthesis vs. irradiance; see

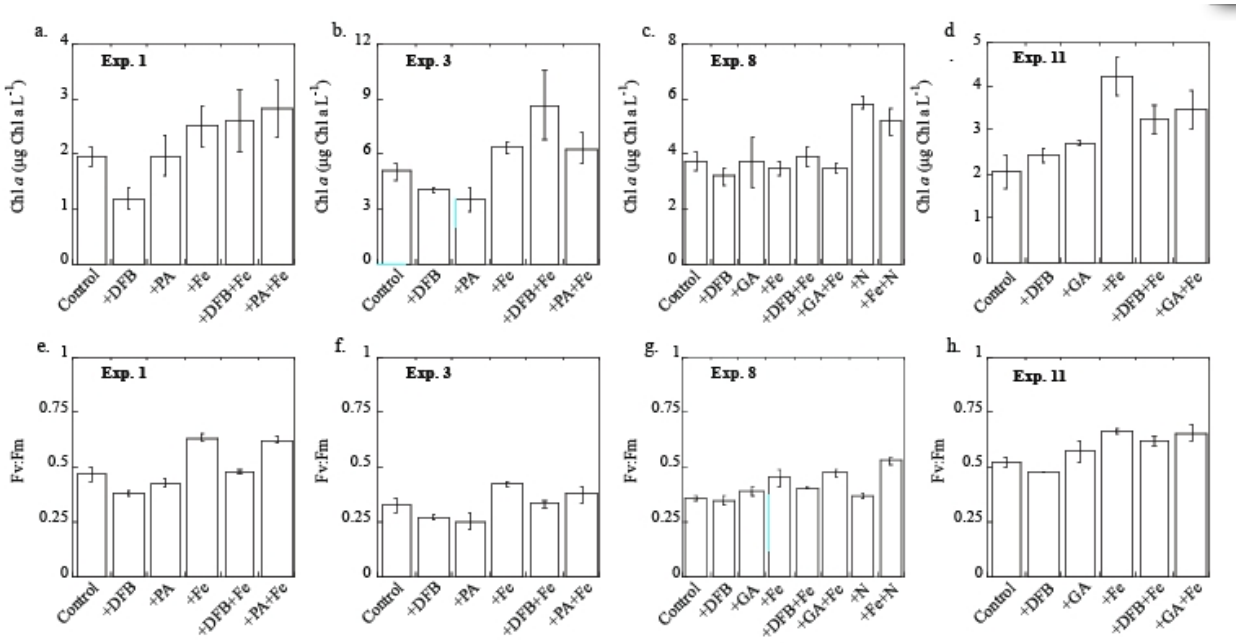

Figure 39: Mean (±sd) chlorophyll *a* (a-d) and photochemical efficiency of photosystem II (Fv:Fm, e-h) responses in four of the Fe/ligand bioassay experiments.

P vs. E section). Additionally, the effect of Fe limitation on photoinhibition and recovery characteristics of the phytoplankton was determined in short-term deck incubations described in the photoinhibition section above.

Preliminary results The responses to the Fe and ligand amendments were variable between experiments. For experiment 1, started in the ice just north of the Pine Island Polynya (Fig. 39a), Chl *a* concentrations in the +Fe treatments were approximately 30% higher than in the control treatment. Fv:Fm responded similarly in the +Fe and +PA+FE treatments, while the +DFB+Fe showed no Fv:Fm change relative to the control (Fig. 39e). In the ligand alone treatments both chl *a* and Fv:Fm decreased relative to the controls while no change was observed in the +PA amended bottles. Within Pine Island Bay the response to the +DFB amendment was similar as in Exp. 1, but the +PA addition resulted in both lower chl *a* concentrations and Fv:Fm (Fig 39b,f). However, when either ligand was added with Fe the chl *a* concentrations were higher in comparison to the control. In the center of the Pine Island Polynya (Fig. 39c,g) there was little chl *a* response to added Fe alone or when added with ligands, however Fv:Fm was higher in the Fe amended treatments. Surprisingly, chl *a* increased approximately 50% in those treatments amended with N. While no increase in Fv:Fm was observed in the +N treatments, higher values were recorded, relative to the control, when N and Fe were added together. These are the first data that we know of suggesting N can play a role in bloom termination in the algal blooms of the Amundsen Sea. Samples for macro-nutrient (NO_3^- and PO_4^{3-}) analysis were also collected and will help to confirm that NO_3^- was at limiting concentrations. Finally, in the sea-ice northwest of the Amundsen Polynya the phytoplankton were clearly Fe limited with strong responses (increases) in both chl *a* and Fv:Fm in those bottles amended with Fe (Fig. 39d,h). Both DFB and GA had similar, if not slightly higher chl *a* concentrations, in comparison to the control when added alone, though little change in Fv:Fm was observed in these treatments. Additions of either ligand with Fe resulted in similar responses to the Fe alone addition.

Overall, the data from Fe/ligand bioassay experiments suggest that the phytolankton communitites in and around the Amundsen Sea are able to access ligand bound Fe, though the between experiment variability suggests a differential ability to utilize this Fe source which may be specific to different algal communities.

Both GA and PA, at times, resulted in equal or slightly higher chl *a* concentrations relative to controls when added alone, and enhanced chl *a* when added with Fe. In contrast, DFB often resulted in lower chl *a* and Fv:Fm when added alone and did not always stimulate chl *a* equal to the Fe addition alone. The results suggest Fe bound to DFB is less available to phytoplankton than Fe bound to either PA or GA. Further analyses characterizing the phytoplankton communities within the experiments will help to understand the connection between different phytoplankton and their ability to use ligand bound Fe.

8.3 Underway Data Acquisition

Remote Sensing

Gert L. van Dijken

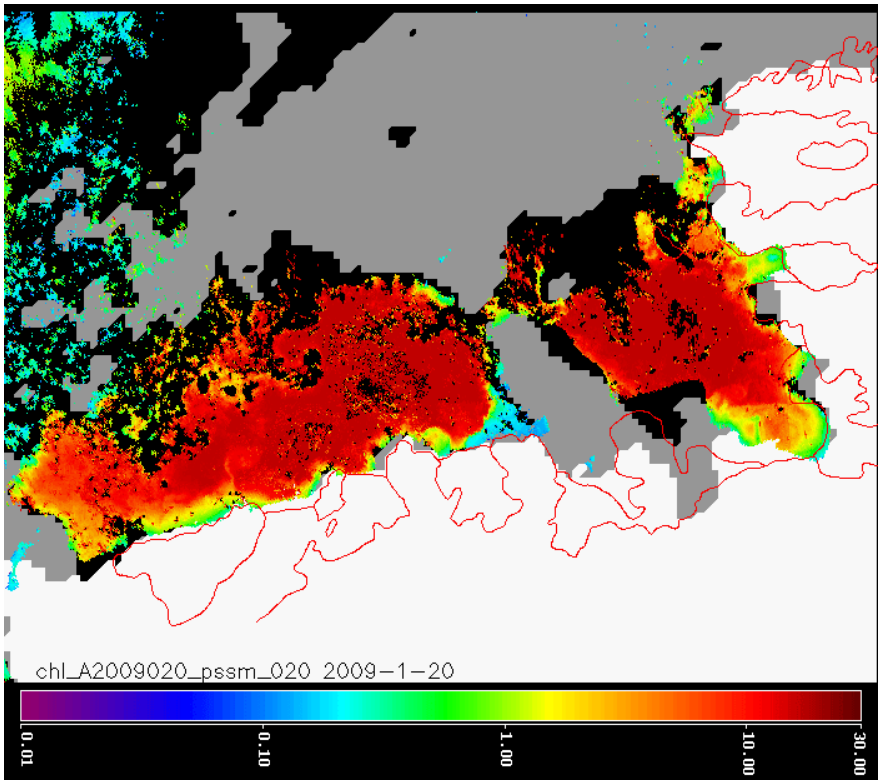

Figure 40: Oceancolor image showing the 2 intense phytoplankton blooms in the Amundsen Sea. This daily composite is based on 5 individual MODIS/Aqua satellite scenes from January 20, 2009. Color legend shows chl *a* concentration (mg chl *a* m^{-3}). PSSM ice cover of the same day derived from SSM/I satellite data is shown as grey. White is continent/ice shelves and red is the coastline.

Ocean color satellite imagery was used to follow the spatial extent and temporal development of the intense phytoplankton blooms in the Pine Island and Amundsen polynyas. An automated system was set up at Stanford University where near real-time satellite imagery acquired by the MODIS/Aqua sensor was downloaded every 3 hours from NASA ftp-servers. The chlorophyll product was extracted, somewhat manipulated and mapped to a common polar stereographic projection. In addition daily composites were generated from the individual scenes (4-6 per day). On these daily chlorophyll composite images ice cover was superimposed (see figure 40). The ice data was generated from SSM/I brightness temperatures, retrieved twice daily from the NSIDC ftp-site and processed to sub-pixel resolution (6.25 km) using the PSSM algorithm. Finally, all processed MODIS scenes and daily composites were automatically e-mailed to the R/V N.B Palmer in PNG

format.

Underway gases/MIMS

Christopher Payne, Philippe Tortell (not on board)

The fine-scale (<10-100 km) distribution and variability of Southern Ocean gases remain poorly described, particularly in ice-covered regions and in the Amundsen Sea polynya. On this cruise we measured real-time underway concentrations of the biogenic gases CO_2, O_2/Ar, N_2/Ar and dimethylsulfide (DMS) using membrane-inlet mass spectrometry (MIMS). During our southbound and northbound transits to and from the Amundsen Sea we observed very little change in gases, with O_2/Ar and CO_2 near atmospheric equilibrium. Once in the ice and in the polynya we observed dramatic changes in all gases on very small time and spatial scales. pCO2 concentrations ranged from 83 μatm to 500 μatm, with the lowest values corresponding to the transit through the blooming phytoplankton in the Pine Island Polynya (PIP). O_2/Ar and CO_2 were strongly anti-correlated throughout the study area, indicating that biological activity rather than physical effects exerted a dominant control on CO_2 and O_2 distributions in this region. DMS concentrations were very low in the Southern Ocean transits and much higher and variable in the ice and polynya . At one point during the initial transit through the PIP, DMS concentrations of 350nM were measured. This is approximately 2x higher than we have measured during 2 previous cruises to the Ross Sea. Large shifts in DMS concentrations were often, but not always, correlated with shifts in both CO_2 and O_2.

References

Arrigo, K.R., and G.L. van Dijken (2003) Phytoplankton dynamics within 37 Antarctic coastal polynya systems. J. Geophysical Res. Vol. 108, C8, 3271

De Baar, H.J.W., K.R. Timmermans, P. Laan , H.H. De Porto, S. Ober,J.J. Blom, M.C. Bakker, J. Schilling, G. Sarthou, M.G. Smit and M. Klunder (2008) Titan: A new facility for ultraclean sampling of trace elements and isotopes in the deep oceans in the international Geotraces program, Marine Chemistry, 2008

Johnson et al., 2007. Developing standards for dissolved iron in Seawater. Eos, Vol 88, n. 11.

De Jong, J.T.M, den Das, J. , Bathman, U., Stoll, M. H.C., Kattner, G., Nolting, R.F., and de Baar, H.J.W. (1998). Dissolved iron at subnanomolar levels in the Southern Ocean as determined by shipboard analysis. Analytica Chimica Acta, 377, 113-124.

Croot P.L., Johanson M. (2000). Determination of iron speciation by cathodic stripping voltammetry in seawater using the competing ligand 2-(2-Thiazolylazo)-p-cresol (TAC). Electroanalysis. 12, No.8, 565-576.

Nishioka J., Takeda S., de Baar H.J.W., Croot P.L., Boye M., Laan P., Timmermans K.R. (2005). Changes in the concentration of iron in the different size fractions during an iron enrichment experiment in the open Southern Ocean. Marine Chemistry. 95, 51-63.

L.J.A. Gerringa, P.M.J. Herman, T.C.W. Poortvliet (1995). Comparison of the linear Van den Berg/Ruzic transformation and a non-linear fit of the Langmuir isotherm applied to Cu speciation data in the estuarine environment. Marine Chemistry. 48, 131-142.

9 Other Sampling and Profiling

9.1 O-18

Chris Little, Stan Jacobs

On selected CTD stations, water samples were drawn for later oxygen isotope analysis. Sampling was focused on waters near and above the pycnocline, likely to contain evidence of glacial meltwater, and in the surface and Tmin layers, more influenced by sea ice melting and freezing. Occasional deep samples were also taken for reference values. The work was done by C Little, K Leonard, R Robertson, and K Mankoff according to the procedures provided (dump, triple rinse and fill, leaving a little head space). In all, 455 d18O samples were taken from 92 CTD/rosette casts; one surface sample was taken from the seawater line. The samples will be analyzed at a laboratory in the US that can achieve an accuracy of better than 0.03 per mil.

9.2 TCO_2

Stan Jacobs, Sharon Stammerjohn, and Robin Robertson

In support of the underway pCO_2 monitoring project (Takahashi & Sweeney, PIs), samples were drawn twice daily for total CO_2 (TCO_2) from the ships uncontaminated seawater line. CTD/rosette casts along two roughly N-S transects across the Amundsen continental shelf were also sampled for TCO_2. The latter sampling was light by Wocean standards, but should be sufficient to define the upper water column above the temperature maximum, i.e., waters that have had recent contact with the sea surface, or have likely mixed with same. It should also complement TCO_2 work done aboard ship in the Amundsen Sea during NBP94-02. Some deeper samples were taken for reference, along with duplicates on two stations, and a reoccupation of site 727 from the 1992 SO4 line. The TCO_2 samples will be returned to US laboratories for processing.

9.3 Drifters

Stan Jacobs and the RPS MTs

Eleven APEX floats were deployed by the RPS MTs in the northern Amundsen Sea for S Riser and R Rupan of the Univ of Washington. Rupan set up the drifters in Punta Arenas prior to the cruise and specified that they be deployed in the Amundsen, but in water deeper than 3000 m and 100 km apart. This relegated them to the region north of the continental rise. All but one drifter, which was launched shortly after leaving the Chilean EEZ (200 nm from the coastline), were ice capable, although icebergs and seamounts in the deployment areas could present operational challenges. The floats reside for most of the time near 1000 m, making a profile once every 10 days first to 2000 m, rising to the surface to transmit data, then returning to 1000 m. Notifications were sent to R&R @ Udub after each 1-2 deployments indicating float number, ship position and other parameters. Drifter data may be logged at http://www.runt.ocean.washington.edu/ice

9.4 ADCP

Pierre Dutrieux

Upper ocean currents are routinely measured aboard the NB Palmer by Ship-mounted Acoustic Doppler Current Profilers (SADCP). Two instruments are currently mounted: a 150 kHz Work Horse and a 38 kHz Ocean Surveyor from RD Instruments. The higher-frequency unit measures currents from 36 to 416 m depth with a 10 m bin vertical resolution, although most measurements rarely reach below 300m. The

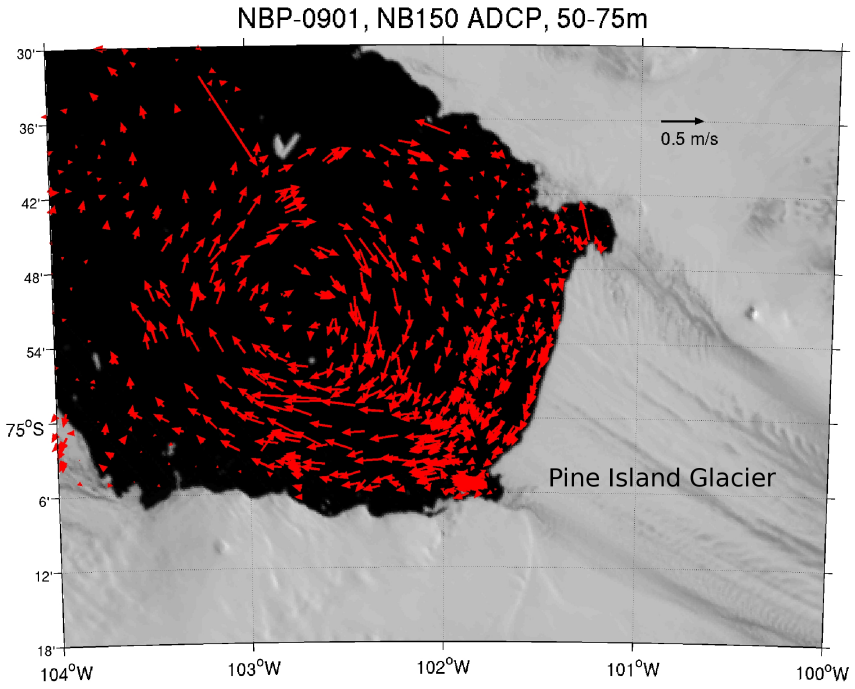

Figure 41: Currents measured from the 150 kHz Work Horse SADCP during NBP09-01 in front of the Pine Island Glacier, averaged as vectors showing speed and direction from 50 to 75 m depth. The background is a MODIS satellite image from December 28, 2008.

lower-frequency device could have been an invaluable instrument to the campaign scientific objectives, with its ability to measure currents down to 1200 m. However, it was nonfunctional again during NBP09-01, as on the last Amundsen Sea cruise.

Preliminary data processing and recording is automatically and routinely done on board using a setup created and maintained by E Firing and J Hummon from the University of Hawaii. The preprocessed data is available in 15 minute bin-averaged Matlab format binary files. Further processing and editing will be necessary at the end of the cruise, and the data will be made available at 2 or 5 minute bin average formats.

Environmental conditions were excellent for SADCP observations in the ice-free Pine Island Bay in early 2009, and the extensive work in front of the Pine Island Glacier resulted in a comprehensive survey of the near surface ocean currents there. Figure 41 shows the measured currents, accurate to ∼2 cm/s in most cases, averaged from 50 to 75 m at the time of the cruise. In general, currents were slightly surface intensified, but consistent in direction over the top 300 m, and were dominated by a cyclonic gyre in front of the glacier. This feature is represented by a doming of the thermocline at the centre of the gyre in CTD observations.

9.5 PIG Frontal Transect

Ken Mankoff, Katherine Leonard, Kathleen Gavahan

On January 28, 2009 between 1400 and 1830 GMT The Nathaniel B. Palmer (NBP) sailed at 5 knots (kts) along a track 0.2 nautical miles (nm) from the Pine Island Glacier (PIG) ice front, from the northern to southern end. Expendable Bathy-Thermographs (XBTs) were deployed at 15 minute intervals to measure temperature. Synchronous with XBTs the following data were obtained: Distance from the ice shelf (obtained from the NBP bridge radar), height of the ice shelf (via sextant), draft of ice shelf (via NBP multibeam), visual description and photography of the ice shelf and local conditions, underway ship data

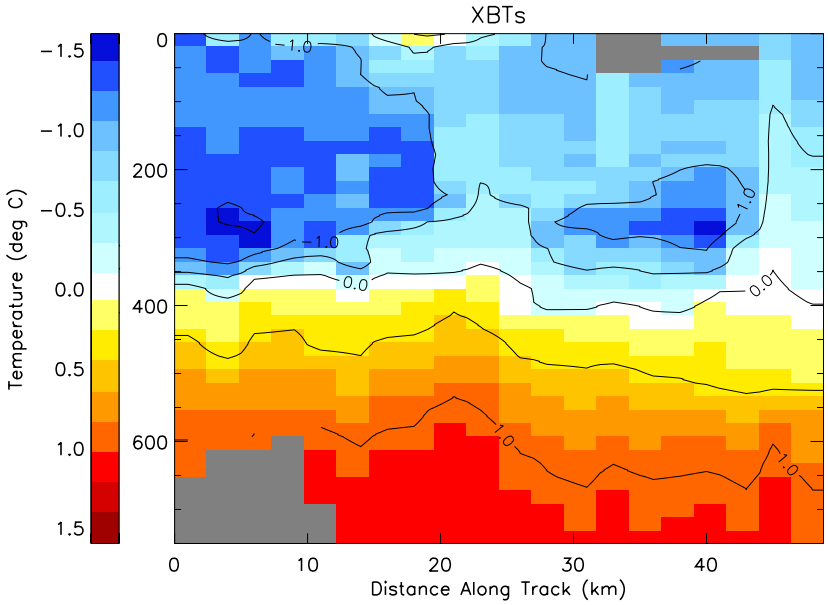

Figure 42: XBTs gridded as if they were evenly spaced along-track. The left side of the image is in the northern notch and the right side in the southern notch. Both contours and colors show temperature.

Latitude	Longitude	Radar (nm)	Obs. (m)	Angle	Height	XBT
-74 45.52	-101 15.39	0.187	336.55	06 40.6	39.4	48
-74 46.50	-101 19.46	0.271	492.22	05 26.4	46.9	49
-74 47.56	-101 21.79	0.265	477.80	06 07.0	51.2	50
-74 48.79	-101 23.61	0.158	279.51	11 17.8	55.8	51
-74 50.03	-101 24.25	0.215	385.14	08 40.6	58.8	52
-74 51.63	-101 24.79	0.195	348.07	09 08.6	56.0	53
-74 52.60	-101 26.01	0.183	325.84	08 24.2	48.1	54
-74 53.96	-101 26.83	0.165	292.48	08 52.0	45.6	55
-74 55.30	-101 28.59	0.165	292.48	09 13.8	47.5	56
-74 56.57	-101 30.37	0.180	320.28	08 08.6	45.8	57
-74 57.87	-101 31.76	0.182	323.98	08 21.8	47.6	58
-74 59.19	-101 32.95	0.162	286.92	10 39.6	54.0	59
-75 00.44	-101 34.81	0.163	288.77	09 57.0	50.7	61
-75 01.63	-101 37.30	0.200	357.34	08 14.4	51.7	62
-75 02.48	-101 41.49	0.200	357.34	09 11.2	57.8	63
-75 03.46	-101 45.36	0.200	357.34	09 29.6	59.8	64
-75 04.47	-101 46.41	0.150	264.68	07 33.4	35.1	65
-75 06.02	-101 42.98	0.335	607.52	02 41.8	28.6	66

Table 8: Sextant angle and associated metadata for Pine Island Glacier freeboard measurements.

(from NBP Thermosalinograph (TSG)), ocean currents (NBP Acoustic Current Doppler Profiler (ADCP)), and bathymetry (NBP multibeam). In addition to this XBT transect, seen in Figure 42, Conductivity Temperature Depth (CTD) profilers were used to profile the water column in close geospatial (within 3 km) and temporal (within 11 days) proximity to the XBT stations. The metadata associated with each sextant reading is shown in Table 8. Additional analysis of data collected is included in a seperate PIG Transect report compiled by K Mankoff.

The PIG transect was performed to add to the limited knowledge base of West Antarctic floating glacial termini and specifically the interactions of PIG with the surrounding bay. Figure 42 shows a steep temperature gradient occurs at approximately 350 m, near the mean draft of the ice shelf. There is a warm vertical intrusion near the center of the image surrounded by two colder regions on either side near 300 m, and an anomalous vertical intrusion in the south notch (right side of figure).

9.6 Snowfall

Katherine Leonard

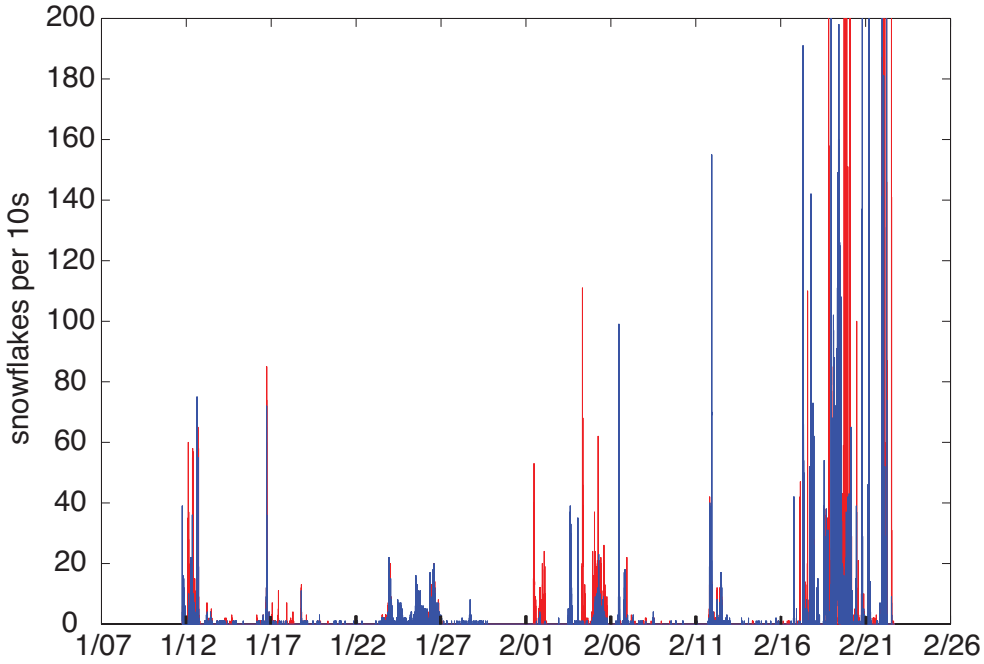

Figure 43: Snowfall measured by the particle counters on top of the ice tower. The red lines represent snowflakes blowing across the ship, the blue lines are snowflakes blowing parallel to the boat's long axis. Data are reported in flakes counted per ten second interval. The vertical scale has been abbreviated at 200, but counts exceeding that number were common at the end of the cruise.

The timing and relative intensity of snowfall events experienced during NBP0901 were measured using photoelectric particle counters mounted on the ship's ice tower, continuing measurements conducted on the ship during cruises NBP07-02 and NBP07-09. These earlier records show shipboard measurements are well correlated with the timing and relative intensity of precipitation forecast by the ECMWF and some other weather models. During the current cruise, two particle counters (Wenglor model YH03NCT08) were mounted on the forward edge of the top of the ice tower with one counter's beam aligned with the ship, and the other oriented across the ship's long axis.

To correlate the absolute magnitude of precipitation events documented on the ship with forecasts and reanalyses, knowledge of the size distribution and water equivalent mass contained in the falling crystals is necessary, so macrophotographs of snowflakes were taken by K. Leonard and M. Stenzel during the rare snowfall events during the Antarctic portion of the cruise. As shown in figure 43, snowfall was more frequent and more intense following our departure from the southern Amundsen Sea. Most snow observed consisted of rimed dendrites, with occasional events close to the continent consisting mostly of plates, sector plates, rare hollow columns, and one snowfall event composed entirely of ice needles up to 3.5mm in length. Snow captured adjacent to the Dotson Ice Shelf in figure 44 consists mostly of sector plates with significant rime

on them. A single hollow column is visible in this photograph, along with a few needles, and a number of crystals so heavily rimed that their identification is questionable. The heavy precipitation experienced north of 67^{o}S typically consisted of rimed dendritic flakes mixed with raindrops.

The most successful photographs (such as that in figure 44) were taken using an auto-focusing Canon 100 mm macro lens and extension tube during heavy snowfall in low-wind conditions or sheltered locations on the ship's deck. More detail for individual snowflakes was acquired using a manually-focused Nikon bellows system with a 55 mm macro, however the paucity of snow during the cruise and the ship's vibration made experimentation with different camera settings and configurations challenging. Several snowfall events were not documented due both to delays in equipment collection and deployment and hesitance by others to wake the snow photographers. Capturing snow also proved difficult in windy conditions.

All snow photographs were illuminated with an LED panel beneath the Petri dish and hemacytometer on which the snow was collected. Most included a blue and a diffusing filter between the light and the Petri dish. The blue light is transmitted through most of a flat-lying snow crystal, while internal structure and crystal edges diffract that light, appearing white in photographs. The Canon system also included a flash with a soft box diffuser covered in a piece of blue filter paper on an extension cable from the camera, which helped illuminate the snow. Two hemacytometers were used, an "improved neubauer" and a "Nageotte bright-line". These slides are typically used for counting blood cells, and have very precise fine-scaled grids. The bright-line hemacytometer has a larger gridded area, with coarser (200 μm) markings than the neubauer, which has a smaller field, with both 250 and 50 μm grids marked on it. These slides were stored in a portable cooler kept at -40^{o}C, along with a "SEAR" snow grain size card and three "Johnny Plastic-Ice XC-24 BR X-Cold Brick" chemical coolant packs. To collect snow, the hemacytometers were placed in Petri dishes set on top of the cold packs on the ship's deck, and wiped clean between photographs. In future, a snowflake collection method that can be deployed more rapidly and under more variable conditions (particularly wind) is recommended. For example, if a freezer for flammable liquids were available, iso-octane in small jars could be used to capture a few flakes per snowstorm and stored at -30 or -40 for later photography in a freezer van with a microscope or other vibration-isolated system.

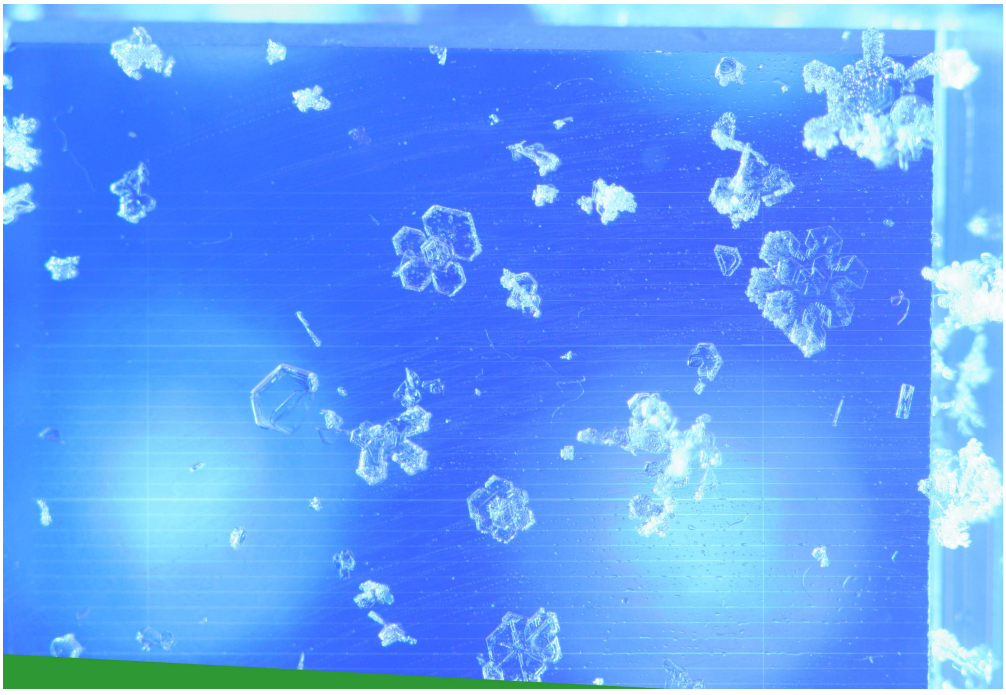

Figure 44: Snow captured during the February 4-5 event while the NBP was conducting a ctd transect along the Dotson Ice Shelf. The white lines are 200 μm (0.0002 m) apart.

The fine weather experienced during NBP09-01 may or may not be representative of typical summer conditions in the Amundsen Sea. December and January are often considered separately from the rest of the year in discussions of Antarctic climatology, due to the high solar angle and incident radiation. Sublimation of falling snow could over-saturate the air with water, while reducing the mean size and total number of falling snowflakes, leading both to the low counts measured with the particle counters and the rime buildup on the unexpectedly large photographed snow crystals. However, the Amundsen experiences high annual snowfall, as evidenced by the thick snow found on sea ice floes during the cruise. Our cruise track could have inadvertently dodged precipitation, the conditions might have been anomalous, or it may not snow very much in January. Post-cruise data analysis and comparison with precipitation forecasts will determine whether the previously observed correlation between snowflake count and modeled precipitation.

10 Education and Public Outreach

NBP-0901 from the Photo-journalists' perspective

Maria Stenzel, Sarah Park

Figure 45: Journalists interview an Emperor Penguin about Circumpolar Deep Water. Photo ©Maria Stenzel, 2009.

More than a year ago we became interested in the West Antarctic Ice Sheet and its interactions with the Southern Ocean. Our curiosity was increased by attending a 'WAIS' meeting and communicating with scientists organizing an expedition to study the topic in more detail near and under the rapidly melting Pine Island Glacier. We believe this research has substantial societal relevance and needs to be fully documented

in ways that are accessible to a wider public audience. We thus inquired about participation in NB Palmer cruise 09-01, and permission was eventually granted, leading to this report.

We have tried to faithfully and accurately cover the science during 0901, from CTD casts, moorings and the Autosub to sea ice studies and phytoplankton experiments. We have also covered many aspects of the physical landscape, which have proven to be useful visual documents for the scientists, in addition to their inherent value in conveying to others the wonders of the regional atmosphere and cryosphere. For example, the configuration and characteristics of ice shelves, the diverse melting and depositional patterns of icebergs, wave action during storms, the nature of sea smoke, wildlife congregations, the top and bottom stages of sea ice formation and melting, the variety of snowflakes, patterns of snowfall and how the wind distributes it. These images have been shared with others and with the scientists working on related studies.

About 24,000 still images and 300 hours of HD video were recorded, including a dozen interviews. The still and video equipment we have used includes Canon digital cameras, various lenses from macro to telephoto, an underwater camera housing unit, Sony XD-CAM EX HD, tripods, various microphones, external hard drives, and laptops. The raw material will require hundreds of hours of editing to be formed into coherent stories, which the scientists will edit for factual content. Our goal is to publish at least one article in a major general audience magazine or newspaper, in tandem with a multimedia piece on that news outlet's website.

The twenty-four hour sunlit days meant that we ran ragged between good light and important events. Of course that could not be avoided, or as one wag noted, "It's been one long day since January 5." As visual journalists, perhaps it would have been helpful to have a cabin with a clear view of the outside rather than being tucked in behind a lifeboat. But that was ameliorated by calls from the bridge crew at any time of day or night to alert us to noteworthy happenings and scenery. Indeed, one of the successful aspects of the cruise was the cooperation we received from everyone aboard. Most scientists were tirelessly willing to explain their work and their hypotheses in ways that the average person can understand. Raytheon staff cheerfully and cleverly modified the underwater camera housing so that it could be fired remotely from a five-meter-long cable, and built an expandable pole extension to lower it through the ice. They willingly drilled extra holes for the camera in the sea ice and skillfully maneuvered the zodiac into position for still and video shots of the Autosub retrieval and other outings. They built a temporary studio for interviews, and escorted us up the science mast numerous times in the cold. Andy Webb volunteered as a grip and technician after completing the successful Autosub missions. Thank you, all, for being of the utmost help.

Blogs

Robin Robertson, Chris Little, Ken Mankoff

Several participants in NBP0901 utilized the limited bandwidth on board to communicate with friends, family, and the broader community. Some efforts were more formalized. A few of these efforts are highlighted below.

Chris Little posted frequent updates to a blog (http://nbp-0901.blogspot.com) devoted to explaining some of the onboard science goals and activities to a broader audience, primarily middle and early high school teachers and students. Before setting forth, Chris worked with his former high school teacher and APECS (Association for Polar Early Career Scientists) to spread the word and develop a format that fostered interaction. The site was set up so that comments were relayed to his NBP email account. One middle school teacher was particularly active, and used temperature and salinity profiles from two Amundsen Sea CTD casts as a teaching tool. He intends to continue to use APECS as a tool for outreach, and the blog website will exist indefinitely. Chris also maintained a blog detailing his experiences on NBP0702 (http://nbp0702.blogspot.com) that is easily found via the NBP0901 website.

Ken Mankoff also posted frequent updates and photos to a blog (http://spacebit.org/category/projects/nbp09-01). Photos were of all aspects of the cruise including scenery, life on the boat, and the science instruments. Text was targeted more toward general public outreach and interest than education. The website

was also announced on the APECS mailing list prior to the cruise.

Robin Robertson sent daily emails and weekly reports to 3 school classes and a unit of Girl Guides Australia. A couple weeks after the cruise started, it was decided to further distribute the emails to all of Girl Guides Australia. The daily emails gave brief accounts of the daily activities and life on the ship, along with location, and air and surface water temperatures. The weekly reports presented the scientific goals and basic knowledge about the topics to explain what we were doing and why. Additionally, one or two photos were sent out with the weekly reports, when possible. The information in these reports was used in various ways. One geography class followed the ship position, science classes used the air and water temperature for temperature dependence on latitude, etc. However, the photos were the biggest hit with the students, according to return emails. Also question occasionally came from the students and were answered.

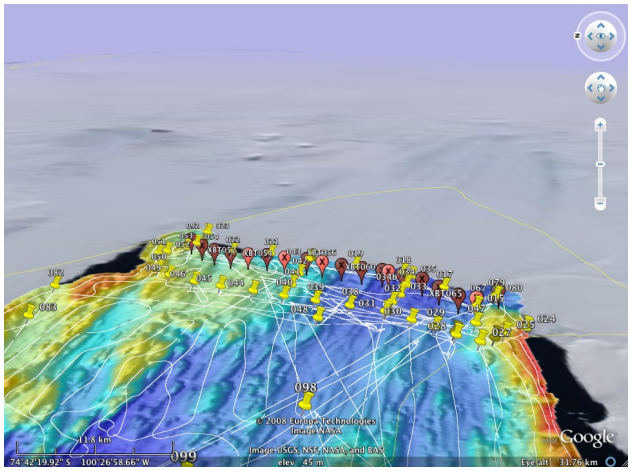

Figure 46: Screenshot of Google Earth showing bathymetric map, ship track, and location of XBTs and CTDs.

The schools involved were Kaleen Primary in Kaleen, Australia (Mrs. Felicity McNeice), George Grant Mason Elementary School in Tuxedo, NY, USA (Mrs. Barbara Voss), and Webatuck Middle School in Millerton, NY, USA (Mrs. Christine Gillette).

Google Earth

Ken Mankoff, Frank Nitsche

Google Earth KML layers were populated with local data to circumvent the lack of internet connectivity. Cruise participants were able to track the ship location, XBTs, and CTD casts in real-time, and see recent data from MODIS and ship bathymetric mapping. A subset of this Google Earth layer will be released on the SpaceBit (http://spacebit.org) website so that the general public can see the cruise track and work locations in a global context.

Appendices

A Cruise Participants

Person	Affiliation
Ben Aaron	Edison Chouest Offshore
Anne Alderkamp	Stanford University
Steve Anderson	Edison Chouest Offshore
Louie Andrada	Edison Chouest Offshore
George Aukon	Raytheon Polar Services
Elbert Bataller	Edison Chouest Offshore
Brandon Bell	Edison Chouest Offshore
Pierre Dutrieux	British Antarctic Survey
Anthony Ford	Edison Chouest Offshore
Lauro Garde	Edison Chouest Offshore
Kathleen Gavahan	Raython Polar Services
Raul Guerrero	Instituto Nacional de Investigacion y Desarollo Pesquero
Eric Hutt	Raython Polar Services
Jullie Jackson	Raython Polar Services
Stan Jacobs	Lamont Doherty Earth Observatory
Adrian Jenkins	British Antarctic Survey
Bill Jirsa	Raython Polar Services
Patrick Laan	Netherlands Institute for Sea Research
Gerald Lakarnafeaux	Edison Chouest Offshore
Katie Leonard	Lamont Doherty Earth Observatory / Columbia University
Mike Lewis	Raython Polar Services
Chris Little	Princeton University
Ted Maksym	British Antarctic Survey
Ken Mankoff	Columbia University / NASA GISS
Steve McPhail	National Oceanography Centre, Southampton
Matt Mills	Stanford University
Alejandra Monje	Edison Chouest Offshore
Dave Munroe	Edison Chouest Offshore
Frank Nitsche	Lamont Doherty Earth Observatory
Ethan Norris	Raython Polar Services
Rogelio Pagdanganan	Edison Chouest Offshore
Sebastian Paoni	Edison Chouest Offshore
Sarah Park	Multimedia Journalist
Chris Payne	University of British Columbia
James Perrett	National Oceanography Centre, Southampton
Johnny Pierce	Edison Chouest Offshore
Danilo Plaza	Edison Chouest Offshore
Vladimir Repin	Edison Chouest Offshore
Robin Robertson	Univ. of New South Wales @ ADFA
Rolly Rogando	Edison Chouest Offshore
Lorenzo Sandoval	Edison Chouest Offshore

continued on next page

continued from previous page

Person	Affiliation
Amy Schaub	Raython Polar Services
Nestor Silverio	Edison Chouest Offshore
Sharon Stammerjohn	University of California, Santa Cruz, Ocean Sciences
Ernest Stelly	Edison Chouest Offshore
Maria Stenzel	Photojournalist
Gary Talbot	Edison Chouest Offshore
Ric Tamayo	Edison Chouest Offshore
Charles Thurozcy	Netherlands Institute for Sea Research
Dmitry Tizon	Raython Polar Services
Gert Van Dijken	Stanford University
Sam Villanueva	Edison Chouest Offshore
Greg Watson	Raython Polar Services
Michael Watson	Edison Chouest Offshore
Andy Webb	National Oceanography Centre, Southampton
Dave White	National Oceanography Centre, Southampton
Scott Worrilow	Woods Hole Oceanographic Institute
Zim Zimmerman	Raython Polar Services

Table 9: Cruise Personnel

B CTD Station Table

No.	Date	Time	Latitude	Longitude	Pres. (dbar)
001	2009-01-10	16:33	65 21.15 S	093 28.57 W	1001
002b	2009-01-12	12:36	69 59.67 S	102 03.67 W	2001
003	2009-01-12	20:25	70 27.70 S	101 55.99 W	2015
004	2009-01-13	09:04	70 59.65 S	102 06.79 W	1772
005	2009-01-13	13:51	71 11.28 S	102 21.86 W	1088
006a	2009-01-14	00:39	71 20.34 S	102 34.23 W	0627
007	2009-01-14	05:31	71 43.65 S	103 02.14 W	0738
008	2009-01-14	19:54	72 07.97 S	104 06.12 W	0579
009	2009-01-15	05:51	72 32.86 S	104 58.41 W	0541
010	2009-01-15	16:26	73 00.49 S	106 21.20 W	0597
011	2009-01-15	23:02	73 26.51 S	106 43.49 W	0882
012	2009-01-16	06:56	74 01.22 S	106 20.07 W	1186
013	2009-01-16	12:02	74 21.64 S	104 53.34 W	1260
014	2009-01-16	19:15	74 43.10 S	104 01.47 W	1083
015	2009-01-17	02:14	75 04.03 S	101 50.82 W	0943
016	2009-01-17	23:35	75 05.51 S	101 46.41 W	0945
017	2009-01-18	01:44	75 02.61 S	101 42.27 W	1047
018	2009-01-18	03:50	75 00.32 S	101 34.85 W	1065
019	2009-01-18	05:26	74 57.28 S	101 31.42 W	0982
020	2009-01-18	06:56	74 54.40 S	101 27.42 W	0832
021	2009-01-18	08:41	74 51.49 S	101 24.69 W	0777
022	2009-01-18	10:31	74 48.78 S	101 23.57 W	0708
023	2009-01-18	12:23	74 46.42 S	101 11.80 W	0713
024	2009-01-19	03:20	75 06.13 S	101 59.39 W	0228
025	2009-01-19	04:09	75 04.85 S	102 01.26 W	0444
026	2009-01-19	05:03	75 04.21 S	102 02.71 W	0624
027	2009-01-19	06:01	75 03.36 S	102 04.06 W	0756
028	2009-01-19	07:17	75 02.24 S	102 01.78 W	0911
029	2009-01-19	08:37	75 01.25 S	101 59.00 W	0920
030	2009-01-19	09:53	75 00.08 S	101 56.25 W	0951
031	2009-01-19	11:25	74 58.70 S	101 53.13 W	0995
032	2009-01-19	12:45	74 59.21 S	101 49.00 W	1018
033	2009-01-19	14:05	74 59.80 S	101 45.71 W	1041
034	2009-01-19	15:27	75 00.34 S	101 41.05 W	1065
035	2009-01-19	17:03	75 00.79 S	101 36.81 W	1081
036	2009-01-19	18:52	74 58.80 S	101 53.07 W	0200
037	2009-01-20	19:58	75 02.23 S	102 00.80 W	0922
038	2009-01-20	23:02	74 56.71 S	101 50.69 W	1004
039	2009-01-21	00:27	74 54.71 S	101 48.66 W	0942
040	2009-01-21	01:49	74 52.81 S	101 46.61 W	0782
041	2009-01-21	03:11	74 53.21 S	101 41.36 W	0769
042	2009-01-21	04:17	74 53.62 S	101 35.72 W	0766
043	2009-01-21	05:26	74 54.17 S	101 27.74 W	0834
044	2009-01-21	11:30	74 50.90 S	101 44.48 W	0675
045	2009-01-21	12:50	74 48.82 S	101 42.40 W	0635

continued on next page

continued from previous page

No.	Date	Time	Latitude	Longitude	Pres. (dbar)
046	2009-01-21	14:03	74 47.06 S	101 40.31 W	0633
047	2009-01-22	09:49	75 03.57 S	101 57.34 W	0798
048	2009-01-22	22:24	74 54.88 S	101 55.76 W	0879
049	2009-01-23	01:42	74 45.28 S	101 37.12 W	0508
050	2009-01-23	02:55	74 44.32 S	101 33.99 W	0541
051	2009-01-23	04:02	74 43.67 S	101 25.19 W	0532
052	2009-01-23	05:01	74 44.18 S	101 23.85 W	0530
053	2009-01-23	05:58	74 45.33 S	101 21.36 W	0599
054	2009-01-23	07:00	74 45.97 S	101 18.93 W	0654
055	2009-01-23	08:08	74 46.44 S	101 17.68 W	0676
056	2009-01-24	00:58	75 01.19 S	103 57.07 W	0634
057	2009-01-24	02:17	75 03.12 S	103 58.20 W	0473
058	2009-01-24	20:58	75 05.44 S	101 46.52 W	0905
059	2009-01-24	22:00	75 05.42 S	101 46.50 W	0901
060	2009-01-24	22:59	75 05.44 S	101 46.53 W	0803
061	2009-01-25	00:14	75 05.42 S	101 46.50 W	0901
062	2009-01-25	00:58	75 05.42 S	101 46.52 W	0901
063	2009-01-25	01:58	75 05.40 S	101 46.51 W	0800
064	2009-01-25	02:59	75 05.42 S	101 46.50 W	0800
065	2009-01-25	03:58	75 05.41 S	101 46.48 W	0800
066	2009-01-25	04:59	75 05.43 S	101 46.51 W	0801
067	2009-01-25	05:58	75 05.44 S	101 46.56 W	0801
068	2009-01-25	06:55	75 05.42 S	101 46.51 W	0800
069	2009-01-25	07:59	75 05.40 S	101 46.47 W	0800
070	2009-01-25	08:57	75 05.45 S	101 46.53 W	0801
071	2009-01-25	09:55	75 05.41 S	101 46.47 W	0800
072	2009-01-25	10:58	75 05.41 S	101 46.46 W	0800
073	2009-01-25	11:58	75 05.42 S	101 46.51 W	0801
074	2009-01-25	12:56	75 05.39 S	101 46.42 W	0800
075	2009-01-25	13:58	75 05.42 S	101 46.51 W	0801
076	2009-01-25	14:58	75 05.41 S	101 46.49 W	0801
077	2009-01-25	15:58	75 05.41 S	101 46.49 W	0803
078	2009-01-25	16:58	75 05.41 S	101 46.49 W	0800
079	2009-01-25	17:58	75 05.47 S	101 46.60 W	0800
080	2009-01-25	18:58	75 05.44 S	101 46.57 W	0800
081	2009-01-25	19:58	75 05.45 S	101 46.56 W	0901
082	2009-01-26	03:59	74 38.59 S	101 42.95 W	0609
083	2009-01-26	05:12	74 38.59 S	101 55.48 W	0630
084	2009-01-26	06:29	74 38.65 S	102 10.56 W	0621
085	2009-01-26	08:52	74 39.46 S	102 35.01 W	0752
086	2009-01-26	10:39	74 43.06 S	102 48.20 W	1012
087	2009-01-26	13:08	74 45.93 S	102 56.74 W	1078
088	2009-01-26	15:05	74 49.66 S	103 09.41 W	1058
089	2009-01-26	18:32	74 53.66 S	103 28.55 W	0872
090	2009-01-26	21:00	74 57.13 S	103 48.74 W	0721
091	2009-01-27	09:06	74 12.50 S	105 35.68 W	1627
092	2009-01-28	12:10	74 46.29 S	101 11.71 W	0667
093	2009-01-28	18:43	75 05.55 S	101 46.52 W	0926

continued on next page

continued from previous page

No.	Date	Time	Latitude	Longitude	Pres. (dbar)
094	2009-01-28	21:58	75 01.52 S	102 44.54 W	0789
095	2009-01-29	00:00	75 03.04 S	102 44.49 W	0628
096	2009-01-29	01:06	75 03.58 S	102 44.66 W	0413
097	2009-01-29	01:59	75 04.09 S	102 44.50 W	0305
098	2009-01-29	13:46	74 54.34 S	102 22.69 W	0945
099	2009-01-29	15:40	74 49.83 S	102 37.55 W	0997
100	2009-01-29	18:37	74 50.82 S	103 17.12 W	1090
101	2009-01-30	13:36	74 45.46 S	104 16.25 W	1224
102	2009-01-30	20:25	74 33.03 S	103 10.60 W	1079
103	2009-01-31	03:11	74 38.43 S	104 23.66 W	1516
104	2009-01-31	17:56	74 09.97 S	104 00.11 W	0316
105	2009-01-31	21:57	73 55.03 S	104 59.86 W	0304
106	2009-02-01	01:16	73 44.98 S	106 00.05 W	0869
107	2009-02-01	04:57	73 35.06 S	106 59.98 W	0605
108	2009-02-01	09:08	73 25.01 S	108 00.13 W	0631
109	2009-02-01	12:17	73 20.01 S	109 00.12 W	0462
110	2009-02-02	07:42	73 08.02 S	112 01.40 W	0408
111	2009-02-02	12:22	72 54.96 S	114 00.11 W	0500
112	2009-02-02	18:03	72 46.44 S	115 45.47 W	0641
113	2009-02-03	02:21	73 09.78 S	115 00.99 W	0759
114	2009-02-03	06:55	73 38.02 S	115 15.30 W	0918
115	2009-02-03	11:45	73 52.62 S	116 49.68 W	1142
116	2009-02-03	15:08	73 48.99 S	117 59.11 W	1209
117	2009-02-03	21:48	73 57.68 S	118 02.71 W	1274
118	2009-02-04	13:22	73 42.76 S	113 17.28 W	0840
119	2009-02-04	18:41	74 10.37 S	113 20.39 W	0588
120	2009-02-04	21:11	74 11.54 S	113 12.72 W	0811
121	2009-02-04	22:50	74 13.01 S	112 52.49 W	0745
122	2009-02-05	00:35	74 13.03 S	112 31.88 W	1184
123	2009-02-05	02:42	74 13.79 S	112 11.64 W	1013
124	2009-02-05	04:17	74 13.22 S	111 56.50 W	0593
125	2009-02-05	07:35	74 11.55 S	112 31.24 W	1066
126	2009-02-06	09:14	74 17.13 S	109 50.71 W	0892
127	2009-02-07	00:08	73 31.65 S	110 24.87 W	0313
128	2009-02-07	19:41	73 02.31 S	110 01.06 W	0431
129	2009-02-07	22:31	73 08.42 S	109 10.70 W	0456
130	2009-02-08	09:14	72 22.04 S	108 48.09 W	0537
131	2009-02-08	17:01	72 17.54 S	106 56.49 W	0683
132	2009-02-09	09:16	71 42.41 S	105 09.47 W	0531
133	2009-02-09	21:27	70 59.29 S	106 01.20 W	1540
134	2009-02-10	01:20	71 02.03 S	105 58.52 W	1084
135	2009-02-10	04:10	71 08.05 S	106 01.81 W	0515
136	2009-02-10	06:03	71 11.89 S	106 03.31 W	0515
137	2009-02-10	13:31	71 45.96 S	106 53.78 W	0527
138	2009-02-10	23:42	71 30.46 S	108 18.70 W	0490
139	2009-02-11	05:45	71 20.08 S	109 46.57 W	0461
140	2009-02-11	10:53	71 39.10 S	110 34.61 W	0471
141	2009-02-12	00:55	71 53.27 S	112 13.25 W	0529

continued on next page

continued from previous page

No.	Date	Time	Latitude	Longitude	Pres. (dbar)
142	2009-02-12	11:21	71 34.07 S	113 01.83 W	0597
143	2009-02-12	15:34	71 27.28 S	113 25.21 W	0633
144	2009-02-12	18:50	71 24.52 S	113 29.90 W	1079
145	2009-02-12	23:55	71 38.71 S	114 23.43 W	0455
146	2009-02-13	08:40	71 59.68 S	115 36.77 W	0445
147	2009-02-13	15:00	72 20.09 S	117 00.39 W	0519
148	2009-02-13	23:06	73 20.24 S	117 51.44 W	0358
149	2009-02-14	04:32	73 55.35 S	118 49.47 W	0751
150	2009-02-14	05:52	73 56.37 S	118 40.10 W	1466
151	2009-02-14	07:43	73 58.50 S	118 30.22 W	1336
152	2009-02-14	09:39	73 59.75 S	118 18.69 W	1061
153	2009-02-14	11:27	74 00.68 S	118 07.86 W	1006
154	2009-02-14	14:07	74 01.12 S	117 54.04 W	1202
155	2009-02-14	16:22	74 01.70 S	117 39.00 W	0639
156	2009-02-15	04:52	72 06.72 S	117 55.36 W	0505
157	2009-02-15	08:26	71 57.16 S	118 26.43 W	0593
158	2009-02-15	10:19	71 54.10 S	118 43.24 W	1113
159	2009-02-17	05:39	66 26.98 S	129 28.23 W	1201
160	2009-02-18	04:02	66 59.99 S	128 58.06 W	4498

Table 10: Table listing of all CTD date, time, location, and maximum pressure

C Pre-cruise Project Plans

C.1 Amundsen Sea Influence on West Antarctic Ice Sheet Stability and Sea Level Rise

Stan Jacobs (Lamont Earth Observatory), Adrian Jenkins (British Antarctic Survey) Hartmut Hellmer (Alfred-Wegener Institute)

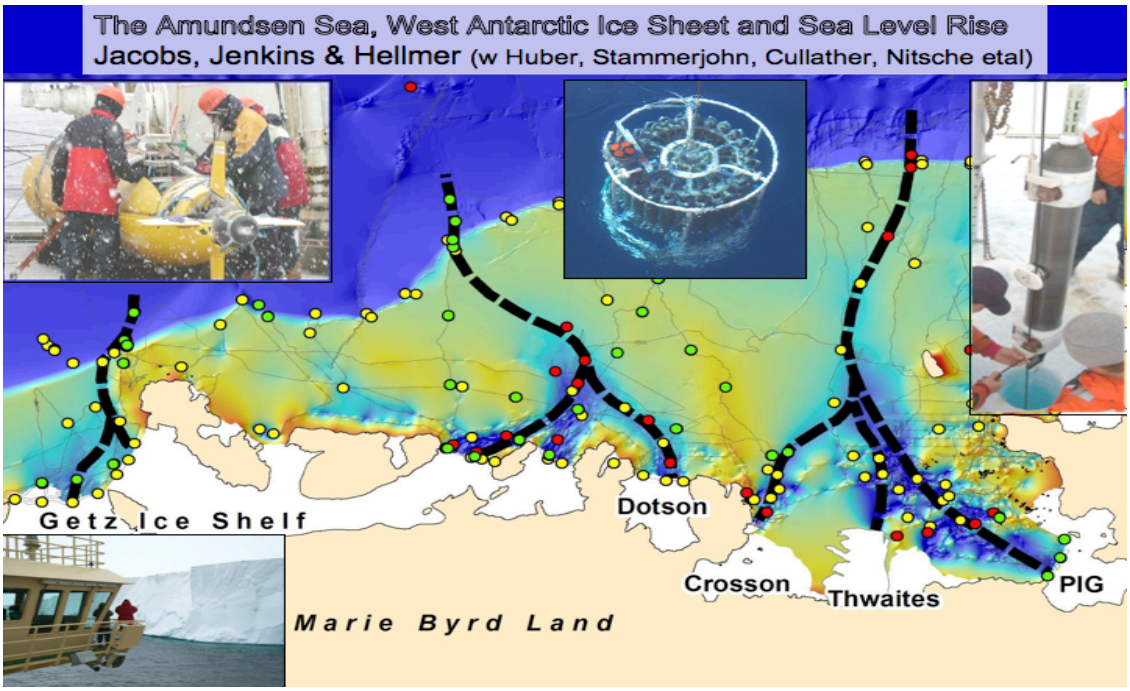

Figure 47: Circumpolar Deep Water crosses the continental shelf break and ponds in deep, glacially-cut troughs on the Amundsen continental shelf, from which it gains access to vulnerable ice shelf grounding lines. Moorings and measurements during NBP09-01 will focus on the eastern and central troughs, shelf break, ice shelf fronts and cavities, sea ice cover and sea floor bathymetry.

Research Objectives

West Antarctica is a marine ice sheet grounded below sea level in an evolving ocean. Its stability in a changing climate hinges on the balance between surface accumulation, ice stream flow, iceberg calving and in situ basal melting of its fringing ice shelves. In the Amundsen Sea's greater Pine Island Bay, deep shelf ice is melting orders of magnitude faster than elsewhere around Antarctica, driven by large intrusions of 'warm' deep water onto the continental shelf. Remote sensing studies have correlated that melting with thinning ice shelves, increased velocity of inflowing ice streams and drawdown of the adjacent ice sheet. Multi-year time series of ocean properties and currents are needed to better understand seasonal and interannual variability of deep water access to the continental shelf and ice shelf cavities. To clarify Amundsen Sea influence on the regional ice shelves and the effects of ice sheet change on the coastal ocean, we will begin to monitor the ocean properties and circulation, within an IPY context. Water column profiling and sampling will provide information about thermohaline variability and meltwater content 15 years after the first observations in this sector. Pack ice investigations will focus on the roles of snow ice and ocean heat transport in sea ice mass balance. Swath mapping of the sea floor will concentrate on the deep troughs and outer shelf depressions that funnel the warm, salty deep water to potentially vulnerable ice shelf grounding zones. The measurements

obtained will be used to model ocean properties, circulation, and interactions with the cryosphere.

Field-Season Overview

During a 54-day cruise of the NB Palmer to the eastern Amundsen Sea (NBP09-01) in Jan-Feb 2009, we will attempt to set 15 arrays of instruments to record temperature, conductivity, pressure and ocean currents near the shelf break, ice shelf fronts, and along/across deep glacial troughs on the continental shelf (figure 47). CTD/rosette/LADCP casts and water sampling will be done at the mooring sites, along nominal N-S and E-W transects and at locations where CTD stations have previously been occupied. Porpoising ocean drifters and XBTs will be deployed at various points along the ship's track. Sea ice cores will be obtained and processed aboard, and buoys set out on the ice to transmit position and mass balance parameters over time. The sea floor will be mapped via multibeam sonar, and a variety of standard and enhanced surface measurements made underway. Water samples will be processed aboard ship for salinity and dissolved oxygen, and returned to US laboratories for CO_2 and oxygen isotope analyses. This work will share time and be coordinated with three other NBP09-01 projects. Moored arrays set during the cruise will be reset/recovered in early 2010/2011.

C.2 Ocean Circulation and Ice Shelf Melting on the Amundsen Sea Continental Shelf

Adrian Jenkins (British Antarctic Survey), Stan Jacobs (Lamont Earth Observatory)

Background

The Antarctic ice sheet, which represents the largest of all potential contributors to sea level rise, appears to be losing mass at a rate that has accelerated over recent decades. Ice loss is focussed in a number of key drainage basins where dynamical changes in the outlet glaciers have led to increased discharge. The most significant recent mass losses have been from the basins that drain along the Amundsen Sea coast. The synchronous response of several independent glaciers, coupled with the observation that thinning is most rapid over their floating termini, is generally taken as an indicator that the changes have been driven from the ocean, but the precise mechanism has remained speculative. Observations have revealed that the deeper parts of the Amundsen Sea shelf are flooded by almost unmodified Circumpolar Deep Water (CDW) with a temperature around 1^oC, and that this drives rapid melting of the floating ice. We need to understand what processes determine the strength of the CDW inflow and how it interacts with the floating ice in order to quantify the past, present and possible future oceanic forcing on the glaciers.

Objectives

This project will use the UK Natural Environment Research Council's autonomous underwater vehicle (Autosub-III) to study how the warm CDW gets beneath the Amundsen sea ice shelves and how it determines the melt rate of the ice shelves. Specifically we aim to: map the seabed beneath the ice shelves; map the underside of the ice shelves; and determine where and how heat is transferred from the inflowing CDW to the outflowing ice-ocean boundary layer. To do this Autosub-III will carry the following instrumentation: Seabird CTD, with dual C and T sensors plus DO sensor and transmissometer; Simrad multi-beam echosounder; upward-looking RDI 300 kHz ADCP; downward-looking RDI 150 kHz ADCP.

Our primary target will be Pine Island Glacier (PIG), which is also the target of a US IPY project that aims to drill through the ice shelf and deploy moored instruments within the cavity. Our spatial survey of water properties beneath the glacier will complement their time-series of observations in one small area. The

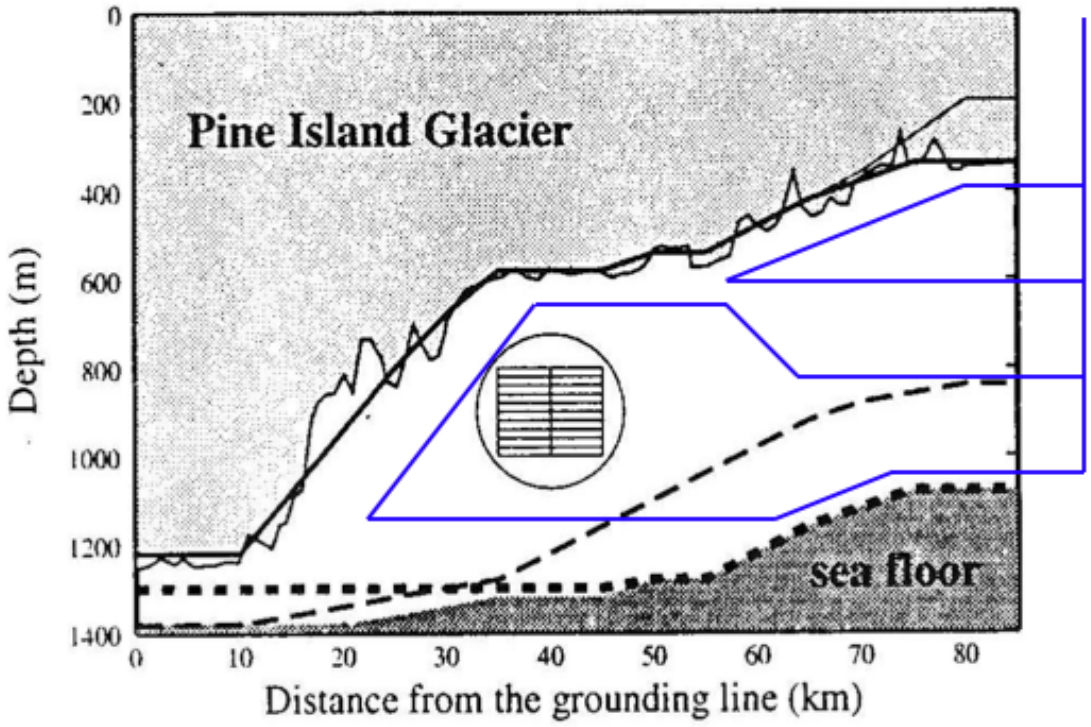

Figure 48: Missions, three each, penetrating 60 and 120 km into cavity (side view). Note grounding line is now thought to be near the break in slope at around 15 km. The seabed depth is completely unknown between there and the ice front. That shown is a guess only.

ideal set of missions would comprise: 3 x 60 km missions to depth 600 m, in the outer half of the cavity; 3 x 120 km missions to depth of 1000 m, extending as far into the cavity as possible (a minimum water column thickness of 100m being the cut-off). A rough cross-section of one short and one long mission is shown below. The other two would run parallel to this. Mission duration for the shorter ones will be around 20 hours, for the longer ones around 30 hours (including deployment and recovery time). Turnaround time will be about 12 hours between missions. In addition a short test mission (8 hours) will be required in open water anywhere on the continental shelf.

Contingency

If ice blocks access to the PIG front, mission tracks will be longer. In this case fewer mission will be run (total run time is limited by battery capacity). If the length of the traverse beneath the sea ice makes work beneath PIG impractical, Thwaites, Crosson, Dotson, Getz of Abbott ice shelves would make worthwhile targets (in that order of priority). We would lose the advantage of a parallel sub-ice shelf mooring project, but the key processes controlling inflow to the cavity and melting within it would be the same.

C.3 Shedding dynamic light on iron limitation: The interplay of iron limitation and dynamic irradiance conditions in governing the phytoplankton distribution in the Ross Sea

Kevin Arrigo (Stanford University)

Research Objectives

The Southern Ocean plays an important role in the global carbon cycle, due to its large size and unique physiochemical characteristics. Approximately 25% of total anthropogenic CO_2 uptake by the oceans takes place in the Southern Ocean, mainly via primary production by phytoplankton. However, changes in the Antarctic climate may impact phytoplankton primary productivity and hence, the carbon export by the Southern Ocean. Primary production in the Southern Ocean is dominated by two phytoplankton groups that bloom in distinct locations and times: diatoms dominate blooms in the shallow mixed layer of the continental shelf, whereas the colony forming Phaeocystis antarctica (Prymnesiophyceae) dominates blooms in the more deeply mixed, open regions. Understanding what controls the dynamics of these two phytoplankton taxa is essential because they dominate virtually all polar waters, they have vastly different nutrient utilization characteristics, and both support very different marine food webs. In addition, this understanding is needed to recognize the potential impact of climate change on the Antarctic phytoplankton community and predict their role in the carbon export in the future. Previous experiments in our laboratory suggest that taxon-specific differences in photoacclimation contribute to the observed distribution. However, photoacclimation does not seem to be the only factor that controls the phytoplankton distribution. Iron (Fe) limitation of the algal communities in both the sub-Arctic and the Southern Ocean is now well documented. Moreover, phytoplankton Fe demand varies as a function of irradiance. Therefore, the main hypothesis of the proposed research is: The interaction between Fe limitation and dynamic irradiance governs phytoplankton distributions in the Southern Ocean.

Field Season Overview

Results from our cruise to the Amundsen Sea in the Antarctic summer 2009 will be compared to results obtained last year during the ANT XXIV/3 cruise. IPY-partner Prof. H.J.W. de Baar (Royal NIOZ, The Netherlands) is sending his expert team to join us to measure concentrations of the total dissolved Fe. At locations harboring one of the two dominant phytoplankton communities at different stages of their respective blooms, photoregulatory processes, pigment ratios, and the effect of the prevailing Fe-levels on the extent to which phytoplankton are protected against photoinhibition when they reside close to the surface, will be determined. In addition, the extent to which the phytoplankton community is Fe-limited and able to use organically bound (ligand bound) Fe will be assessed in bottle experiments. Phytoplankton samples will be incubated over six days with the addition of dissolved Fe and/or a ligand (e.g., the siderophore ferrioxamine B), whereas in control experiments no Fe will be added. Increases in phytoplankton biomass will be determined from cell counts and POC content.

We will need to sample regions with phytoplankton at different stages of bloom development. Transect work would be ideal, as would be the ability to sample some stations more than once. Depending on cruise track, we would be interested in sampling the Amundsen polynya (centered at 115^{o}W) while in transit to Pine Island Bay. We would like to sample one station each day, preferably in the morning. On even days, we will require 40 L of water to be collected from a single depth ($\sim$50 m) using the standard rosette that accompanies the CTD package. A second cast will be performed at this station using trace-metal clean Niskin bottles attached to a Kevlar wire that will sample from multiple depths near the ocean surface (<300 m). These water samples will be used to quantify Fe concentrations as well as ligand abundance and characteristics. On odd days, we also will require 40 L of water to be collected from a single depth ($\sim$50 m) using the standard rosette that accompanies the CTD package. The second cast will be performed at this station using a trace-metal clean rosette and will sample from a single depth near the ocean surface ($\sim$50 m). This water will be used to conduct incubation experiments that will each last several days.

C.4 Collaborative Research: Sampling the ocean - sea ice interaction in the Pacific center of the Antarctic Dipole

Xiaojun Yuan (Lamont Earth Observatory), Janet Sprintall (Scripps Institution of Oceanography), Douglas Martinson (Lamont Earth Obsservatory)

Project Summary

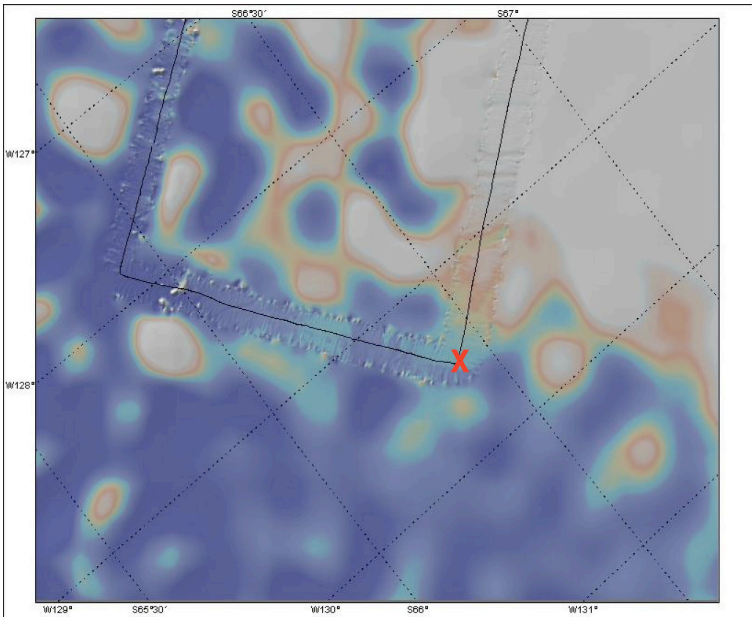

Figure 49: Target mooring site and topography.

The Antarctic Dipole (ADP) presents the strongest tropical-polar teleconnection climate signal in the Southern Ocean, with poles centered within the Ross Gyre of the Pacific sector and the central Weddell Gyre of the Atlantic sector. The ADP is a standing mode pattern characterized by out-of-phase relationships in the surface air temperature, sea surface temperature, and sea ice fields. The opposing large-scale spatial patterns of the ADP within the Pacific and Atlantic centers are clearly associated with both positive and negative phases of ENSO. Outside these sectors the anomalies are not coherent or distinct. Furthermore, the anomalous signals persist in the subpolar waters for nearly a year after the demise of the ENSO event in the tropics. While the atmospheric and sea surface signatures of the ADP have received much recent attention, little is known about the role of the upper ocean in maintaining and reinforcing the ADP climate anomalies in the Southern Ocean. Clearly the upper ocean has a longer memory and larger heat capacity than the atmosphere to preserve anomalous climate signals.

Objectives

The main objective of this proposal is to investigate the response of the upper ocean and the variability in the air-sea-ice system in the centers of the ADP in the Southern Ocean. Specifically, we are motivated by the desire to better understand the local and regional processes underlying the response of the ADP to climate forcing on synoptic to ENSO time scales. Our key goal is to determine the role of the upper ocean in maintaining the ADP climate signal in the Southern Ocean. Specifically, this international program will document and investigate the processes of ocean-sea ice interaction that amplify and maintain the strong ADP signal in the subpolar South Pacific.

Fieldwork overview

To achieve our goal, multi-year mooring deployments are planned within each center of the ADP in the western Ross gyre and the central Weddell Gyre. While German scientists have led the monitoring effort in the Weddell Gyre, this project is to support the U.S. led effort to deploy a mooring in the Pacific center of

the ADP in west of the Amundsen Sea. The target mooring site is at 66.45^{o}S, 129.47^{o}W, where the largest ADP climate signal frequently appears in sea ice and surface temperature fields; high resolution topography data are available; and sea floor is relatively flat. The moorings will be initially deployed in austral summer 2008-9, redeployed in austral summer 2010-11, and recovered in austral summer 2012-13. The mooring will consist of an ice profiling sonar, McLane Moored Profiler (MMP), discrete SeaBird temperature, conductivity and pressure sensors, as well as a current meter. This mooring will resolve the upper ocean stratification and velocity between 75 and 550m over a variety of time scales from daily to interannual. The ice profiling sonar will be installed at the top of the mooring to provide simultaneous measurements of the ice draft. A full depth CTD station at the mooring site is planned during the first deployment for ballasting the MMP and providing background stratification. In case of severe weather that prohibits the deployment at the target site, the mooring can be deployed at an alternative site, as close as possible to the target site. Combined with satellite measurements of sea ice concentration/drift, winds, sea surface and air temperatures, the direct measurements of the stratification and sea ice thickness from the mooring data will allow us, for the first time, to unambiguously determine the dynamical processes of the coupled upper ocean-air-ice system in the Southern Ocean that link these polar regions to large-scale climate variability.


Photo © Maria Stenzel 2009